Operator control of a Heisenberg chain by locally acting on a single end qubit

A thesis submitted in partial fulfillment of the requirements for the degree of
Master of Science in Physics

Department of Physics, University of Basel, Switzerland

Supervisor: Prof. Dr. Christoph Bruder
Co-Supervisor: Dr. Vladimir M. Stojanović
Author: Rahel Heule

July 27, 2010

Abstract

As recently proved by Burgarth *et al.* [Phys. Rev. A **79**, 060305(R) (2009)], a Heisenberg spin chain can be controlled completely by acting locally on one of the spins at its ends. This is the starting point for the present thesis. We consider mainly an isotropic spin-$\frac{1}{2}$ Heisenberg chain of length three and apply a control field to the first spin. The control is chosen to be an element of the set of piecewise constant functions. Controlling the field in x- and y-direction is sufficient for universal quantum computation. We perform operator control, i.e. we find control functions such that the time evolution operator of the system reaches a specified target unitary at some fixed final time, and analyse the time dependence of the control fields found for some concrete gates. The implementation is performed by maximizing the fidelity between the respective target gate and the dynamic time evolution of the system. Throughout this work we use as standard gate a spin-flip gate which flips the last spin in the chain and is achievable by control of the x-field only, but we implement as well entangling gates like the controlled-NOT and square root of SWAP. We analyse the sensitivity of the fidelity to random noise and search for smooth optimal control fields by applying filtering techniques in the Fourier space. Concretely, we make use of two different filters having a smoothing effect, namely of an ideal low-pass and a Gaussian filter. Furthermore, we extend the three-spin system adding one more spin to the chain and estimate a minimal time for the implementation of the spin-flip and CNOT gate depending on the number of spins whereas we include results stemming from a chain of two, three, and four spins. Finally, we describe how a quantum error correction circuit consisting of five qubits may be implemented by local control of a Heisenberg spin chain of length five.

Contents

1 Introduction

The thesis is organized in the following way. We start by overviewing basics of quantum information, computation and control (Section 2). Doing this we focus on unitary operators and quantum gates and give a definition for universal gates in the context of quantum circuits. In Section 3 we introduce the concepts of control theory and answer the question of controllability for a given quantum control system from a Lie algebra perspective. Furthermore, we collect a few facts about Lie algebras and Lie groups and note the *Lie Algebra Rank Condition* which associates the set of reachable states for a control system with the system's dynamical Lie algebra. This condition provides at the same time a criterion for complete controllability.

After having introduced the relevant theoretical background with regard to quantum control systems, in Section 4 the actual work starts. We briefly review the argument of [1] concerning local controllability of quantum networks. The proof that a Heisenberg spin chain can be controlled completely by applying a control field either to the first or last spin in the chain, is the starting point for the further work. We set up a quantum control system by an isotropic Heisenberg spin-$\frac{1}{2}$ chain whereas we operate locally with a control field on the first spin. This system is fully controllable which means here that the set of unitaries reachable from the identity is the special unitary group $su(n)$. Hence, any unitary contained in $su(n)$ can be achieved by adjusting the controls in an appropriate manner. We apply a control field to the first spin which points in x- and y-direction and is sufficient for complete controllability. The shape of the control field is chosen to be piecewise constant. Performing local operator control we implement spin-flip gates and the entangling gates CNOT and $\sqrt{\text{SWAP}}$. In order to find optimal control fields which drive the system's time evolution operator from the identity to the desired target gate, we numerically maximize the fidelity between the target and the dynamic time evolution of the system. Fields which implement a respective gate to high accuracy are called optimal throughout this work. As standard target unitary we consider the gate which flips the last spin in the chain and can be achieved by controlling only the x-field. Having reached optimal control fields we disturb them by random noise and analyse the sensitivity of the fidelity to the noise. Furthermore, we tend to reach optimal control fields which are smoother than the piecewise constant ones and nevertheless correspond to high fidelities. To this end we apply ideal-low pass and Gaussian filters to the Fourier transformed optimal piecewise constant controls. The filtering effects a smoothing of the control fields. We analyse how the strength of the control fields influences the smoothing procedure.

In Section 5 we extend the Heisenberg three-spin chain to a chain of arbitrary length. Due to the computational burden it is unfortunately not possible to go beyond four spins. However, two, three, and four spins can be done and we compare the implementation of spin-flip and CNOT gates for varying number of spins. In particular, we are interested how the minimal time, which is needed to achieve those gates, depends on the number of spins. The thesis is completed by Section 6 where we describe one possible application of local operator control. We present a quantum error correction circuit which can be realized by local operator control applied to a Heisenberg five-spin chain. Finally, the results are summarized in Section 7.

2 Basics of quantum computation, information, and control

This section introduces the fundamentals of quantum computation, information, and control, mainly based on [2], [3], and [4].

2.1 Quantum bits

While classical computation and information is based on the *bit*, the basic unit of classical computer information, the quantum analogue is given by the *quantum bit*, or *qubit* for short. Qubits are mathematical objects which can be realized as real physical systems. A classical bit has a state which is either equal to 0 or equal to 1. Accordingly, a quantum bit also has a state. Each

qubit represents a two-level quantum system associated with a two-dimensional complex vector space on which an inner product, denoted by $\langle \cdot, \cdot \rangle$, is defined (Hilbert space). The state of the qubit is described by a normalized vector contained in the Hilbert space. Since a qubit is a two-level system, there exist two possible states for it denoted in the Dirac notation by $|0\rangle$ and $|1\rangle$ which correspond to the states 0 and 1 for a classical bit. But in contrast to classical bits a qubit can be additionally in a state other than $|0\rangle$ or $|1\rangle$, namely in a state resulting from a linear combination of both. The special states $|0\rangle$ and $|1\rangle$, which represent the states in which the qubit may be measured, form an orthonormal basis for the two-dimensional Hilbert space, known as *computational basis*. A pure qubit state is a linear combination of the basis states.

Now we assume the existence of two qubits. In the corresponding classical case there are four possible states: 00, 01, 10 and 11. The *computational basis* of a two-qubit system consists analogously of the four basis states $|00\rangle$, $|01\rangle$, $|10\rangle$, and $|11\rangle$. As in the case of a single qubit a pair of qubits can exist in a superposition of these four states. Another important orthonormal basis for the two-qubit state space (four-dimensional Hilbert space) is the *Bell basis* consisting of the four maximally entangled states $\frac{|00\rangle+|11\rangle}{\sqrt{2}}$, $\frac{|00\rangle-|11\rangle}{\sqrt{2}}$, $\frac{|10\rangle+|01\rangle}{\sqrt{2}}$, and $\frac{|01\rangle-|10\rangle}{\sqrt{2}}$. The Bell basis is maximally correlated while the computational basis is uncorrelated.

As mentioned before, qubits are not only mathematical objects but can also be realized in different physical systems, e.g. as the two different polarizations of a photon, as the two states (ground state and excited state) of an electron orbiting an atom or as the alignment of a nuclear spin in a magnetic field. In particular, the spin of the electron or in general every system with spin $\frac{1}{2}$ is described very well by the qubit model since the Hilbert space of a system with spin $\frac{1}{2}$ is two-dimensional. In this work we will consider a physical N-qubit system realized by an isotropic Heisenberg spin-$\frac{1}{2}$ chain of length N.

2.2 Quantum entanglement

Entanglement of quantum systems may be produced by the interaction between two or more systems. It refers to the situation where the state of the whole composite system cannot be written as the tensor product of states of the single systems. Consider for instance a two-qubit system which is composed of two single qubits. We write the corresponding four-dimensional Hilbert space as the tensor space $\mathcal{H} = \mathcal{H}_1 \otimes \mathcal{H}_2$ where $\mathcal{H}_1$ and $\mathcal{H}_2$ are the two-dimensional Hilbert spaces each associated with one of the two single qubits. There exist two-qubit states which can be decomposed into the tensor product of two single-qubit states, such as $|\psi\rangle = |01\rangle = |0\rangle \otimes |1\rangle$. In this case we may conclude that one qubit is in the state $|0\rangle$ while the other is in the state $|1\rangle$. But there are other states in the Hilbert space $\mathcal{H}$ which cannot be written as the tensor product of two single-qubit states, for instance $|\psi\rangle = \frac{|00\rangle+|11\rangle}{\sqrt{2}}$. In such a case it is not possible to separate the states of the two single qubits by writing $|\psi\rangle = |\psi_1\rangle \otimes |\psi_2\rangle$ for two single-qubit states $|\psi_1\rangle$ and $|\psi_2\rangle$, and the two qubits are said to be entangled. This entanglement can be illustrated by imaging that the two qubits are sent to two different locations A and B. If we measure the qubit at location A the result of this measurement will determine the outcome of a measurement of the qubit at location B which means that the measurement outcomes are correlated.

Separable and entangled pure states:

We consider a quantum system composed of N subsystems. Its state is described by a vector $|\psi\rangle$ in the tensor space

$$\mathcal{H} := \mathcal{H}_1 \otimes \mathcal{H}_2 \otimes \cdots \otimes \mathcal{H}_N, \tag{2.2.1}$$

where H_j, $j \in \{1, \ldots N\}$, is the Hilbert state of the j-th subsystem.

Definition 2.1. *[2] If a state $|\psi\rangle \in \mathcal{H}$ can be written as*

$$|\psi\rangle = |\psi_1\rangle \otimes |\psi_2\rangle \otimes \cdots \otimes |\psi_N\rangle, \qquad (2.2.2)$$

with $|\psi_j\rangle$ being a state in the space H_j of the j-th subsystem, it is called separable, otherwise entangled.

2.3   Qubit state space

The state space of a single qubit is two-dimensional. In general, a N-qubit system has an underlying state space of 2^N dimensions. We assume that $|0\rangle$ and $|1\rangle$ form an orthonormal basis for the state space of a single qubit. A pure single-qubit state can then be represented as a linear combination of the normalized basis states $|0\rangle$ and $|1\rangle$:

$$|\psi\rangle = \alpha |0\rangle + \beta |1\rangle, \qquad (2.3.1)$$

with $|\alpha|^2 + |\beta|^2 = 1$, since the probabilities $|\alpha|^2$ to measure a qubit in the state $|0\rangle$ and $|\beta|^2$ to measure it in the state $|1\rangle$ must sum to one. This relation can geometrically be seen as the condition that the qubit's state is normalized to length 1. Due to this we may write

$$|\psi\rangle = e^{i\gamma} \left(\cos\frac{\theta}{2} |0\rangle + e^{i\phi} \sin\frac{\theta}{2} |1\rangle \right), \qquad (2.3.2)$$

where θ, ϕ and γ are real numbers. The factor $e^{i\gamma}$ can be ignored since it has no observable effects which means that the statistics of measurement (probabilities to measure certain outcomes) are not affected by ignoring it. Or shortly, global phases are irrelevant in quantum mechanics. The real numbers θ and ϕ represent geometrically a point on the unit sphere in the three-dimensional space. This sphere is known as *Bloch sphere* and allows the visualization of the state of a single qubit. The Bloch sphere can be considered as a two-dimensional space which corresponds to the surface of a sphere. Each pure single-qubit state can therefore be represented as a point on the unit sphere with spherical coordinates θ and ϕ. The corresponding vector $(\sin\theta\cos\phi, \sin\theta\sin\phi, \cos\theta)$ is called *Bloch vector*. The Bloch sphere description holds for the states of any two-level quantum system. However, there is not known an easy generalization of the Bloch sphere having the same simple geometrical representation for systems with more than two, say d, levels, such as for multiple qubits (qudits). If we consider a system where the qubit is represented by a single spin $\frac{1}{2}$, then $|0\rangle$ and $|1\rangle$ correspond to the two possible states of a spin $\frac{1}{2}$, namely to spin up and spin down, respectively.

The Bloch sphere picture can be generalized to mixed states. A mixed state is described by a density matrix which is a Hermitian, positive-semidefinite matrix of unit trace. The state space of a qubit which contains all possible density matrices is a subset of all Hermitian operators with a trace equal to one. The set of all Hermitian operators form a real vector space on which a scalar product (Hilbert-Schmidt inner product) between two elements A and B of the space is defined by $\langle A, B \rangle = \text{tr}(AB)$. A standard choice for a basis of this vector space is the set of the Pauli matrices, i.e. $\{\sigma_0, \sigma_x, \sigma_y, \sigma_z\} = \{\mathbb{1}, \vec{\sigma}\}$. This set represents an operator basis for a single qubit. We state that except $\mathbb{1}$ all other basis operators are traceless. Hence, an arbitrary density matrix, which has a unit trace as we know, describing a qubit in a mixed state may be written in the Bloch sphere representation as

$$\rho = \frac{\mathbb{1} + \vec{r} \cdot \vec{\sigma}}{2}, \qquad (2.3.3)$$

where $\vec{r}$ is the generalized Bloch vector for the state ρ, which is a real three-dimensional vector with $|\vec{r}| \leq 1$.

2.4 Unitary operators and quantum gates

We briefly review an important postulate of quantum mechanics:

Postulate 2.2. *[3] The evolution of a closed quantum system is described by a unitary transformation. That is, the state $|\psi\rangle$ of the system at time t_0 is related to its state at time t_f by a unitary time evolution operator U which depends only on the times t_0 and t_f,*

$$|\psi(t_f)\rangle = U(t_f, t_0) |\psi(t_0)\rangle . \tag{2.4.1}$$

Closed in this context means that the considered system is not interacting with other systems. All real systems interact at least somewhat with the environment, but there are interesting systems which can be approximated well by unitary evolution. The unitary property of the time evolution operator ensures that the norm of the state $|\psi\rangle$ on which it acts is let invariant. The norm is given by $\sqrt{\langle\psi|\psi\rangle}$ and it is not affected by unitary transformations since unitary operators preserve the inner product $\langle\cdot,\cdot\rangle$ between states. To see this, we consider two states $|\psi\rangle$ and $|\phi\rangle$. The inner product of $U|\psi\rangle$ and $U|\phi\rangle$ is the same as the inner product of $|\psi\rangle$ and $|\phi\rangle$,

$$\langle\psi|U^\dagger U|\phi\rangle = \langle\psi|\phi\rangle . \tag{2.4.2}$$

Postulate 2.3. *[3] The time evolution of the state of a closed quantum system is described by the Schrödinger equation,*

$$i\hbar\frac{d|\psi\rangle}{dt} = H|\psi\rangle . \tag{2.4.3}$$

It is common in practice to absorb the *Planck's constant* $\hbar$ into the Hamiltonian of the system H by effectively setting $\hbar = 1$.

Considering a quantum control system, it is important to note that the quantum computer interacts with some external control and is hence turned into an *open* quantum system which is affected by noise. The dynamics of an open system, i.e. of the system of interest, called *principal system*, interacting with an *environment*, is described by a general quantum operation ε. Suppose the system is initially in state ρ, then its final state is $\varepsilon(\rho)$ which is not necessarily related by a unitary transformation to the initial state. If no measurement is included into the process, then the quantum operation ε has to be trace-preserving, since it maps density operators to density operators which all fulfill $\mathrm{tr}(\varepsilon(\rho)) = 1$. The principal system and the environment form together a closed quantum system whose evolution is a unitary transformation.

Quantum computing: Gates

Quantum (logic) gates are part of a quantum computer circuit. They operate on a certain number of qubits. That is, they manipulate the information which is contained in the states of the qubits and convert it to other forms. As it follows from Postulate 2.2, quantum gates act as unitary transformations on the states of the considered N-qubit system. The action is hence *linear* which means that the transformation of an arbitrary state is entirely determined by the transformations of the basis states for a given basis of the corresponding state space (Hilbert space). Assume that we consider a two-dimensional single-qubit system for which the states $|0\rangle$ and $|1\rangle$ form an orthonormal basis and let act a certain quantum gate U on an arbitrary state $|\psi\rangle = \alpha|0\rangle + \beta|1\rangle$. Due to the linearity we obtain the transformed state as

$$U|\psi\rangle = \alpha U|0\rangle + \beta U|1\rangle . \tag{2.4.4}$$

Since quantum gates are linear unitary operators, they can be represented by unitary matrices. Gates which act on N qubits are described by $2^N \times 2^N$ unitary matrices. In this work all matrix representations of quantum gates are given in the computational basis even if not explicitly mentioned. We note that the unitary property is the only constraint on quantum gates which means that every unitary matrix specifies a valid quantum gate. In contrast to classical gates

quantum gates are *always* reversible (invertible) because they are unitary. Due to the unitarity, the inverse of a matrix representing a quantum gate is its complex conjugate transpose (adjoint) and hence also a unitary matrix. In particular, if a gate is Hermitian in addition, for instance one described by a real symmetric matrix, then the gate is equal to its inverse.

We have seen that pure states $|\psi\rangle$ evolve under unitary transformations as $|\psi\rangle \to U|\psi\rangle$. In order to generalize the case of pure states to mixed states, we have to use the density operator formalism. An arbitrary density operator ρ which describes a system in a mixed state transforms under unitary evolution as

$$\rho \to U\rho U^\dagger. \tag{2.4.5}$$

An important task in quantum control is to achieve some given quantum gate, the target unitary, by controlling the dynamic time evolution operator. For this purpose a time-dependent control field is applied to the system. The goal is to find a control field which leads to a maximal fidelity between target unitary and the dynamic time evolution of the system. In the following we consider a few interesting single- and multiple-qubit gates whereof some will be relevant in this work.

2.4.1 Single-qubit operations

Operations on a single qubit are represented by 2×2 unitary matrices. Among these, the most important are the Pauli matrices:

$$X = \begin{pmatrix} 0 & 1 \\ 1 & 0 \end{pmatrix}, \qquad Y = \begin{pmatrix} 0 & -i \\ i & 0 \end{pmatrix}, \qquad Z = \begin{pmatrix} 1 & 0 \\ 0 & -1 \end{pmatrix}. \tag{2.4.6}$$

The X matrix is often called the quantum NOT gate, analogously to the classical NOT gate, and sometimes as well referred to as the *bit-flip* matrix since it takes $|0\rangle$ to $|1\rangle$ and $|1\rangle$ to $|0\rangle$. On the other hand, the Z matrix is sometimes called *phase-flip* matrix. It leaves $|0\rangle$ invariant and transforms $|1\rangle$ to $-|1\rangle$ where the added factor of -1 is known as a relative *phase factor*.

Other interesting single-qubit gates are the Hadamard gate (denoted H), phase gate (denoted S) and $\frac{\pi}{8}$ gate (denoted T):

$$H = \frac{1}{\sqrt{2}} \begin{pmatrix} 1 & 1 \\ 1 & -1 \end{pmatrix}, \qquad S = \begin{pmatrix} 1 & 0 \\ 0 & i \end{pmatrix}, \qquad T = \begin{pmatrix} 1 & 0 \\ 0 & e^{i\frac{\pi}{4}} \end{pmatrix}. \tag{2.4.7}$$

We will explain in Section 2.4.3 the universal property of these three gates. The following two algebraic relations between them are worth to be kept in mind:

$$H = (X + Z)/\sqrt{2} \quad \text{and} \quad S = T^2, \tag{2.4.8}$$

as well as the observation that the $\frac{\pi}{8}$ gate is the square root of the phase gate which itself is the square root of the Z gate due to the relation $e^{i\frac{\pi}{4}} = \sqrt{i} = \sqrt{\sqrt{-1}}$. If we use the Bloch sphere picture, we can visualize the single-qubit gates as compositions of rotations and reflections of the sphere. The Pauli matrices generate the *rotation operators* about the x, y and z axes:

$$R_x(\theta) \equiv e^{-i\theta X/2} = \cos\frac{\theta}{2}\mathbb{1} - i\sin\frac{\theta}{2}X = \begin{pmatrix} \cos\frac{\theta}{2} & -i\sin\frac{\theta}{2} \\ -i\sin\frac{\theta}{2} & \cos\frac{\theta}{2} \end{pmatrix}, \tag{2.4.9}$$

$$R_y(\theta) \equiv e^{-i\theta Y/2} = \cos\frac{\theta}{2}\mathbb{1} - i\sin\frac{\theta}{2}Y = \begin{pmatrix} \cos\frac{\theta}{2} & -\sin\frac{\theta}{2} \\ \sin\frac{\theta}{2} & \cos\frac{\theta}{2} \end{pmatrix}, \tag{2.4.10}$$

$$R_z(\theta) \equiv e^{-i\theta Z/2} = \cos\frac{\theta}{2}\mathbb{1} - i\sin\frac{\theta}{2}Z = \begin{pmatrix} e^{-i\theta/2} & 0 \\ 0 & e^{i\theta/2} \end{pmatrix}. \tag{2.4.11}$$

2.4.2 Multiple-qubit operations

Two and more qubit gates may provide entanglement of states. Therefore we first define the property of gates which are said to be entangling. The definition of a 2-qubit entangling gate is given as follows:

Definition 2.4. *[4] A 2-qubit gate is said to be an entangling gate if for some input product state $|\psi\rangle\,|\phi\rangle$ the output of the gate is not a product state (i.e. the output qubits are entangled).*

One of the most useful type of multi-qubit quantum logic gates is the *controlled operation* which corresponds to the logical statement 'if A is true, then do B'. The prototypical controlled operation is the 2-qubit controlled-NOT or CNOT gate which is the most commonly encountered 2-qubit gate. This quantum gate has two input qubits which are called *control* and *target* qubit, respectively. The action of the CNOT gate on a 2-qubit state $|c\rangle\,|t\rangle$ may be summarized as follows: If the control qubit $|c\rangle$ is set to $|1\rangle$, then the NOT gate acts on the target qubit $|t\rangle$ and flips it, otherwise the target qubit is left invariant. In the matrix representation the CNOT gate is given by

$$\mathrm{CNOT} = \begin{pmatrix} 1 & 0 & 0 & 0 \\ 0 & 1 & 0 & 0 \\ 0 & 0 & 0 & 1 \\ 0 & 0 & 1 & 0 \end{pmatrix}. \tag{2.4.12}$$

The CNOT gate is an entangling gate, that is, this gate leads to a correlation between target and control qubit. Its action may be expressed as $|c\rangle\,|t\rangle \to |c\rangle\,|t \oplus c\rangle$ where $\oplus$ stands for addition modulo two. We can interpret the CNOT gate as a generalization of the classical XOR gate if we consider the control and target qubit as the input of the XOR whose output is stored in the target qubit.

There exist many possible controlled gates. Any 2-qubit controlled-unitary operation can be constructed in the same manner as the controlled-NOT according to the following rule: If the control qubit is set to $|1\rangle$ then the unitary operator U, being a single-qubit gate, is applied to the target qubit otherwise the identity. In the case of the CNOT gate the unitary in question is the NOT gate. In principle any single-qubit gate can be used to construct a controlled-unitary gate. Beside the controlled-NOT gate one often encounters the controlled-Z (CZ) and the controlled-phase (CS) gate. These two gates are like the CNOT gate entangling gates and represented for their action on 2-qubit states $|c\rangle\,|t\rangle$ by the unitary matrices

$$\mathrm{CZ} = \begin{pmatrix} 1 & 0 & 0 & 0 \\ 0 & 1 & 0 & 0 \\ 0 & 0 & 1 & 0 \\ 0 & 0 & 0 & -1 \end{pmatrix}, \tag{2.4.13}$$

and

$$\mathrm{CS} = \begin{pmatrix} 1 & 0 & 0 & 0 \\ 0 & 1 & 0 & 0 \\ 0 & 0 & 1 & 0 \\ 0 & 0 & 0 & i \end{pmatrix}. \tag{2.4.14}$$

So far we have treated controlled gates which perform conditioning on a single control qubit. Extensions are controlled gates which condition on multiple, say n, control qubits and perform a k-qubit unitary operation on the k target gates if all n control qubits are equal to 1. One example of multiple-qubit conditioning is the *Toffoli gate* which is a controlled operation with three inputs; two control qubits $|c_1\rangle$ and $|c_2\rangle$ and one target qubit $|t\rangle$. If both control qubits are set to 1, the target qubit is flipped otherwise it is left alone: $|c_1\rangle\,|c_2\rangle\,|t\rangle \to |c_1\rangle\,|c_2\rangle\,|t \oplus c_1 c_2\rangle$. The Toffoli gate in its matrix representation:

$$\text{Toffoli} = \begin{pmatrix} 1 & 0 & 0 & 0 & 0 & 0 & 0 & 0 \\ 0 & 1 & 0 & 0 & 0 & 0 & 0 & 0 \\ 0 & 0 & 1 & 0 & 0 & 0 & 0 & 0 \\ 0 & 0 & 0 & 1 & 0 & 0 & 0 & 0 \\ 0 & 0 & 0 & 0 & 1 & 0 & 0 & 0 \\ 0 & 0 & 0 & 0 & 0 & 1 & 0 & 0 \\ 0 & 0 & 0 & 0 & 0 & 0 & 0 & 1 \\ 0 & 0 & 0 & 0 & 0 & 0 & 1 & 0 \end{pmatrix}. \tag{2.4.15}$$

The reversible quantum Toffoli gate allows to simulate the irreversible classical gates NAND and FANOUT. With these two gates any classical gate can be performed. Hence, quantum computers can perform any computation doable by a classical computer.

A further example of a multiple-qubit gate, not a controlled one, is the 2-qubit SWAP gate which exchanges the state of the first qubit to the second qubit, and vice versa. It is described by the matrix

$$\text{SWAP} = \begin{pmatrix} 1 & 0 & 0 & 0 \\ 0 & 0 & 1 & 0 \\ 0 & 1 & 0 & 0 \\ 0 & 0 & 0 & 1 \end{pmatrix}. \tag{2.4.16}$$

More useful than the ordinary SWAP gate is the 2-qubit quantum gate obtained by taken the 'square root' of SWAP which we will denote $\sqrt{\text{SWAP}}$. In contrast to the SWAP operation the $\sqrt{\text{SWAP}}$ acts as an entangling gate and it is represented by the matrix

$$\sqrt{\text{SWAP}} = \begin{pmatrix} 1 & 0 & 0 & 0 \\ 0 & \frac{1}{2}(1+i) & \frac{1}{2}(1-i) & 0 \\ 0 & \frac{1}{2}(1-i) & \frac{1}{2}(1+i) & 0 \\ 0 & 0 & 0 & 1 \end{pmatrix} \quad \text{with} \quad \frac{1}{2}(1+i) = \frac{1}{\sqrt{2}}e^{i\frac{\pi}{4}}. \tag{2.4.17}$$

Since the matrix representing the SWAP gate is diagonalizable, the matrix describing the 'square root' of SWAP can be derived by calculating $\sqrt{\text{SWAP}} = P^{-1}D^{1/2}P$ where D is a diagonal matrix with the eigenvalues of the SWAP operator on its diagonal. We can choose P^{-1} to be the matrix with the eigenstates of the SWAP gate as columns. The square root of D is formed by taking the square root of all the entries on the diagonal. We can imagine the action of the $\sqrt{\text{SWAP}}$ gate as swapping the states of the two qubits but stopping midway, a classical impossibility. The 'square root' of SWAP may hence be obtained by pulsing the SWAP operation for just half the duration. Most commonly the $\sqrt{\text{SWAP}}$ operation is realized by a Heisenberg interaction like $H = J(t)\vec{S}_1 \cdot \vec{S}_2$ by switching the time-dependent coupling constant $J(t)$ between the spins $\vec{S}_1 = \frac{1}{2}\vec{\sigma}_1$ and $\vec{S}_2 = \frac{1}{2}\vec{\sigma}_2$, where $\vec{\sigma}_i$ with $i = 1, 2$ denotes the spin Pauli vector and $\hbar$ is set equal to 1. Then we may write

$$\sqrt{\text{SWAP}} = e^{i\frac{\pi}{8}} \cdot e^{-i\frac{\pi}{2}\vec{S}_1\vec{S}_2} = e^{i\frac{\pi}{8}} \cdot e^{-i\frac{\pi}{8}\vec{\sigma}_1\vec{\sigma}_2}. \tag{2.4.18}$$

2.4.3 Universality of quantum gates

Here we point out an essential theorem concerning the universality of quantum gates which reveals the importance of entangling gates. According to [4] a universal set of gates is defined as follows:

Definition 2.5. *[4] A set of gates is said to be universal if for any integer $n \geq 1$, any n-qubit unitary operator can be approximated to arbitrary accuracy by a quantum circuit using only gates from that set.*

Definition 2.6. *[4] A set of gates is said to be universal for 1-qubit gates if any 1-qubit unitary gate can be approximated to arbitrary accuracy by a quantum circuit using only gates from that set.*

The following theorem explains why the entangling gates such as the CNOT or $\sqrt{\text{SWAP}}$ gates are useful:

Theorem 2.7. *[4] A set composed of an arbitrary entangling 2-qubit gate acting on any pair of qubits, together with all 1-qubit gates operating on every qubit, is universal for n-qubit operations for any integer $n \geq 1$.*

Using a set as described by Theorem 2.7, any n-qubit unitary can be implemented *exactly* which means that such a set is universal in a stronger sense than required by Definition 2.5. A set composed of a 2-qubit entangling gate and all 1-qubit gates is in general *infinite*. A *finite* universal set of quantum gates can be found by looking for a finite set of 1-qubit gates which is universal for 1-qubit operations. In Ref. [3] such a set is provided by the Hadamard, phase and $\frac{\pi}{8}$ gates. Therefore we can conclude that any unitary operator can be approximated to arbitrary accuracy using Hadamard, phase and $\frac{\pi}{8}$ gates as well as one 2-qubit entangling gate.

2.4.4 Average gate fidelity

An important task in quantum computation and quantum information is to determine the quality of quantum gates. A simple formula for the average fidelity of a noisy quantum gate is developed by Nielsen [5]. The final formula which he derives is given by

$$\bar{F}(\varepsilon, U) = \frac{\sum_j \text{tr} \left(U U_j^\dagger U^\dagger \varepsilon(U_j) \right) + d^2}{d^2(d+1)}, \tag{2.4.19}$$

where ε represents a trace-preserving quantum operation. Nielsen assumes that ε acts on a qudit which means on a d-dimensional quantum system, with d finite. The average gate fidelity $\bar{F}(\varepsilon, U)$ quantifies how well ε approximates a certain quantum gate U. If ε implements U perfectly, we obtain $\bar{F}(\varepsilon, U) = 1$, otherwise the value for $\bar{F}(\varepsilon, U)$ is lower and the implementation noisy. The set of unitary operators $U_j/\sqrt{d}$ forms an orthonormal unitary operator basis for a qudit (i.e. for the complex vector space $\mathbb{C}^{d \times d}$): $\text{tr}(U_j^\dagger U_k) = \delta_{jk} d$.

Within the scope of quantum computation, quantum operations are commonly called quantum channels. In the derivation of formula (2.4.19) Nielsen starts from the integral expression for the average fidelity of a quantum channel

$$\bar{F}(\varepsilon) = \int d\psi \, \langle \psi | \varepsilon(\rho) | \psi \rangle, \tag{2.4.20}$$

which quantifies how well ε preserves quantum information. The integral is over the uniform Haar measure $d\psi$ on the space of pure states $|\psi\rangle$ and ρ denotes the density matrix $|\psi\rangle \langle \psi|$. The Haar measure is normalized such that $\int d\psi = 1$ which ensures that it can be interpreted as a probability measure and it is invariant under arbitrary unitary transformations, i.e. $d\psi = d\psi'$ if $|\psi'\rangle = U |\psi\rangle$ for any unitary U. According to (2.4.20), the average gate fidelity $\bar{F}(\varepsilon, U)$ may be written as

$$\bar{F}(\varepsilon, U) = \int d\psi \, \langle \psi | U^\dagger \varepsilon(\rho) U | \psi \rangle. \tag{2.4.21}$$

The uniform Haar measure defines a measure for uniformly distributed random quantum states. Since each (pure) quantum state may be produced by operating unitarily on a fixed reference state, the Haar measure also provides a measure for uniformly generated random unitary operators. We point out that the application of Nielsen's formula (2.4.19) requires a uniform starting distribution of states and operators, respectively.

Bagan *et al.* [6] have derived a general expression for $\bar{F}$ in terms of the $SU(d)$ group generators which is equivalent to Eq. (2.4.19). Due to the invariance of $d\psi$ the relation $\bar{F}(\varepsilon, U) = \bar{F}(\varepsilon', \mathbb{1}) = \bar{F}(\varepsilon')$, where $\varepsilon'(\rho) = \varepsilon(U^\dagger \rho U)$, is fulfilled. Without any loss of generality it is hence

sufficient to only consider the simpler form $\bar{F}(\varepsilon)$ as done in [6]. We note that all (locally) compact Lie groups, thus in particular $SU(d)$ and as well $U(d)$, carry a Haar measure. Hence, the integral over the measure $d\psi$ (2.4.20) may be rewritten as an integral over dU which is the Haar measure of $SU(d)$ normalized such that $\int dU = 1$. Using the Haar measure of $SU(d)$ Bagan *et al.* obtain the following formula for the average gate fidelity:

$$\bar{F}(\varepsilon) = \frac{1}{d} + \frac{2}{d(d+1)} \sum_{j=1}^{d^2-1} \text{tr}\left(T_j \varepsilon(T_j)\right), \tag{2.4.22}$$

where $\{T_j\}$ are the Hermitian and traceless generators of $SU(d)$ with the normalization $\text{tr}(T_j T_k) = \delta_{jk}/2$. We give additionally the expression for the average gate fidelity $\bar{F}(\varepsilon, U)$ which is straightforward derived as

$$\bar{F}(\varepsilon, U) = \frac{1}{d} + \frac{2}{d(d+1)} \sum_{j=1}^{d^2-1} \text{tr}\left(U T_j U^\dagger \varepsilon(T_j)\right), \tag{2.4.23}$$

and which is equivalent to formula (2.4.19). We note that, if the quantum operation ε implements the gate U perfectly, its mapping is given by

$$\varepsilon : \rho \to \varepsilon(\rho) = U \rho U^\dagger \quad \forall \rho. \tag{2.4.24}$$

Inserting this map into Eqs. (2.4.19) and (2.4.23), we obtain in both cases $\bar{F}(\varepsilon, U) = 1$ as expected. If the implementation is noisy a value between 0 and 1 will be returned and the quantum map ε may be interpreted as a characterization of the noise.

3 Controllability and Lie algebras

In this work we are concerned with finite dimensional quantum control systems, say of dimension n with an associated n-dimensional complex Hilbert space $\mathcal{H}$. The dynamics of the system, assumed to be closed, is described by the Schrödinger equation, given here both for the controlled time evolution of the state and of the unitary by setting $\hbar = 1$:

$$\frac{\partial}{\partial t} |\psi(t)\rangle = -iH(u(t)) |\psi(t)\rangle, \tag{3.0.25}$$

$$\dot{U}(t) = -iH(u(t))U(t), \quad U(0) = \mathbb{1}. \tag{3.0.26}$$

We note that the Hamiltonian of the system $H(u)$ depends on some time-dependent functions, denoted $u(t)$, which represent the *controls* of the system and are chosen in an appropriate set of functions $\bar{\mathcal{U}}$. For every value of u the Hamiltonian is required to be Hermitian. The control of the system may often be realized by a set of control functions $u_k(t) \in \mathbb{R}$ which are coupled to the system via time-independent Hermitian interaction Hamiltonians H_k ($k = 1, 2, ..., m$). The Heisenberg spin-$\frac{1}{2}$ chain which will be considered in this work belongs to this class. The total Hamiltonian associated with such a quantum control system has then the form

$$H(t) = H_0 + \sum_{k=1}^{m} u_k(t) H_k, \tag{3.0.27}$$

where H_0 describes the free evolution of the system. Using this Hamiltonian, the controlled evolution of the state $|\psi(t)\rangle$ is determined by

$$\frac{\partial}{\partial t} |\psi(t)\rangle = -i[H_0 + \sum_{k=1}^{m} u_k(t) H_k] |\psi(t)\rangle, \tag{3.0.28}$$

and the time evolution of the unitary operator by

$$\dot{U}(t) = -i[H_0 + \sum_k u_k(t)H_k]U(t), \quad U(0) = \mathbb{1}. \qquad (3.0.29)$$

We note that $-iH(u)$, $-iH_0$, and $-iH_k$ are skew-Hermitian matrices. Since we will work with unitaries rather than with states, we formulate the quantum control problem in terms of operators. The goal of a typical quantum control problem is to find a final time $t_f > 0$ and controls $u_k(t) \in \mathbb{R}$ which drive the time evolution operator $U(t)$ from $U(0) = \mathbb{1}$ at $t_0 = 0$ into a desired target unitary $U(t_f)$ at t_f.

The set of unitary matrices $\mathcal{R}$ that can be obtained by changing the control for the quantum control system in consideration, i.e. the reachable set of states for this system, is always a subset of the Lie group of unitary matrices of dimension n, $U(n)$, with n being the dimension of $\mathcal{H}$ [2]. The reachable set $\mathcal{R}$ is a Lie group as will be stated in Section 3.2. If the set of possible matrices that can be reached is equal to $U(n)$ or $SU(n)$ (we remember that global phases are irrelevant in quantum mechanics and that any element of $U(n)$ may be expressed as the product of an element of $SU(n)$ and a phase), the system is said to be controllable. In order to describe the reachable set of the system, we refer throughout this work to the case where the controls are assumed to belong to the set of piecewise constant functions with values in a set $\mathcal{U}$. It is even sufficient to take $\mathcal{U} = \{0, 1\}$. This choice allows to switch the control on and off and leads to the same reachable set as in any other case where $\mathcal{U}$ contains at least two or more different elements.

Operator controllability, also called complete controllability, of a quantum control system guarantees the existence of controls to achieve any desired target unitary:

Definition 3.1. *[7] The quantum control system 3.0.26 and the special case 3.0.29 are operator controllable if there exist control functions $u(t)$ or $u_k(t)$ which drive the unitary operator $U(t)$ from $\mathbb{1}$ (at $t_0 = 0$) to U_{target} (at t_f), for any $U_{target} \in U(n)$ (or $SU(n)$).*

3.1 Lie Algebras and Lie groups

Lie algebras and Lie groups give information about the controllability of quantum control systems. For this reason we present a brief survey of Lie algebra and Lie group theory borrowed from [2]. We have collected facts which are relevant for this work. More detailed discussion is found in [2].

Lie algebras:

We will work with Lie algebras of matrices which are called *linear Lie algebras*. The Lie bracket of these Lie algebras is the standard matrix commutator. The Lie algebra of all the $n \times n$ matrices with real (complex) entries is denoted by $gl(n, \mathbb{R})$ $(gl(n, \mathbb{C}))$ and called the *general linear Lie algebra* over the real (complex) numbers.

Subalgebras:

All subalgebras of $gl(n, \mathbb{R})$ $(gl(n, \mathbb{C}))$ are called *linear Lie algebras*. A few examples of subalgebras of $gl(n, \mathbb{R})$:

- $sl(n, \mathbb{R})$ (or $sl(n)$): *special linear Lie algebra*
  Lie algebra of $n \times n$ real matrices with trace equal to zero.

- $o(n, \mathbb{R})$ (or $o(n)$): *orthogonal Lie algebra*
  Lie algebra of $n \times n$ real skew-symmetric matrices A, i.e. $A^T = -A$.

- $so(n, \mathbb{R})$ (or $so(n)$): *special orthogonal Lie algebra*
  Lie algebra of $n \times n$ real skew-symmetric matrices with trace equal to zero.

- **$u(n)$: unitary Lie algebra**
  Lie algebra of $n \times n$ complex skew-Hermitian matrices A, i.e. $A^\dagger = -A$. We note that this Lie algebra is considered as a Lie algebra over the real field, not over the complex field. In particular, all matrices $-iH$ with H being Hermitian are contained in $u(n)$.

- **$su(n)$: special unitary Lie algebra**
  Lie algebra of $n \times n$ complex skew-Hermitian matrices with trace equal to zero. Again, we point out that this is a Lie algebra over the real field. In particular, all matrices $-iH$ with H being Hermitian and traceless are contained in $su(n)$.

The Lie algebras $u(n)$ and $su(n)$ are marked bold since they represent the relevant Lie algebras in quantum control theory.

Lie algebra generated by a set of elements:

Let $\{x_1, ..., x_m\}$ be a set of elements of a Lie algebra $\mathcal{L}$. Then a subalgebra of $\mathcal{L}$ is spanned by the set of all (repeated) commutators of $\{x_1, ..., x_m\}$. Such a subalgebra is called the Lie algebra generated by $\{x_1, ..., x_m\}$. It is the smallest subalgebra of $\mathcal{L}$ containing $\{x_1, ..., x_m\}$ and we will denote it by $\{x_1, ..., x_m\}_{\mathcal{L}}$. In general, we define as the generators of a Lie algebra the set of elements which allows us to construct a basis for the considered Lie algebra containing only the generators and some of its repeated commutators.

Bases for specific Lie algebras:

- $su(2)$:
  Spanned by skew-Hermitian traceless matrices. A basis is for instance provided by the set $\{iX, iY, iZ\}$ with X, Y and Z being the Pauli matrices. We state that $su(2)$ is generated by the set $\{iX, iY\}$ since the commutator of iX and iY is linearly dependent on iZ.

- $u(2)$:
  Spanned by the above given basis for $su(2)$, containing additionally the unit matrix which is not traceless.

- $su(3)$:
  Spanned by skew-Hermitian traceless matrices. A basis is for instance provided by the set $\{i\lambda_k\}_{k=1}^{8}$, where the λ_k's are the Gell-Mann matrices.

- $u(3)$:
  Spanned by the above given basis for $su(3)$, containing additionally the unit matrix which is not traceless.

Lie groups and their subgroups:

A real (complex) Lie group is a group which is additionally a real (complex) analytic differentiable manifold such that the group operations of multiplication (group composition) and inversion are analytic maps, i.e. the mapping $(x, y) \mapsto x^{-1}y$ has to be a smooth mapping of the product manifold into the group. The dimension of the Lie group is the dimension of the underlying manifold. If the dimension of the manifold is finite, the manifold is automatically analytic as well as the group operations of multiplication and inversion. Therefore Lie groups are finite-dimensional by definition.

Examples of Lie groups:

An example of a Lie group is the *general linear group*, $Gl(n, \mathbb{C})$, which is the group of $n \times n$ nonsingular (invertible) matrices having complex entries. The matrix multiplication is the group composition. All subgroups of $Gl(n, \mathbb{C})$, as for instance the unitary group $U(n)$ or the special unitary group $SU(n)$ which are the relevant ones for quantum systems, are Lie groups as well. We note that the matrix multiplication and inversion only require analytic operations.

Correspondence between Lie groups and Lie algebras:

The Lie algebra associated to a Lie group of matrices is isomorphic (in the sense of vector spaces) to the space of tangent vectors of the Lie group at the identity. The matrices obtained by differentiating curves in the Lie group at the identity at time $t = 0$ generate the corresponding Lie algebra. In particular, the dimension of the Lie algebra is equal to the one of the tangent space which itself has the dimension of the Lie group seen as an analytic manifold.

Exponential map:

The unique connected Lie subgroup of $Gl(n, \mathbb{R})$ ($Gl(n, \mathbb{C})$), which corresponds to a Lie algebra of matrices $\mathcal{L}$, is generated by the associated one-dimensional (one-parameter) subgroups:

$$e^{\mathcal{L}} := \{e^{A_1} e^{A_2} \cdots e^{A_m}, \quad A_1, A_2, ..., A_m \in \mathcal{L}\}. \tag{3.1.1}$$

The map from the Lie algebra $\mathcal{L}$ to the corresponding Lie group $e^{\mathcal{L}}$ with $A \in \mathcal{L}$, $e^A \in e^{\mathcal{L}}$ where e^A is defined by the usual power series is called exponential map. This definition does not hold for Lie groups which are not matrix groups. In such cases a more abstract definition should be used.

3.2 Controllability test: The dynamical Lie algebra

In this section we explain how Lie algebra and Lie group techniques provide information about the controllability of quantum systems. At first we point to the theorem which states that the reachable set $\mathcal{R}$ of a quantum control system can be identified with a connected Lie group:

Theorem 3.2. *[2] The set of reachable states $\mathcal{R}$ of a general quantum control system such as described by Eq. (3.0.26) is the connected Lie group associated with the Lie algebra $\mathcal{L}_0$ generated by $\mathrm{span}_{u \in \mathcal{U}}\{-iH(u)\}$. For the special system described by Eq. (3.0.29) $\mathcal{R}$ is the connected Lie group associated with the Lie algebra $\mathcal{L}_0$ generated by $\{-iH_0, -iH_1, ..., -iH_m\}$. In short: $\mathcal{R} = e^{\mathcal{L}_0}$.*

We mention that Theorem 3.2, which tests the controllability of a quantum system, is known as the *Lie Algebra Rank Condition* and proved in any detail in [2]. From Theorem 3.2 there may directly be derived the following criterion for operator controllability, i.e. for complete controllability:

Theorem 3.3. *[7] The quantum systems (3.0.26) and (3.0.29) are operator controllable if and only if $\mathcal{L}_0 = u(n)$ (or $\mathcal{L}_0 = su(n)$), where $\mathcal{L}_0$ is the Lie algebra generated by $\mathrm{span}_{u \in \mathcal{U}}\{-iH(u)\}$ and $\{-iH_0, -iH_1, ..., -iH_m\}$, respectively.*

We call the Lie algebra $\mathcal{L}_0$ the dynamical Lie algebra associated with the considered quantum system and note that it is always a subalgebra of $u(n)$. Theorems 3.2 and 3.3 both state that the system is operator controllable (complete controllable) if $\dim(\mathcal{L}_0) = n^2 = \dim(u(n))$, i.e $\mathcal{L}_0 = u(n)$ and $e^{\mathcal{L}_0} = U(n)$. The system is even called controllable in the case where $\dim(\mathcal{L}_0) = n^2 - 1 = \dim(su(n))$, i.e. $\mathcal{L}_0 = su(n)$ and $e^{\mathcal{L}_0} = SU(n)$, since global phases are irrelevant in quantum mechanics. We conclude that every system whose dynamical Lie algebra $\mathcal{L}_0$ is generated by matrices with trace equal to zero is controllable if $\mathcal{L}_0 = su(n)$. The set of elements which generate the Lie algebra is in the case of complete controllability called universal. If the system is controllable, every unitary matrix can be obtained by choosing an appropriate set of control functions.

Procedure to construct a basis of $\mathcal{L}_0$:

An algorithm to compute a basis in terms of iterated commutators for the dynamical Lie algebra $\mathcal{L}_0$ associated with the system 3.0.29 is described in Table I of Ref. [8]. In order to construct a basis all possible (repeated) commutators of the generators have to be computed.

Uniform finite generation of compact Lie groups:

We point out a corollary which has a significant importance for our further work and is shown within the proof of the controllability test (Theorem 3.2) presented in Ref. [2].

Corollary 3.4. *[2] Consider a connected Lie group $e^{\mathcal{L}}$ corresponding to a Lie algebra $\mathcal{L}$. Then: Every element U in $e^{\mathcal{L}}$ can be written in the form*

$$U = e^{At_r} \cdots e^{At_1}, \tag{3.2.1}$$

with the indeterminates A in the set $S := \{A_1, ..., A_s\}$ of generators of $\mathcal{L}$ and $t_1, ..., t_r \geq 0$. The number r will depend on U.

Assume that $\mathcal{L}$ is the dynamical Lie algebra of a certain quantum control system, then we may conclude that any element of the reachable set of unitaries for this system can be expressed in the form (3.2.1).

Furthermore it can be shown (see e.g. Ref. [9] for a detailed proof) that if the connected Lie group $e^{\mathcal{L}}$ is *compact* then the number r is uniformly bounded and $e^{\mathcal{L}}$ is said to be *uniformly finitely generated*. Uniform boundedness of the number r means that there exists an integer $n > 0$ such that each element of the group $e^{\mathcal{L}}$ can be written as in (3.2.1) with $r \leq n$. Every connected compact Lie group is uniformly finitely generated by any set of generators of the corresponding Lie algebra. Connected and compact Lie groups are for instance $U(n)$ or $SU(n)$.

Switching controls and universality of quantum gates from a Lie algebra perspective:

In the following we point out a physical interpretation, which will turn out to be very important for our purposes, resulting from the uniform finite generation of connected compact Lie groups. We consider a quantum control system and assume that the control allows to switch between the two Hamiltonians H_1 and H_2 of dimension at least two associated with the skew-Hermitian matrices $-iH_1$ and $-iH_2$. These two skew-Hermitian operators represent two possible evolutions, $e^{-iH_1 t}$ and $e^{-iH_2 t}$, of the considered quantum control system. In the language of quantum computation such evolutions are called quantum logic gates. Allowing switching controls means that the experimental set-up must be adjusted in a way so that different evolutions may be induced. Let $\mathcal{L}_0$ be the dynamical Lie algebra generated by $-iH_1$ and $-iH_2$ through commutation. Any unitary $U \in e^{\mathcal{L}_0}$ can be achieved by the described switching set-up and according to (3.2.1) be expressed in the form

$$U = e^L = \cdots e^{-iH_2 t_4} e^{-iH_1 t_3} e^{-iH_2 t_2} e^{-iH_1 t_1}, \quad L \in \mathcal{L}_0. \tag{3.2.2}$$

Definition 3.5. *[2] The set of gates $\{e^{-iH_1 t}, e^{-iH_2 t}\}$ is said to be universal if all (special) unitary evolutions can be achieved by switching between them.*

Corollary 3.4 implies that the set $\{e^{-iH_1 t}, e^{-iH_2 t}\}$ is universal if and only if the skew-Hermitian operators $\{-iH_1, -iH_2\}$ generate the whole Lie algebra $u(n)$ or $su(n)$. We note that in such a case the number r of gates which is needed to generate any (special) unitary evolution is uniformly bounded due to the compactness of the Lie groups $U(n)$ and $SU(n)$. That is, any unitary can be achieved by a finite number of gates.

An approximate result restricted to finite products is derived in Refs. [10] and [11] resulting in the following theorem which modifies the above corollary slightly:

Theorem 3.6. *[11] Let H_1 and H_2 be $n \times n$ Hermitian matrices ($n \geq 2$) and let $\mathcal{L}_0$ be the Lie algebra generated by the set of skew-Hermitian operators $\{-iH_1, -iH_2\}$ through commutation, then for any $L \in \mathcal{L}_0$, the unitary matrix $U = e^{iL}$ can be approximated by finite products of the form (3.2.2), with each t_j positive.*

Almost any quantum logic gate is universal:

We may interpret the Hamiltonian H_1 as the intrinsic Hamiltonian of the quantum control system, inducing the system's free evolution, and the Hamiltonian H_2 as an interaction Hamiltonian due to some external force which is acting as a control and can be applied at will. By turning the control on and off for successive time intervals and various numbers of intervals, any unitary of the form (3.2.2) can be reached. We note that almost every pair of skew-Hermitian matrices (any two operators $-iH_1$ and $-iH_2$) generate the entire Lie algebra $u(n)$. This result is often referred to as the statement that 'almost every quantum logic gate is universal'. In the following we give the theorem which states this universality and is proved and discussed in detail in Ref. [11]:

Theorem 3.7. *[11] For almost all Hermitian $n \times n$ matrices H_1 and H_2 ($n \geq 2$), every unitary $n \times n$ matrix can be exactly represented in the form 3.2.2 with each $t_j > 0$.*

In the whole discussion of this section we have assumed that the time intervals t_j are positive since negative values are from a practical point of view impossible. This restriction leads to an interesting conclusion pointed out in [11]. We might expect that unitaries close to the identity can be achieved or at least approximated in arbitrarily short times. However, Ref. [11] states that this is not the case due to the restriction to positive t_j and that in short times only unitaries which are, roughly speaking, 'on one side' of the identity are reachable.

4 Local operator control of a Heisenberg three-spin chain

4.1 Motivation

In Ref. [1] Burgarth *et al.* give a sufficient criterion for complete controllability of a many-body quantum system by manipulating the (local) Hamiltonian of one of its subsystems. Assume we are considering a network of interacting qubits. Then the question arises how many qubits we have to control for universal quantum computation. Burgarth *et al.* derive how the answer to this question depends on the type of interaction and the connectedness of the network. They state that if the interaction Hamiltonian is general enough, concretely algebraically propagating, then it is sufficient to control the qubits on an infectious subgraph of the system. For more details on algebraically propagating Hamiltonians and infectious subgraphs we refer to [1]. Here we confine ourself to mentioning the main result relevant for our purposes:

Theorem 4.1. *[1] Any Heisenberg spin chain of arbitrary length can be (algebraically) controlled by operating on a single spin at one of its ends.*

Theorem 4.1 holds since the subgraph consisting of a single spin at one end of the chain infects the whole system and since the Heisenberg interaction is algebraically propagating. The latter statement is proved in [1] explicitly for spin $\frac{1}{2}$, but it is true for arbitrary spin because the proof only uses the commutation relations of the spin matrices. We conclude that controlling the first or last spin of a Heisenberg spin chain is enough for complete controllability. This is, what we intend to do in the following: Local control of a Heisenberg spin chain.

4.2 Sketch of the problem

We consider an isotropic Heisenberg spin-$\frac{1}{2}$ chain of length three and apply a control field to the first spin. Operating on the first spin, we tend to implement various target unitaries. For this purpose we control the dynamic time evolution operator $U(t)$. That is, we want to find control fields such that $U(t)$ is driven from the identity at $t_0 = 0$ to respective gates at some final time $t_f > 0$. At first we derive the Hamiltonian of the quantum control system which we just have set-up. The Hilbert space associated with the three-spin chain has 2^3 dimensions. We divide the Hamiltonian of the system into two parts and write

$$H = H_0 + H_c. \tag{4.2.1}$$

The Hamiltonian H_0 describes the system's free evolution and contains the effective spin interaction given by the isotropic Heisenberg nearest-neighbour model

$$
\begin{aligned}
H_0 &= J(\vec{S}_1 \cdot \vec{S}_2 + \vec{S}_2 \cdot \vec{S}_3) \\
&= J(S_{1x}S_{2x} + S_{1y}S_{2y} + S_{1z}S_{2z} + S_{2x}S_{3x} + S_{2y}S_{3y} + S_{2z}S_{3z}),
\end{aligned}
\tag{4.2.2}
$$

where J is the coupling constant between adjacent spins and positive for an antiferromagnetic chain. We set J equal to 1 throughout this work. The spin matrices S_{ij} with $i = 1, 2, 3$ and $j = x, y, z$ are expressed by $S_{ij} = \frac{\hbar}{2}\sigma_{ij}$, where σ_{ij} denote the usual Pauli matrices. The Planck's constant $\hbar$ will be set equal to 1 in all numerical calculations for which reason the units given to the physical quantities have to be understood as natural units. In particular, all times are given in units of $1/J$. The control Hamiltonian H_c is obtained as

$$
H_c = \vec{h}(t) \cdot \vec{S}_1.
\tag{4.2.3}
$$

We assume that the control-field is pointing in x- and y-direction by setting the z-component equal to zero:

$$
\vec{h}(t) = \begin{pmatrix} h_x(t) \\ h_y(t) \\ 0 \end{pmatrix}.
\tag{4.2.4}
$$

Then we may write the control Hamiltonian as

$$
H_c = h_x(t)S_{1x} + h_y(t)S_{1y},
\tag{4.2.5}
$$

and the total Hamiltonian as

$$
H = H_0 + h_x(t)S_{1x} + h_y(t)S_{1y}.
\tag{4.2.6}
$$

In order to enable universal quantum computation, it is sufficient to control the field only in x- and y-direction since S_x and S_y imply S_z in the Lie completion, i.e. $[S_x, S_y] = iS_z$. Applying the control field (4.2.4) to the first spin, the system is complete controllable. That is, any target unitary operator contained in the special unitary group $SU(8)$ is achievable. To prove the complete controllability, we have to show that the dimension of the dynamical Lie algebra $\mathcal{L}_0$ generated by the set of skew-Hermitian and traceless matrices $\{-iH_0, -iS_{1x}, -iS_{1y}\}$ is $d^2 - 1$ with $d = 8$ being the dimension of the Hilbert space, i.e. $\mathcal{L}_0 = su(8)$ (according to Theorems 3.2 and 3.3). To this end we use the algorithm described in Table I of [8] and state that the dimension is indeed $d^2 - 1 = 63$. Therefore the system is complete controllable and the set of generators $\{-iH_0, -iS_{1x}, -iS_{1y}\}$ is called universal.

Using the standard basis $|\sigma_{1z}\sigma_{2z}\sigma_{3z}\rangle = |\sigma_{1z}\rangle \otimes |\sigma_{2z}\rangle \otimes |\sigma_{3z}\rangle$ of the Hilbert space, the full Hamiltonian H is represented by the Hermitian matrix

$$
H = \begin{pmatrix}
\frac{1}{2} & 0 & 0 & 0 & \frac{1}{2}h_- & 0 & 0 & 0 \\
0 & 0 & \frac{1}{2} & 0 & 0 & \frac{1}{2}h_- & 0 & 0 \\
0 & \frac{1}{2} & -\frac{1}{2} & 0 & \frac{1}{2} & 0 & \frac{1}{2}h_- & 0 \\
0 & 0 & 0 & 0 & 0 & \frac{1}{2} & 0 & \frac{1}{2}h_- \\
\frac{1}{2}h_+ & 0 & \frac{1}{2} & 0 & 0 & 0 & 0 & 0 \\
0 & \frac{1}{2}h_+ & 0 & \frac{1}{2} & 0 & -\frac{1}{2} & \frac{1}{2} & 0 \\
0 & 0 & \frac{1}{2}h_+ & 0 & 0 & \frac{1}{2} & 0 & 0 \\
0 & 0 & 0 & \frac{1}{2}h_+ & 0 & 0 & 0 & \frac{1}{2}
\end{pmatrix},
\tag{4.2.7}
$$

where h_+ and h_- denote $h_x(t) + ih_y(t)$ and $h_x(t) - ih_y(t)$, respectively.

In this work we will implement the target unitaries $11X$, $1X1$, $1\mathrm{CNOT}$, and $1\sqrt{\mathrm{SWAP}}$ (recall Sections 2.4.1 and 2.4.2 where we have presented the respective gates). We concentrate mainly on the implementation of $11X$ which effects a flip of the last spin by leaving the other two spins invariant. In the following we list the matrix representations of the mentioned four gates (the identity matrix $\mathbb{1}$ has to be considered as a 2×2 matrix):

1.

$$
11X \equiv \mathbb{1} \otimes \mathbb{1} \otimes X =
\begin{pmatrix}
0 & 1 & 0 & 0 & 0 & 0 & 0 & 0 \\
1 & 0 & 0 & 0 & 0 & 0 & 0 & 0 \\
0 & 0 & 0 & 1 & 0 & 0 & 0 & 0 \\
0 & 0 & 1 & 0 & 0 & 0 & 0 & 0 \\
0 & 0 & 0 & 0 & 0 & 1 & 0 & 0 \\
0 & 0 & 0 & 0 & 1 & 0 & 0 & 0 \\
0 & 0 & 0 & 0 & 0 & 0 & 0 & 1 \\
0 & 0 & 0 & 0 & 0 & 0 & 1 & 0
\end{pmatrix}
\tag{4.2.8}
$$

2.

$$
1X1 \equiv \mathbb{1} \otimes X \otimes \mathbb{1} =
\begin{pmatrix}
0 & 0 & 1 & 0 & 0 & 0 & 0 & 0 \\
0 & 0 & 0 & 1 & 0 & 0 & 0 & 0 \\
1 & 0 & 0 & 0 & 0 & 0 & 0 & 0 \\
0 & 1 & 0 & 0 & 0 & 0 & 0 & 0 \\
0 & 0 & 0 & 0 & 0 & 0 & 1 & 0 \\
0 & 0 & 0 & 0 & 0 & 0 & 0 & 1 \\
0 & 0 & 0 & 0 & 1 & 0 & 0 & 0 \\
0 & 0 & 0 & 0 & 0 & 1 & 0 & 0
\end{pmatrix}
\tag{4.2.9}
$$

3.

$$
1\mathrm{CNOT} \equiv \mathbb{1} \otimes \mathrm{CNOT} =
\begin{pmatrix}
1 & 0 & 0 & 0 & 0 & 0 & 0 & 0 \\
0 & 1 & 0 & 0 & 0 & 0 & 0 & 0 \\
0 & 0 & 0 & 1 & 0 & 0 & 0 & 0 \\
0 & 0 & 1 & 0 & 0 & 0 & 0 & 0 \\
0 & 0 & 0 & 0 & 1 & 0 & 0 & 0 \\
0 & 0 & 0 & 0 & 0 & 1 & 0 & 0 \\
0 & 0 & 0 & 0 & 0 & 0 & 0 & 1 \\
0 & 0 & 0 & 0 & 0 & 0 & 1 & 0
\end{pmatrix}
\tag{4.2.10}
$$

4.

$$
1\sqrt{\mathrm{SWAP}} \equiv \mathbb{1} \otimes \sqrt{\mathrm{SWAP}} =
\begin{pmatrix}
1 & 0 & 0 & 0 & 0 & 0 & 0 & 0 \\
0 & \frac{1}{2}(1+i) & \frac{1}{2}(1-i) & 0 & 0 & 0 & 0 & 0 \\
0 & \frac{1}{2}(1-i) & \frac{1}{2}(1+i) & 0 & 0 & 0 & 0 & 0 \\
0 & 0 & 0 & 1 & 0 & 0 & 0 & 0 \\
0 & 0 & 0 & 0 & 1 & 0 & 0 & 0 \\
0 & 0 & 0 & 0 & 0 & \frac{1}{2}(1+i) & \frac{1}{2}(1-i) & 0 \\
0 & 0 & 0 & 0 & 0 & \frac{1}{2}(1-i) & \frac{1}{2}(1+i) & 0 \\
0 & 0 & 0 & 0 & 0 & 0 & 0 & 1
\end{pmatrix}
\tag{4.2.11}
$$

We notice that the unitaries $11X$ and $1X1$ have a zero trace while the trace of $1\mathrm{CNOT}$ and $1\sqrt{\mathrm{SWAP}}$ does not vanish. Furthermore, the gates $11X$, $1X1$, and $1\mathrm{CNOT}$ are not only unitary but as well Hermitian. They are moreover contained in the special unitary group $SU(8)$ since their determinant is equal to 1 whereas $1\sqrt{\mathrm{SWAP}}$ has a determinant of -1 and is therefore not included in the special unitary group. From a controllability perspective, the issue that the group $SU(8)$ does not contain the gate $1\sqrt{\mathrm{SWAP}}$ is of no further relevance since any unitary of the group $U(8)$ may be achieved as the product of an element of $SU(8)$ and an (irrelevant) phase.

The gate fidelity which quantifies how well the dynamic unitary $U(t)$ approximates the target unitary U_{target} can be calculated as

$$F = \frac{1}{d}|\text{tr}(U^\dagger(t)U_{target})|, \tag{4.2.12}$$

where d indicates the dimension of the Hilbert space. We note that this gate fidelity is trivially related to the average gate fidelity defined in Section 2.4.4 by Eqs. (2.4.19) and (2.4.23). This may be seen directly if we assume for the calculation of the average gate fidelity unitary transformations, thus replacing the general quantum operation ε by a unitary operator U. Pedersen *et al.* [12] derive an expression for the average fidelity of the unitary transformation U as follows,

$$\bar{F} = \frac{1}{d(d+1)}[d + |\text{tr}(U^\dagger U_{target})|^2]. \tag{4.2.13}$$

Hence, $\bar{F}$ and F are related by

$$\bar{F} = \frac{1}{d+1}(1 + dF^2), \tag{4.2.14}$$

and yield both the same physical information.

We are interested in achieving a fidelity which is as high as possible which is why we have to maximize the function for the fidelity defined in Eq. (4.2.12). Before we can turn towards the maximization of the fidelity and its numerical implementation we have to discuss the calculation of the dynamic time evolution $U(t)$. In the next subsection we present two strategies in order to compute the dynamic unitary, one of them can be applied to all targets, the other one can be used only for a certain class of gates. To decide on the way of calculating $U(t)$ means that we simultaneously are determining the pulse shape of the control field. In order to simplify the calculation of the dynamic unitary and to ensure that the theorem of controllability is applicable, we choose the control field as a piecewise constant function varying in time. That is, we discretize the action time of the control field by dividing it into a certain number of time intervals N_t, each of them of length T, and assume that in each time interval the field is constant. In order to maximize the fidelity, we treat the number of time intervals and the length of the intervals as parameters while we leave the amplitude of the field in each interval variable. The field amplitudes are hence our free control parameters over which we will maximize. We will perform the maximization for different sets of parameters, i.e. for different sets $\{N_t, T\}$.

4.3 Calculation of the fidelity

We present two different methods in order to calculate the dynamic unitary $U(t)$. Both of them assume that the pulse shape of the control field is represented by a piecewise constant function.

Procedure A: Switch between control fields in x- and y-direction

Assume that we want to achieve a certain target unitary at a final time t_f. At $t_0 = 0$ we apply a control field to the first spin of the Heisenberg chain and let the system evolve during the time t_f. The control sequence is hence limited by the beginning time t_0 and the final time t_f. We note that the time t_f corresponds to the total evolution time of the system as well as to the action time of the control field. In order to calculate $U(t_f)$, the full dynamic time evolution operator of our quantum control system at t_f, we divide the action time of the control field into a certain number of time intervals N_t of fixed length T. We may interpret N_t as the number of control pulses and T as the duration of each pulse or as the switching time. Furthermore we assume that the control field is applied alternately in x- and y-direction for successive time intervals whereas in each time interval either h_x shall be constant and h_y equal to zero or h_y constant and h_x zero. The evolution time of the system, t_f, is thus equal to the product $N_t T$.

The matrix representation of the Hamiltonians $H_x = H_0 + h_x S_{1x}$ (h_x constant, h_y zero) and $H_y = H_0 + h_y S_{1y}$ (h_y constant, h_x zero) follows directly from Eq. (4.2.7):

$$H_x = \begin{pmatrix} \frac{1}{2} & 0 & 0 & 0 & \frac{h_x(t)}{2} & 0 & 0 & 0 \\ 0 & 0 & \frac{1}{2} & 0 & 0 & \frac{h_x(t)}{2} & 0 & 0 \\ 0 & \frac{1}{2} & -\frac{1}{2} & 0 & \frac{1}{2} & 0 & \frac{h_x(t)}{2} & 0 \\ 0 & 0 & 0 & 0 & 0 & \frac{1}{2} & 0 & \frac{h_x(t)}{2} \\ \frac{h_x(t)}{2} & 0 & \frac{1}{2} & 0 & 0 & 0 & 0 & 0 \\ 0 & \frac{h_x(t)}{2} & 0 & \frac{1}{2} & 0 & -\frac{1}{2} & \frac{1}{2} & 0 \\ 0 & 0 & \frac{h_x(t)}{2} & 0 & 0 & \frac{1}{2} & 0 & 0 \\ 0 & 0 & 0 & \frac{h_x(t)}{2} & 0 & 0 & 0 & \frac{1}{2} \end{pmatrix} \qquad (4.3.1)$$

$$H_y = \begin{pmatrix} \frac{1}{2} & 0 & 0 & 0 & -\frac{ih_y(t)}{2} & 0 & 0 & 0 \\ 0 & 0 & \frac{1}{2} & 0 & 0 & -\frac{ih_y(t)}{2} & 0 & 0 \\ 0 & \frac{1}{2} & -\frac{1}{2} & 0 & \frac{1}{2} & 0 & -\frac{ih_y(t)}{2} & 0 \\ 0 & 0 & 0 & 0 & 0 & \frac{1}{2} & 0 & -\frac{ih_y(t)}{2} \\ \frac{ih_y(t)}{2} & 0 & \frac{1}{2} & 0 & 0 & 0 & 0 & 0 \\ 0 & \frac{ih_y(t)}{2} & 0 & \frac{1}{2} & 0 & -\frac{1}{2} & \frac{1}{2} & 0 \\ 0 & 0 & \frac{ih_y(t)}{2} & 0 & 0 & \frac{1}{2} & 0 & 0 \\ 0 & 0 & 0 & \frac{ih_y(t)}{2} & 0 & 0 & 0 & \frac{1}{2} \end{pmatrix} \qquad (4.3.2)$$

The full time evolution operator $U(t_f)$ is then found as the product of alternately applied matrices $U_x = e^{-iH_x T}$ and $U_y = e^{-iH_y T}$:

$$U(t_f) = \prod_{j=N_t/2}^{1} U_{y,j} U_{x,j} = U_{y,N_t/2} \cdot U_{x,N_t/2} \cdot \ldots \cdot U_{y,1} \cdot U_{x,1}. \qquad (4.3.3)$$

The complex conjugate transpose of $U(t_f)$ is given by

$$U^\dagger(t_f) = (\prod_{j=N_t/2}^{1} U_{y,j} U_{x,j})^\dagger = \prod_{j=1}^{N_t/2} U_{x,j} U_{y,j} = U_{x,1}^\dagger \cdot U_{y,1}^\dagger \cdot \ldots \cdot U_{x,N_t/2}^\dagger \cdot U_{y,N_t/2}^\dagger. \qquad (4.3.4)$$

If we use this method for computing the dynamic unitary, the fidelity depends on N_t variable field amplitudes $h_{x,1},...,h_{x,N_t/2}$, $h_{y,1},...,h_{y,N_t/2}$. These field amplitudes play here the role of the free control parameters over which we will maximize. In order to obtain optimal fidelities, we perform several maximizations with varying number of time intervals and length of these and hence different evolution times. Instead of fixing the pulse duration and maximizing over the field amplitudes we could equivalently fix the amplitudes and treat the pulse timings as free control parameters [13]. We prefer maximizing over the field amplitudes since this method allows to fix the total evolution time and estimate the minimal time which is needed to implement the desired gate.

We note that the controllability test theorems (recall Theorems 3.2 and 3.3) can be applied to the above chosen method for the calculation of the dynamic time evolution operator. This may be verified by recalling the discussion about switching controls in Section 3.2. There we have pointed out that if the set of skew-Hermitian matrices $\{-iH_1, -iH_2\}$ generates the whole Lie algebra $u(n)$ (or $su(n)$), then it is possible to implement all (special) unitary matrices by switching between the two quantum logic gates $e^{-iH_1 t}$ and $e^{-iH_2 t}$. In our particular case we switch between the evolutions U_x and U_y for which reason we have to look at the set $\{-iH_x, -iH_y\}$ with $H_x = H_0 + h_x S_{1x}$ and $H_y = H_0 + h_y S_{1y}$. Since we are allowed to perform scalar multiplications in Lie algebras we may instead consider the set $\{-i(H_0 + S_{1x}), -i(H_0 + S_{1y})\}$. A straightforward

calculation of the dynamical Lie algebra generated by this set using the algorithm provided in Ref. [8] (see Table I) shows that the algebra is equal to $su(n)$. We conclude that switching between e^{-iH_xT} and e^{-iH_yT} is indeed enough to generate any special unitary time evolution.

Procedure B: Control of the field in x-direction only

For the achievement of a certain class of target unitary operators it is sufficient to control only the field in x-direction. To this class belongs the gate $11X$ as can be shown using Lie algebra techniques. The Hamiltonian of the system simplifies in this case to

$$H = H_0 + h_x(t)S_{1x}. \tag{4.3.5}$$

In order to prove that the unitary $11X$ may be reached by controlling only the x-field, we have to calculate a basis for the dynamical Lie algebra $\mathcal{L}_X$ associated with the system (4.3.5). This Lie algebra is generated by the set $\{-iH_0, -iS_{1x}\}$ and it is a subalgebra of $su(8)$. We compute its dimension using the algorithm provided in Table I of [8] and obtain a dimension of 18. If and only if there exists a matrix A contained in this subalgebra such that $U_{target} = e^A$, the desired gate U_{target} belongs to the Lie group associated with $\mathcal{L}_X$ and can therefore be reached. If we add $-i(11X)$ to $\mathcal{L}_X$, the dimension of the algebra does not increase which means that $-i(11X)$ is contained in the algebra. Furthermore, since $11X$ is not only unitary but as well Hermitian, i.e. $(11X)^2 = \mathbb{1}$, we find a matrix A, namely $A = -i\frac{\pi}{2}(11X)$ which is an element of the considered algebra and fulfills $e^{-i\frac{\pi}{2}(11X)} = -i(11X)$. Hence, we conclude that up to an irrelevant global phase $-i(11X) \in \mathcal{L}_X$ implies $11X \in e^{\mathcal{L}_X}$ with $e^{\mathcal{L}_X}$ being the Lie group whose elements build the reachable set for the system. Thus, controlling the x-field is indeed sufficient to implement $11X$. We state that in general any unitary U, which is additionally Hermitian and where $-iU$ is contained in the dynamical Lie algebra $\mathcal{L}_0$ of the quantum control system, is up to an irrelevant phase an element of the reachable set $e^{\mathcal{L}_0}$ of the system.

Proof. $-iU \in \mathcal{L}_0 \Rightarrow e^{-i\frac{\pi}{2}U} \in e^{\mathcal{L}_0}$,
$e^{-i\frac{\pi}{2}U} = \cos\left(-\frac{\pi}{2}U\right) + i\sin\left(-\frac{\pi}{2}U\right) = \sum_{k=0}^{\infty}(-1)^k\frac{(-\frac{\pi}{2}U)^{2k}}{(2k)!} + i\sum_{k=0}^{\infty}(-1)^k\frac{(-\frac{\pi}{2}U)^{2k+1}}{(2k+1)!}$.
Due to $U^2 = \mathbb{1}$ it follows $e^{-i\frac{\pi}{2}U} = \mathbb{1}\cos\left(-\frac{\pi}{2}\right) + iU\sin\left(-\frac{\pi}{2}\right) = -iU \Rightarrow U \in e^{\mathcal{L}_0}$. $\qquad\square$

In the Appendix A.1 we calculate explicitly a basis for $\mathcal{L}_X$. The calculation reveals that together with $11X$ as well $1X1$ is contained in $\mathcal{L}_X$. Since $1X1$ is unitary and Hermitian, it can be achieved by control of the x-field for the same reasons as $11X$. Using the derived basis, it can furthermore be shown that also the gate $1\sqrt{\text{SWAP}}$ is generated by an element of $\mathcal{L}_X$ and hence achievable (see A.1). For all gates contained in $e^{\mathcal{L}_X}$ the above described procedure A may be modified by applying a field in x-direction only. We calculate the time evolution operator at the final time t_f at which we desire to achieve the target unitary in an analogous way as for procedure A, however taking into account only the x-field which means that in all time intervals the x-field is acting:

$$U(t_f) = \prod_{j=N_t}^{1} U_{x,j} = U_{x,N_t} \cdot \ldots \cdot U_{x,2} \cdot U_{x,1}. \tag{4.3.6}$$

The fidelity depends hence on the N_t variables $h_{x,1},...,h_{x,N_t}$.

Since the Lie algebra generated by $\{-iH_{x,1}, -iH_{x,2}\}$ with $H_{x,1} = H_0 + h_{x,1}S_{1x}$ and $H_{x,2} = H_0 + h_{x,2}S_{1x}$ is equal to $\mathcal{L}_X$ for any values of $h_{x,1}$ and $h_{x,2}$ provided they are different, the calculation of the unitary evolution given by Eq. (4.3.6) where we switch between evolutions $e^{-iH_{x,j}}$ is sufficient to achieve any unitary in the Lie group $e^{\mathcal{L}_X}$.

A few remarks

a) Numerical computation of $U(t_f)$: Spectral representation

We calculate $U_x = e^{-iH_x t}$ and $U_y = e^{-iH_y t}$ numerically by using the spectral representation of H_x and H_y. For this purpose we briefly review the spectral theorem:

An arbitrary normal operator A on a m-dimensional complex Hilbert space, i.e. any continuous linear operator for which the relation $[A, A^\dagger] = 0$ is fulfilled, can be written in the spectral form $A = \sum_{n=1}^{m} \lambda_n P_n$, where the λ_n's denote the - not necessarily distinct - eigenvalues of A. The eigenprojectors P_n are given by $|n\rangle \langle n|$ with $|n\rangle$ being the normalized eigenstates of the operator A. This statement holds since every normal operator is diagonalizable over the complex numbers by a unitary transformation. That is, the eigenvectors of the operator A build a basis for the associated m-dimensional Hilbert space. Using the orthogonal property of the eigenprojectors, i.e. $P_n P_{n'} = \delta_{nn'} P_n$, an analytic function f depending on A can be calculated as

$$f(A) = \sum_{n=1}^{m} f(\lambda_n) P_n. \tag{4.3.7}$$

Accordingly, the exponential of the operator A is given by $e^A = \sum_{n=1}^{m} e^{\lambda_n} P_n$. We note that every function of a normal operator is normal as well.

Applying this result to the unitary time evolution operators U_x and U_y, which are analytic functions depending on the Hermitian (and hence normal) matrices H_x and H_y, we obtain

$$U_x = e^{-iH_x t} = \sum_{n_x=1}^{m} e^{-i\lambda_{n_x} t} P_{n_x}, \tag{4.3.8}$$

$$U_y = e^{-iH_y t} = \sum_{n_y=1}^{m} e^{-i\lambda_{n_y} t} P_{n_y}, \tag{4.3.9}$$

with λ_{n_x} and λ_{n_y} being the eigenvalues as well as $|n_x\rangle$ and $|n_y\rangle$ being the eigenvectors of H_x and H_y, respectively. Equations (4.3.8) and (4.3.9) are spectral decompositions of the unitaries U_x and U_y. We note that their eigenvalues are given by $e^{-i\lambda_{n_x} t}$ and $e^{-i\lambda_{n_y} t}$, respectively.

We write a Fortran 90 program which calculates the fidelity (4.2.12) numerically by making use of the spectral decompositions (4.3.8) and (4.3.9). The program calls suitable routines from the Fortran libraries EISPACK or LAPACK in order to compute the eigenvalues and eigenvectors of H_x and H_y.

b) Properties of H_x and H_y:

Independent of the choice of h_x and h_y, the trace of H_x and H_y is always equal to 0. Since H_x (real symmetric) and H_y (complex) are Hermitian matrices (only real eigenvalues) and thus diagonalizable, there exist complex $m \times m$ matrices Q_x and Q_y which are unitary (so-called unitary transformations) such that $H'_x = Q_x H_x Q_x^\dagger$ and $H'_y = Q_y H_y Q_y^\dagger$ are Hermitian diagonal matrices. If we set h_x equal to h_y, then H_x and H_y are similar matrices, i.e. they are related by a (unitary) similarity transformation Q of the form $H_x = Q H_y Q^\dagger$. Due to the Hermitian property of the Hamiltonians, H_x and H_y being similar implies $H'_x = H'_y$. Hence, Q can be found as the product $Q_x^\dagger Q_y$. If H_x and H_y are similar, they have the same eigenvalues and same determinant.

We give the eigenvalues of H_x calculated by Mathematica. Two of them have the form

$$\frac{1 - h_x}{2} \quad \text{and} \quad \frac{1 + h_x}{2}. \tag{4.3.10}$$

The other six eigenvalues are the roots of the following two cubic equations in λ:

$$-h_x^2 + h_x^3 + (-4 - 2h_x^2)\lambda + (4 - 4h_x)\lambda^2 + 8\lambda^3 = 0, \tag{4.3.11}$$

$$-h_x^2 - h_x^3 + (-4 - 2h_x^2)\lambda + (4 + 4h_x)\lambda^2 + 8\lambda^3 = 0. \tag{4.3.12}$$

We state that all eigenvalues of H_x are algebraic functions in h_x. The eigenvalues of H_y are obtained by replacing h_x with h_y in the expressions for the eigenvalues of H_x.

c) Properties of U_x and U_y:

At first we mention that the matrices $U_x = e^{-iH_x t}$ and $U_y = e^{-iH_y t}$ are unitary which ensures that the whole time evolution operator $U(t_f)$ has the required unitary property. Because of the relation $\det(e^A) = e^{\text{tr}(A)}$ which is valid for arbitrary matrices A with entries in the complex field, the determinant of U_x and U_y is always equal to 1. The unitaries U_x and U_y are diagonalizable making use of the same unitary transformation as used for the diagonalization of H_x and H_y. The diagonalized matrices are thus given by

$$U_x' = Q_x U_x Q_x^\dagger = Q_x e^{-iH_x t} Q_x^\dagger = e^{-iQ_x H_x Q_x^\dagger t} = e^{-iH_x' t}, \tag{4.3.13}$$

$$U_y' = Q_y U_y Q_y^\dagger = Q_y e^{-iH_y t} Q_y^\dagger = e^{-iQ_y H_y Q_y^\dagger} = e^{-iH_y' t}. \tag{4.3.14}$$

As in the case of H_x and H_y, the time evolution operators U_x and U_y are similar if h_x is equal to h_y, related by the same similarity transformation $Q = Q_x^\dagger Q_y$. The eigenvalues and the trace of U_x and U_y correspond to each other in this case. Due to the unitary property of U_x and U_y their eigenvalues are lying on the unit circle which means that they are complex numbers with norm one. Looking at the eigenvalues of U_x and U_y, which are given by $e^{-i\lambda_{n_x} t}$ and $e^{-i\lambda_{n_y} t}$ with λ_{n_x} and λ_{n_y} being the eigenvalues of H_x and H_y, this becomes obvious.

Since H_x is a real symmetric and H_y a complex Hermitian matrix, $U_x^\dagger$ and $U_y^\dagger$ are found as

$$U_x^\dagger = (e^{-iH_x t})^\dagger = e^{iH_x^\dagger t} = e^{iH_x t} = \sum_{n_x=1}^m e^{i\lambda_{n_x} t} P_{n_x}, \tag{4.3.15}$$

$$U_y^\dagger = (e^{-iH_y t})^\dagger = e^{iH_y^\dagger t} = e^{iH_y t} = \sum_{n_y=1}^m e^{i\lambda_{n_y} t} P_{n_y}. \tag{4.3.16}$$

The eigenvalues of $U_x^\dagger$ and $U_y^\dagger$ are the complex conjugated eigenvalues of U_x and U_y. Furthermore, since H_x is a symmetric matrix, U_x and $U_x^\dagger$ are symmetric as well.

d) Periodicity:

The components of the matrices U_x and U_y show a quasi-periodic behaviour with wave character which can be attributed to the factors $e^{-i\lambda_{n_x} t} = \cos(\lambda_{n_x} t) - i\sin(\lambda_{n_x} t)$ and $e^{-i\lambda_{n_y} t} = \cos(\lambda_{n_y} t) - i\sin(\lambda_{n_y} t)$, respectively (see Fig. 1 where the real part of the first matrix element of U_x is plotted). Increasing t decreases the length of the period along the h_x- and h_y-axis. We expect that the function for the fidelity has many local maxima which occur in an approximate periodic manner.
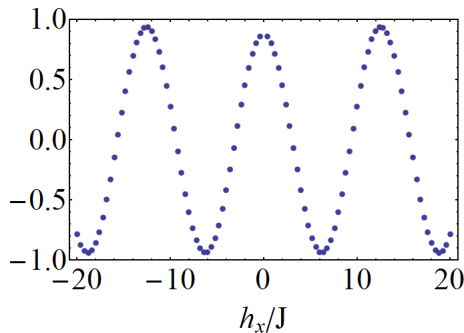
Figure 1: Real part of the first matrix element of the time evolution operator U_x plotted for a sequence of values of the control field h_x/J in the interval $[-20, 20]$. The time interval length T is set to 1.0.

e) Properties of the fidelity:

As derived before the fidelity F between the target unitary U_{target} and the dynamic unitary $U(t)$ is determined by the formula $F = \frac{1}{d}|\text{tr}(U^\dagger(t) \cdot U_{target})|$ with d being the dimension of the Hilbert space. We may write $U(t)$ in the general form $U(t) = U_n \cdot U_{n-1} \cdot \ldots \cdot U_2 \cdot U_1$ which is valid for procedure A and B. The fidelity depends in both cases on n variables.

We collect a few properties of the fidelity F for the implementation of the gate $11X$:

1. The fidelity between $11X$ and $U(t_f)$ is equal to zero at any final time t_f if the system is evolving freely. Free evolution means here that no control field is applied and the dynamic time evolution $U(t_f)$ governed only by the free Heisenberg Hamiltonian (4.2.2).

2. The fidelity remains invariant if $U(t)$ is replaced by $U(t)_{inverse} = U_1 \cdot U_2 \cdot \ldots \cdot U_{n-1} \cdot U_n$. We state the direction of time in which a sequence of control amplitudes is applied does not change the fidelity.

3. The fidelity remains invariant under parity transformation. That is under the transformation $h_x \to -h_x$ and/or $h_y \to -h_y$. We state that the fidelity is point symmetric with respect to zero in the space of all variables h_x and in the space of all variables h_y and hence in the whole n-dimensional space.

We emphasize that these observations are valid for the gate $11X$ without claim of generality.

4.4 Maximization of the fidelity

The fidelity is a function of N_t variables which are represented by a point x in a N_t-dimensional space. The number of variables correspond to the number of time intervals. We maximize the fidelity $F(x)$ by minimizing $-F(x)$. In order to minimize this function numerically, we use a multidimensional variable metric method (quasi-Newton method) which performs successive line minimizations. This method requires in addition to the calculation of the function itself the computation of the function's gradient. We implement the *Broyden-Fletcher-Goldfarb-Shanno* (BFGS) algorithm, a variant of *Davidon-Fletcher-Powell* minimization [14]. Since this minimization routine requires the gradient of the function which shall be maximized, we have to implement the partial derivatives of the fidelity with respect to the N_t variables. For this purpose we choose a method of polynomial extrapolation developed by Ridders [14]. We implement the whole minimization program - calculation of the fidelity and its gradient included - in Fortran 90.

The BFGS-algorithm works in the following way: First we have to choose randomly an initial guess for the variables of the fidelity. We denote this initial point by x_0 which is a vector consisting of N_t components. A possible guess could be for instance a constant one like $x_0 = 1.0$ (all components set equal to 1.0). Such a guess would in the case of procedure B (only x-field)

correspond to a control field which is constant in time both in its amplitude and direction while using procedure A the field would be constant in its amplitude but not in its direction due to the switching between x- and y-field. Performing line minimizations, the algorithm generates iteratively x_{k+1} starting from x_k such that $-F(x_{k+1}) < -F(x_k)$ which means that the fidelity increases at each iteration point. This procedure ensures the convergence to a local minimum. The algorithm terminates if x_{k+1} is too close to x_k or if the gradient of the fidelity is sufficiently close to zero. In the first case the algorithm is not able to find a line direction along which the fidelity can be increased further. The tolerance for convergence on x is given by the minimization routine as $tol_x = 4.0\epsilon$ where ϵ denotes the machine epsilon (machine precision). The machine epsilon gives the smallest number such that $1 + \epsilon > 1$. According to the IEEE standard for floating point arithmetic, ϵ is in the case of double precision of the order of $2.2 \cdot 10^{-16}$. The convergence criterion tol_g for zeroing the gradient is an input parameter of the minimization routine. We point out that the accuracy of the results is dependent on the choice of tol_g. We set $tol_g = 10^{-5}$. The found local maxima of the fidelity are only to a certain accuracy the highest ones which can be reached. Decreasing tol_g would allow to obtain slightly higher fidelities. It is not possible to calculate an upper bound for the difference between the obtained optimal fidelities and the ones which could be obtained using a slower tol_g since we do not know the explicit dependence of the fidelity on the variables, but we estimate it to be of the order of the chosen tol_g and smaller by comparing for a given function $F(x)$ the results for varied tol_g. We conclude that setting tol_g equal to 10^{-5} is certainly sufficient to determine optimal fidelities.

In all numerical calculations the Planck's constant $\hbar$ is set equal to 1. Therefore the values of the physical quantities are given in natural units. For the control field amplitudes h_x and h_y we define the dimensionless quantities h_x/J and h_y/J where J is the Heisenberg coupling constant.

4.4.1 Implementation of the gate 11X: Procedure A

We implement the target unitary $11X$ by maximizing the function for the fidelity (recall Eq. (4.2.12)). The dynamic unitary $U(t_f)$ is calculated by applying procedure A. At first we analyse the shape of the fidelity for $T = 1.0$ and $U(t_f) = U_{y,1}U_{x,1}$ by looking at the contour plot in Fig. 2 where the fidelity versus the plane $(h_{x,1}, h_{y,1})$ is plotted. The plot reveals that there exist many local maxima which occur periodically. Replacing the target unitary operator $11X$ by $11Y$ exchanges the axes $h_{x,1}$ and $h_{y,1}$ in the plot of Fig. 2.
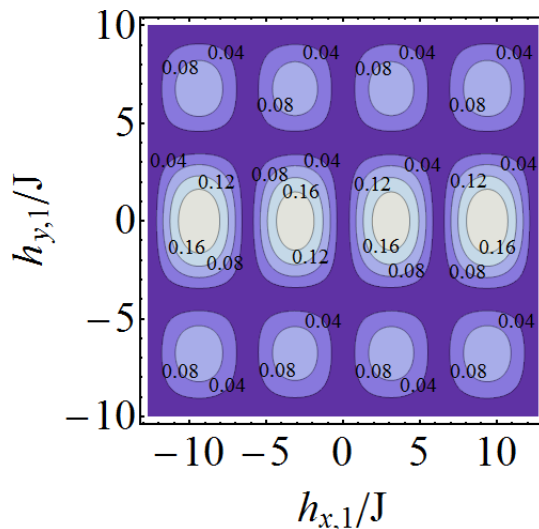

Figure 2: Contour plot of the fidelity versus $(h_{x,1}, h_{y,1})$ for $U(t_f) = U_{y,1}U_{x,1}$ and $T = 1.0$. The horizontal axis is the $h_{x,1}$-axis, the vertical one the $h_{y,1}$-axis.

Numerical maximization:

We start our search for optimal fidelities by varying the number of time intervals N_t and the length T of these, i.e. the total time $t_f = N_t T$ is variable. At first we observe that the returned maximal values for the fidelity are dependent on the initial guess and perform therefore for a given set of parameters $\{N_t, T\}$ runs over several randomly chosen initial guesses. We proceed by increasing the number of time steps N_t and varying for any value of N_t the interval length T.

a) Computational burden: Iterations and matrix multiplications

An increase of N_t and hence of the number of variables on which the fidelity depends forces the minimization routine to perform more iterations in order to reach a local maximum. This can be attributed to the increasing number of degrees of freedom which is equal to the number of variables. Hence, the minimization program becomes more and more time-consuming with increasing N_t. For the length of the time intervals T the contrary holds. For increasing T tendentially less iterations have to be done due to the reduced length of the period between successive local maxima. We state that the closer the initial guess is to a local maxima the less iterations should be needed to reach it. Another reason, why an increase of N_t leads to the fact that the program takes more time, is the number of matrix multiplications which increases for more N_t. Due to the computational burden in performing matrix multiplications and iterations, the number of initial guesses which can be run is limited. For this reason we concentrate on varying the parameters N_t and T and not on covering the whole N_t-dimensional space by trying a lot of guesses for fixed parameters.

b) Optimal fidelities:

At first we realize the following: Independent of the value given to the time interval length T we observe that the higher fidelities can be achieved the higher the number of time intervals N_t is. For any T we are able to achieve optimal fidelities if the number of time steps is high enough. However, the contrary does not hold. Fixing N_t it is not possible to produce higher and higher fidelities only by increasing T. The explanation is intuitive: The control field amplitude is fixed during the duration T. An increase of N_t, on the other hand, allows to adjust the amplitudes more times. It seems that a sufficient high number of time intervals is the most important condition if we want to reach fidelities as high as possible. Nevertheless, it cannot be ruled out that even for only a few time steps there exist very high fidelities at certain values for T somewhere in the N_t-dimensional space of variables. The dependence of the maximization procedure on the initial guess, however, prevents us from covering the whole space of variables.

We notice that for increasing N_t and increasing fidelities the values of the reached local maxima seem to be less dependent on the initial guess than for smaller N_t. In order to show this reduced dependence, we calculate for fixed T and increasing N_t the average of all fidelities which are reached for different guesses. We observe that the standard deviation of the single samples is decreasing with increasing number of time intervals (see Table 1).

In Fig. 3 we show one example of an optimal control field which is achieved for $N_t = 70$ and $T = 0.5$. The amplitudes h_x and h_y are indicated as green and blue bars, respectively. The values of the variables h_x and h_y which are returned from the numerical maximization procedure are dependent on the initial guess. If there exist local maxima close to the initial guess the returned values for the field variables will be close to the initial values. In Fig. 3 almost all variables are positive which can be attributed to the fact that all variables h_x and h_y are chosen positive in the corresponding initial guess.

N_t	N_{guess}	average	maximum	sd of the single samples
10	33	0.63	0.82	0.114
20	33	0.78	0.90	0.058
30	33	0.89	0.94	0.025
40	17	0.96	0.99	0.014
50	17	0.99	$1 - 10^{-4}$	0.006
60	9	$1 - 10^{-4}$	$1 - 10^{-6}$	10^{-4}
70	9	$1 - 10^{-8}$	$1 - 10^{-9}$	10^{-8}

Table 1: Average reached fidelities for $T = 1.0$ and varying N_t. The number of initial guesses is denoted by N_{guess}. The third column contains the average of all achieved fidelities, the fourth the highest produced fidelity and the last the standard deviation (sd) of the single samples.
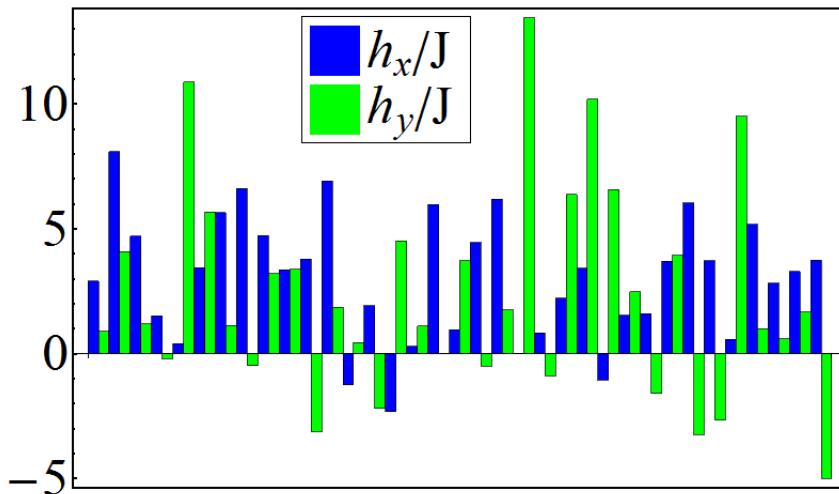
Figure 3: This optimal control field is reached for $N_t = 70$ and $T = 0.5$ and corresponds to a fidelity of $1 - 10^{-10}$.

c) Dependence on the total evolution time t_f:

Furthermore, we consider different total times t_f and search for the highest possible fidelity which is reachable for a given t_f. We expect that there exists a minimal total time below which no optimal fidelities can be achieved no matter how many time intervals or iterations are used [15]. In order to estimate such a minimal time, we perform runs over different total evolution times t_f whereas for every fixed t_f we start with $N_t = 2$ and increase the number of time intervals in steps of 2 until optimal fidelities are reached or the found maxima are not increasing anymore. Since the above considerations have shown that the initial guess becomes less and less important for increasing N_t we use here for every given set of parameters $\{t_f, N_t\}$ only one guess, namely a constant one where we set all initial field components equal to 1.

Firstly, we state that for larger total times higher fidelities are achievable. For every fixed t_f the higher fidelities can be reached the more N_t is increased. We observe that for very short evolution times the returned fidelities are far away from optimal and cannot be increased even not if we use many time steps. For instance, we obtain for the total times $t_f = 5.0$ and $t_f = 8.0$ fidelities of maximal 0.59 and 0.85, respectively. It cannot be excluded that for other guesses than the one which we have chosen higher fidelities can be achieved but in the case of $t_f = 5.0$ it seems very improbable that there exist higher fidelities than the one we found. Starting from an evolution time of at least 10.0, we find optimal fidelities with values of 0.9 and above. Increasing t_f and N_t we can achieve fidelities which are arbitrarily close to 1.0. We remark that not only an increase of N_t but also of t_f reduces the dependence on the initial guess of the maximal reached fidelity values.

In Section 5.2.1 we give an estimate of the minimal time required to implement respective gates to high accuracy by comparing Heisenberg chains of two, three, and four spins.

4.4.2 Implementation of the gate 11X: Procedure B

Now we intend to implement the same gate as before but using procedure B for the calculation of the dynamic unitary evolution $U(t_f)$. In order to obtain maximal values for the fidelity we proceed analogously to the previous section. At first we observe that in contrast to procedure A the maximal reachable fidelities cannot be increased further and further just by increasing N_t and/or t_f. It seems that if we go beyond a certain number of time intervals N_t or a certain total time t_f no further increase is possible. We achieve optimal fidelities in the range 0.9 to 0.999. Furthermore, we see that for equal total times t_f and assumed that N_t is high enough most guesses lead to the same fidelity. As in procedure A optimal fidelities are only reachable for evolution times which are larger than a minimal time. For $t_f = 5.0$, $t_f = 10.0$, and $t_f = 15.0$ we obtain no optimal fidelities. The values 0.55, 0.80, and 0.88, respectively, are the highest fidelities we found for these three cases (see Table 2).

t_f	maximal F
5.0	0.55
10.0	0.80
15.0	0.88
20.0	0.95
25.0	0.999
30.0	0.92

Table 2: Highest fidelities which are reached for different total times t_f.

Optimal fields:

Three optimal fields which all correspond to a total evolution time of 25.0 and a fidelity of 0.999 are shown in Fig. 4. The field plotted in (a) is achieved for the parameters $N_t = 25$ and $T = 1.0$ while the fields plotted in (b) and (c) are reached for two different initial guesses at $N_t = 50$ and $T = 0.5$.

We briefly mention some observations concerning the correlation between initial guess and the field values returned by the optimization program.

If we choose a N_t-dimensional guess $x = (x_1, x_2, ..., x_{N_t-1}, x_{N_t})$ for which the condition

$$x_k = x_{N_t-k+1} \quad \forall k \quad \text{with} \quad k \in \{1, ..., N_t\} \tag{4.4.1}$$

is fulfilled, in most of the considered cases the values of the field associated with the returned maximal fidelity obey as well the above condition, at least approximately. Figure 4(c) shows such an example. The property of such fields can be described as a left-right symmetry in time.

Furthermore, we look at two different initial guesses x^1 and x^2 which are related by $x_k^1 = x_{N_t-k+1}^2$ $\forall k$. In all considered cases both guesses lead to the same fidelity with fields which are related by the same condition as the two initial guesses. This means that one field is the inverse (with respect to time) of the other. That such two fields lead to the same fidelity was already mentioned in the discussion of Section 4.3 (see Paragraph *Properties of the fidelity*).
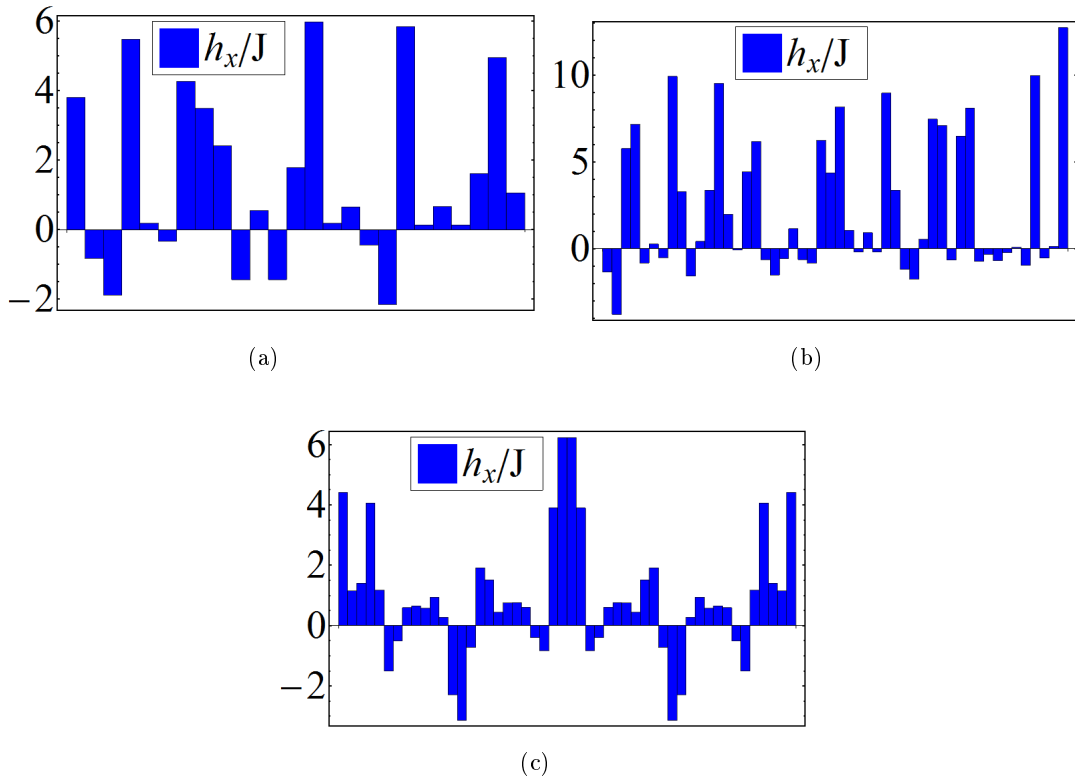
Figure 4: These three optimal fields correspond all to a total time of 25.0 and a fidelity of 0.999 which is the highest one reached for the given total time. The field plotted in (a) belongs to the parameters $N_t = 25$ and $T = 1.0$ while the fields plotted in (b) and (c) are reached for two different initial guesses at $N_t = 50$ and $T = 0.5$.

Since it turned out that using procedure B it is not as intuitive as with procedure A to achieve optimal fidelities, we will in the following use procedure A in order to implement other target unitaries even if they could be reached by controlling the field in x-direction only.

4.4.3 Implementation of other gates: Procedure A

In addition to $11X$, we implement the target unitaries $1X1$, 1CNOT and $1\sqrt{\text{SWAP}}$ and are able to show that they can be approximated to a very high accuracy, i.e. with optimal fidelities arbitrarily close to 1. The reason for implementing the gate $1X1$ is the expectation that this gate may be easier to achieve than $11X$. Easier in the sense that it is reachable within a smaller total evolution time of the system because the second spin which shall be flipped is 'closer' to the first spin where the control field is applied than the third spin. But we have to take into account that the gate $1X1$ not only causes a flip of the second spin but as well lets the third spin invariant which may not be 'easier' to achieve. The unitaries CNOT and $\sqrt{\text{SWAP}}$ are entangling gates and therefore of interest. The dependence of the optimal achieved fidelities on the parameters N_t and T as well as on the total time $t_f = N_t T$ is for these three gates very similar to the gate $11X$ whose implementation we already discussed. For this reason we will not go into the results in detail here. However, we emphasize that every considered target unitary can be achieved to a high accuracy by increasing the number of time steps N_t and/or the total evolution time t_f. The minimal total time and the number of time intervals needed to achieve optimal fidelities may differ from gate to gate but since we are limited in the number of guesses and since the difference may be quite small, no significant differences could be observed.

We measure the distance between the implemented target gates and the $d \times d$ unit matrix in order to obtain a quantity which may specify how 'easy/difficult' the achievement of the target is. For this purpose we use the Hilbert-Schmidt inner product defined for two operators A and B, which act on states of the d-dimensional Hilbert space of the considered system, as $\langle A, B \rangle = \text{tr}(A^\dagger B)$.

This inner product induces a norm, known as the unitarily invariant Hilbert-Schmidt (Frobenius) norm, as follows

$$||A|| = \sqrt{\frac{1}{d}\langle A, A\rangle} = \sqrt{\frac{1}{d}\text{tr}(A^\dagger A)}. \tag{4.4.2}$$

Then the distance between an arbitrary target U_{target} and the $d \times d$ unit matrix $\mathbb{1}$ is derived as

$$||U_{target} - \mathbb{1}|| = \sqrt{\frac{1}{d}\text{tr}[(U_{target} - \mathbb{1})^\dagger(U_{target} - \mathbb{1})]}. \tag{4.4.3}$$

Another quantity, which may describe the overlap between a certain target gate and the unit matrix, is of course our well-known fidelity, given by

$$F = \frac{1}{d}|\text{tr}(U_{target}^\dagger \mathbb{1})|. \tag{4.4.4}$$

gate	distance	fidelity
$11X$	≈ 1.4	0
$1X1$	≈ 1.4	0
$1CNOT$	1	0.5
$1\sqrt{\text{SWAP}}$	≈ 0.7	≈ 0.79

Table 3: Distance and fidelity between the implemented gates and the unit matrix.

Table 3 summarizes the distance and fidelity between the implemented gates and the unit matrix. Considering the calculated values, we note that there exist certainly gates which are much closer in terms of the fidelity or the Hilbert-Schmidt measure to the unit matrix and should hence be 'easier' to achieve. We may construct gates which are very close to the unit matrix but not equal to it using the rotation operators defined in Eqs. (2.4.9), (2.4.10), and (2.4.11) and choosing the rotation angle θ very small. In order to find gates which are very close to the unit matrix, we examine the fidelity and distance between the unit matrix and the gates $11R_x$, $11R_y$, and $11R_z$ depending on θ (see Table 4). We note that the following relations hold

$$||11R_x - \mathbb{1}|| = ||11R_y - \mathbb{1}|| = ||11R_z - \mathbb{1}||, \tag{4.4.5}$$

and

$$\frac{1}{d}|\text{tr}[(11R_x)^\dagger \mathbb{1}]| = \frac{1}{d}|\text{tr}[(11R_y)^\dagger \mathbb{1}]| = \frac{1}{d}|\text{tr}[(11R_z)^\dagger \mathbb{1}]|. \tag{4.4.6}$$

θ	distance (approximate)	fidelity (approximate)
$\pi/2$	0.765	0.707
$\pi/3$	0.518	0.866
$\pi/4$	0.390	0.924
$\pi/8$	0.196	0.980
$\pi/16$	0.098	0.995

Table 4: Distance and fidelity between the unit matrix and the gates $11R_x$, $11R_y$, and $11R_z$ depending on θ.

In order to examine if a gate whose initial fidelity is very high, may be achieved in significant shorter evolution time, we implement the rotation operator $11R_y$ for $\theta = \frac{\pi}{16}$. Having already a fidelity of 0.995 at time $t = 0$, we expect that there will be produced even higher fidelities after short evolution time. Of course, if we reduce the number of time steps and let the length of these converge to zero, we obtain the initial fidelity. As soon as we let the system evolve over a longer time, the fidelity decays first continuously before increasing again. Hence, it could not be observed that the gate $11R_y$ is achievable in significant shorter time than the other implemented

gates. One possible explanation for this behaviour is already given in Section 3.2 at the very end, where we point out that the restriction to positive time intervals T may effect that unitaries close to the identity cannot be achieved in arbitrarily short times.

4.5 Sensitivity of the fidelity

We analyse the sensitivity of the fidelity to optimal control fields which are disturbed by random noise of varying strength. For this purpose we add uniformly generated random numbers to the optimal field values and recalculate the fidelity for the disturbed values. The strength of the random noise is determined by the extent of the interval in which the random numbers are generated, hence by the width of the uniform distribution. In order to quantify the noise strength, we introduce the parameter δ which limits the range of the random numbers. For fixed strength we generate random numbers in the open interval $(-\delta, +\delta)$. The generation of the random numbers is performed by using the routine ran which is recommended for the use on purely serial machines by the authors of [14]. This routine is completely portable to all Fortran 90 environments and implements the 'minimal' random number generator developed by Park and Miller combined with a Marsaglia shift sequence. It returns a uniform random deviate between 0.0 and 1.0 (endpoints excluded). The period of this generator is about $3.1 \cdot 10^{18}$. For each δ we generate a few hundred sequences of random numbers and disturb the optimal control field by adding the random numbers to the field values. In so doing, we obtain a few hundred disturbed fields for which we recalculate the fidelity. Then we compute the average fidelity $\bar{F}$ of the collected samples. This average fidelity gives us a reliable value for the fidelity between a gate and its implementation which is affected by random noise. We examine the dependence of the average fidelity on the strength of the random noise by varying the strength parameter δ and plotting $\bar{F}$ versus δ.

Standard deviation of the average fidelity:

The standard deviation of the calculated average fidelity $\sigma_{\bar{F}}$ for a certain δ is given by $\frac{\sigma_F}{\sqrt{N}}$ where N indicates the number of collected samples and σ_F the standard deviation of the single samples which can be calculated using the formula

$$\sigma_F = \sqrt{\frac{1}{N-1} \sum_{i=1}^{N} (F_i - \bar{F})^2}, \tag{4.5.1}$$

where the F_i's denote the single samples.

We remark that σ_F is dependent on the value of δ. For $\delta = 0.01$ the standard deviation of the single samples can be calculated to be of the order of 10^{-5}. Increasing δ increases σ_F such that we obtain for $\delta = 1.0$ a σ_F of the order of 0.1. The standard deviation of the average is increasing until δ reaches values which are large enough to enable a saturation of the average fidelity which results in a slight decrease of the standard deviations with values of the order of 10^{-2}. Since the standard deviation of the average is very small, we will not include it as error bars in the plots of the average fidelity versus δ. Such plots are presented and discussed in the subsequent Sections 4.5.1 and 4.5.2 for various optimal fields which are differing in N_t and T.

4.5.1 Procedure A

In this chapter we analyse data obtained for implementing gates by applying a control field in x- and y-direction to the first spin in the chain. That is, we refer throughout this chapter to the case where we compute the dynamic time evolution operator $U(t_f)$ by means of the in Section 4.3 presented procedure A. We discuss the sensitivity of optimal fidelities to random noise applied to the optimal control fields. The average fidelity $\bar{F}$ is calculated as the average of 1600 collected samples. We look at various optimal control fields which are essentially differing in their total action time, i.e. in the number of time steps N_t and the length T of these. In cases where we have more than one optimal field available for the same parameters we take one with high fidelity.

At first we consider the implementation of the spin-flip gate $11X$ and perform a sensitivity analysis of the fidelity for various optimal control fields. Figure 5 contains plots of $\bar{F}$ versus δ for random noise affected optimal fields which are differing in N_t and T. While in plot 5(a) the number of time steps is fixed ($N_t = 70$) and the length of the steps varied, in 5(b) the contrary holds; T is set to 0.5 and N_t is varied. Table 5 collects how well these optimal fields approximate the gate $11X$ if no random noise is present:

T	Fidelity
0.5	$1 - 10^{-10}$
1.0	$1 - 10^{-9}$
1.5	$1 - 10^{-10}$
2.5	$1 - 10^{-10}$

(a)

N_t	Fidelity
30	0.99
40	0.99
50	0.999
60	$1 - 10^{-6}$
70	$1 - 10^{-10}$

(b)

Table 5: Optimal fields and corresponding fidelity: (a) $N_t = 70$ and (b) $T = 0.5$. If random noise is applied to these fields, the fidelity is decaying as it is shown below by Fig. 5.

(a)

(b)
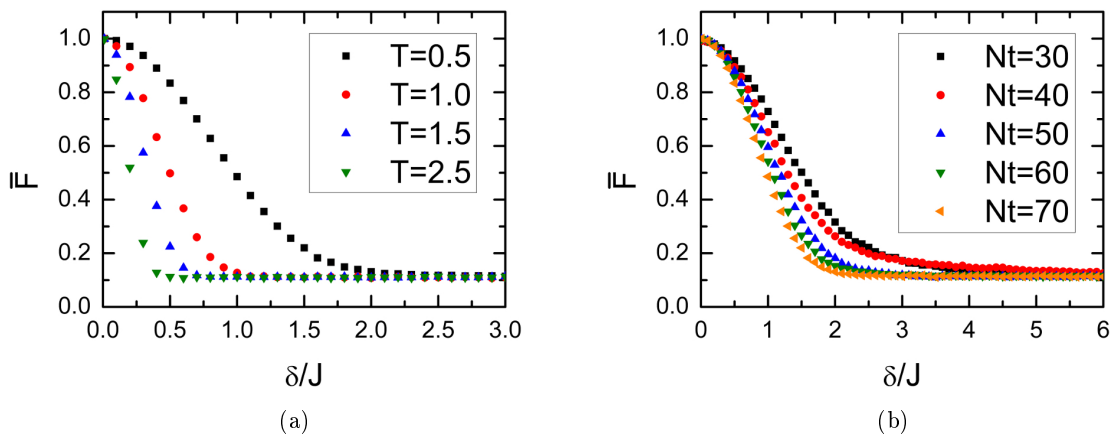
Figure 5: Average fidelity $\bar{F}$ versus δ for random noise affected optimal fields which are achieved for different parameter sets $\{N_t, T\}$. (a) $N_t = 70$ and (b) $T = 0.5$.

As we expect and as it is clearly visible in Fig. 5 the average fidelity is decreasing more and more the stronger the effect of the random noise becomes. Analysing the plots in 5(a), we observe furthermore that for fixed N_t the fidelity becomes more sensitive to random noise if the time length T and hence the total action time of the control field is increased. A similar observation is revealed by the plots in 5(b). If we fix T and increase N_t, then the fidelity is decaying more rapidly. We may state that the more time the random noise has to act and disturb the optimal field the stronger is its effect on the sensitivity of the fidelity. However, even for equally acting time of the random noise there is a difference in the decay of the fidelity depending on how the parameters N_t and T are chosen. This phenomenon will be shown later.

Looking at Fig. 5, we notice that the average fidelity saturates if δ, the parameter which determines the strength of the random noise, is sufficiently large. We see that for every optimal control field analysed in Figs. 5(a) and 5(b) the average fidelity converges to the same saturation value for large δ. In order to examine this universal property of the saturation value further, we consider two additional figures (see Fig. 6). In 6(a) we plot the decay of the fidelity for five random noise affected optimal control fields all achieved for the parameters $N_t = 60$ and $T = 1.5$. The fidelity between the gate $11X$ and the evolution induced by those fields lies above 0.999 for all five cases. We see immediately that the decay curve of the average fidelity does not

differ in all cases. Figure 6(b) is equivalent to Fig. 6(a) in the sense that all fields analysed there are reached for the same set of parameters. But in comparison to the fields of 6(a) the control fields in 6(b) act during a much shorter time which is determined by the parameters $N_t = 40$ and $T = 0.4$. For this evolution time not all initial guesses given to the minimization routine as input produce control fields with optimal fidelities. The fields analysed in 6(b) belong to fidelities between 0.699 and 0.992. However, although not all fields are optimal, all curves saturate to the same value.

(a) (b)
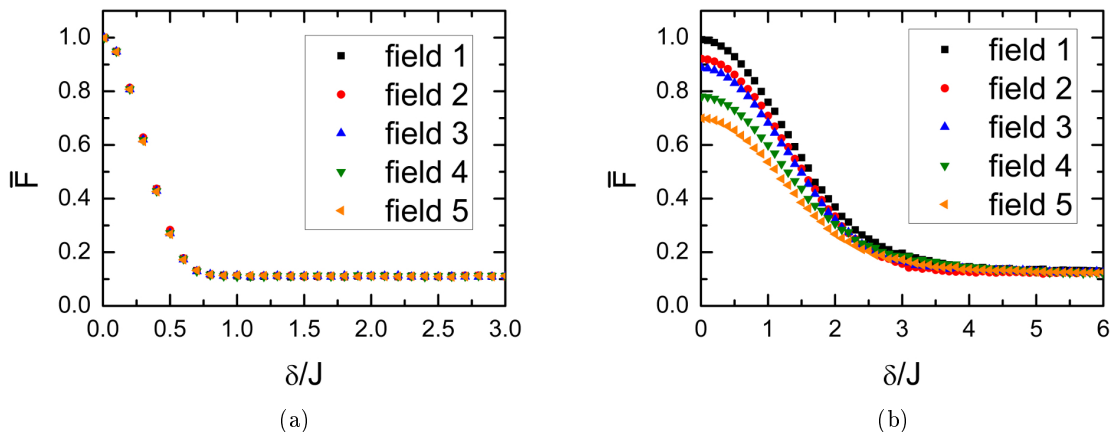
Figure 6: Average fidelity $\bar{F}$ versus δ for random noise affected fields. In (a) all five fields are optimal if no random noise is present with fidelities above 0.999 and correspond to the parameters $N_t = 60$ and $T = 1.5$. The five fields analysed in (b) are achieved for $N_t = 40$ and $T = 0.4$ and only the field corresponding to the black curve induces a fidelity of above 0.99.

We state that, if we start from optimal fields, the shape of the decay curve is dependent on the parameters N_t and T, but not on the values of the field components. That is, the behaviour of the fidelity under randomness in the control field is in particular not dependent on the strength of the field. The saturation occurs for values of δ which are such large that the random noise has driven the control field far away from optimal. We hence conclude that the saturation of the average fidelity is an intrinsic property of the considered quantum control system and completely independent of the shape of the control field. Furthermore, the value of the saturation may be computed using Eqs. (2.4.19) or (2.4.23) which give an expression for the average gate fidelity $\bar{F}(\varepsilon, U)$. The quantum control system, which is considered here, is determined by the Hamiltonian (4.2.6) and thus allows to generate any unitary contained in the Lie group $SU(d)$ with $d = 8$. Hence, it seems intuitive to use formula (2.4.23), which is derived explicitly in terms of the $SU(d)$ group generators, in order to evaluate the saturation value. We assume that the action of the quantum operation ε is given by

$$\varepsilon : \rho \rightarrow \varepsilon(\rho) = \frac{\mathbb{1}}{d} \quad \forall \rho. \tag{4.5.2}$$

This choice provides that the image of any (pure) state is a maximally mixed state. If the density matrix is proportional to the identity matrix, the pure states, which form an orthonormal basis of the d-dimensional Hilbert space of the system, are equal-weighted. That is, the probability for each basis state to be prepared is equal to $1/d$. The density matrix expresses in this case a complete and hence maximal ignorance ('mixedness') about which pure state has been prepared. Such states are referred to as maximally mixed states and may be interpreted as the quantum analogue of the uniform probability distribution. Assuming that the quantum map ε is acting as defined in (4.5.2), we assume simultaneously that the quantum system undergoes full randomization. We note that every density matrix may be written as

$$\rho = \frac{\mathbb{1}}{d} + \sum_{j=1}^{d^2-1} k_j T_j, \quad k_j \in \mathbb{R}, \tag{4.5.3}$$

where the sum is a linear combination of the Hermitian and traceless generators $\{T_j\}$ of $SU(d)$. Due to $\varepsilon(\rho) = \frac{1}{d}$ it follows by linearity and trace-preserving that all T_j are mapped by ε to 0. Hence, we see immediately that the sum in (2.4.23) evaluates to 0 which means that the average gate fidelity $\bar{F}(\varepsilon, U)$ is given by

$$\bar{F}(\varepsilon, U) = \frac{1}{d}. \tag{4.5.4}$$

For $d = 8$ we expect thus a saturation value of 0.125. Figures 5 and 6 seem to confirm this expectation. In Section 5.2.2 we will briefly come back to this issue and discuss it in the context of spin chains of varying length whereas we will determine the value of the saturation by linear fitting the numerical data. We note that Eq. (4.5.4) is only applicable in cases where any unitary contained in $SU(d)$ may be generated by adding random noise to the control field and where the generation is uniform. The first condition means that the random noise must be strong enough, as already pointed out, and that the number of time steps N_t as well as the total evolution time $t_f = N_t T$ must be large enough. In all cases shown in Figs. 5 and 6 the parameter sets $\{N_t, T\}$ seem to allow full randomization since the saturation converges to a value close to $1/d$.

Next, we compare the sensitivity of the fidelity for implementations of the gates $11X$, $1X1$, 1CNOT and $1\sqrt{\text{SWAP}}$. For this purpose we plot in Fig. 7 the average fidelity $\bar{F}$ versus the strength of the random noise for control fields corresponding all to an evolution time of $t_f = 30.0$, but differing in the parameters N_t and T. Figure 7(a) belongs to the gate $11X$, 7(b) to $1X1$, 7(c) to 1CNOT, and 7(d) to $1\sqrt{\text{SWAP}}$.
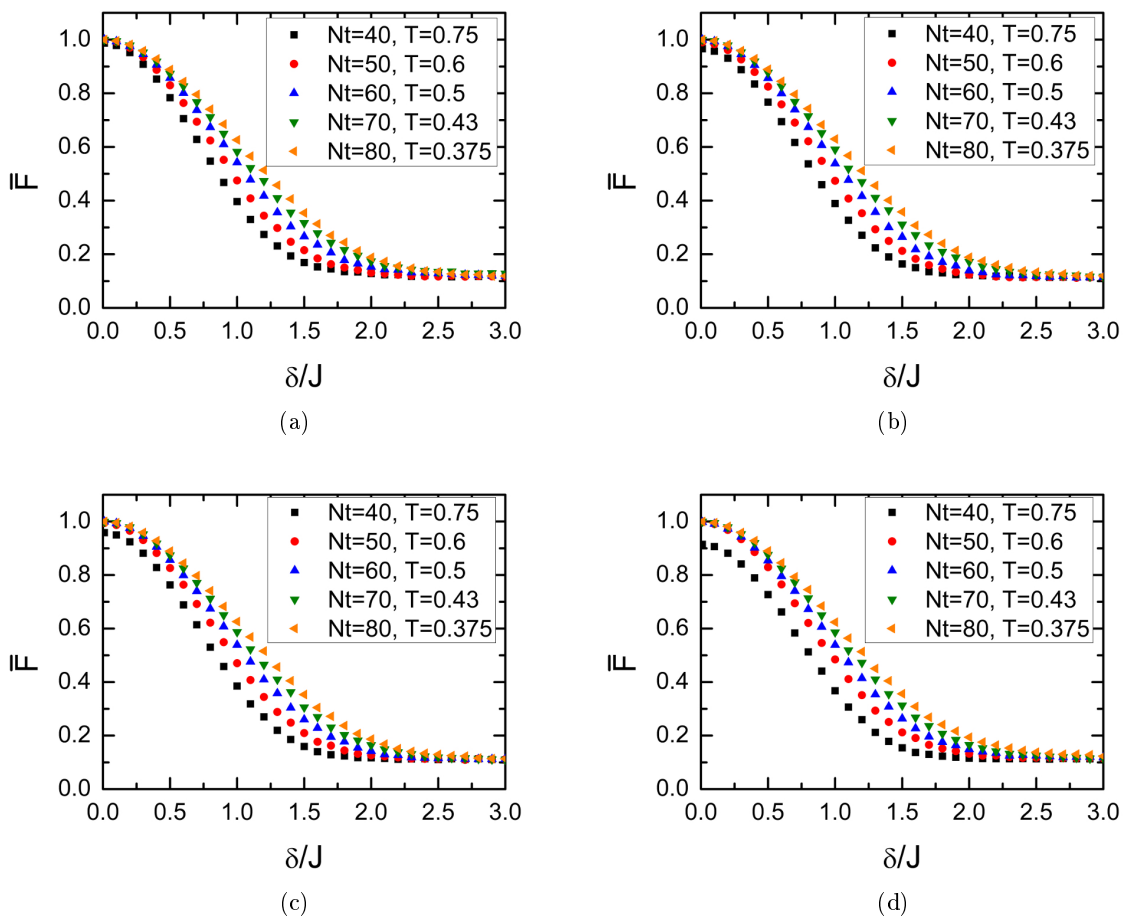

Figure 7: Average fidelity $\bar{F}$ versus δ for random noise affected optimal fields (optimal refers here to a fidelity above 0.9) which are all achieved for a total evolution time $t_f = 30.0$ but are differing in the parameters N_t and T. Figures (a)-(d) correspond to different gates: (a) $11X$, (b) $1X1$, (c) 1CNOT, and (d) $1\sqrt{\text{SWAP}}$.

We observe that the decay curve is not dependent on the gate. A deviation is only visible if the undisturbed gate fidelity is differing from gate to gate for given N_t and T. Furthermore, we state that even for equally total time, there is a difference in the decay of the average fidelity depending on the parameters set $\{N_t, T\}$. The behaviour illustrated in Fig. 7 bears resemblance to the *motional narrowing* [16] occurring in nuclear magnetic resonance (NMR) experiments in that for shorter time intervals ('pulse timings') T (or equivalently larger 'switching rate' $1/T$) the system is less affected by the randomness in the control field.

4.5.2 Procedure B

After having discussed the sensitivity of the fidelity for gates achieved by applying a control field in x- and y-direction, we now address ourself to the case where we are controlling only the x-field. We review that control of the x-field is enough for implementing our standard spin-flip gate $11X$. The sensitivity of the fidelity to random noise for implementations of the spin-flip gate is analysed analogously to the proceeding in the previous section. Figure 8 contains plots of $\bar{F}$ versus δ for random noise affected optimal fields. The data plotted in 8(a) correspond to optimal control fields which are achieved by taking 70 time steps and differ in T. In 8(b) T is fixed to 0.5 while N_t is varied and in 8(c), finally, the total evolution time is equal to 25.0 for all fields while N_t and T are variable.
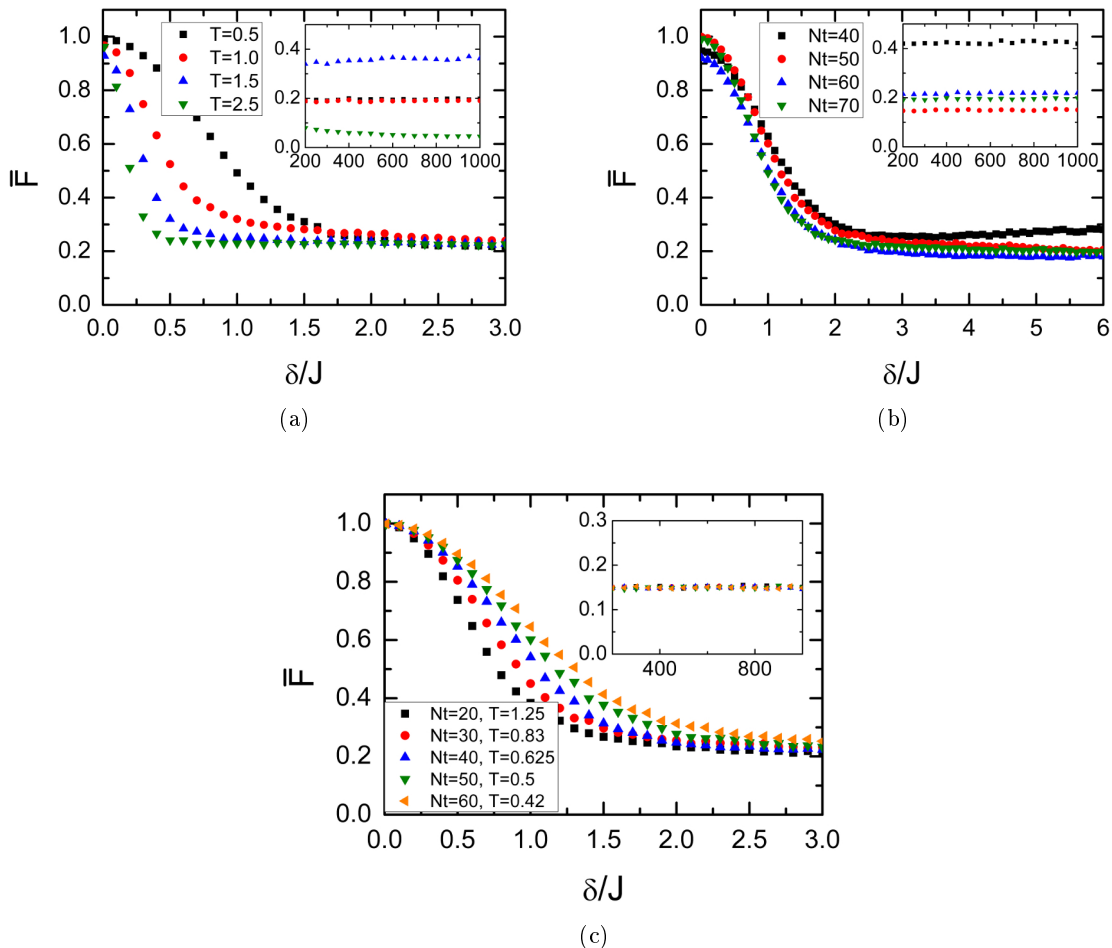

(a)

(b)

(c)

Figure 8: Average fidelity $\bar{F}$ versus δ for random noise affected optimal fields (optimal refers here to a fidelity above 0.9). Fixed parameters are: (a) $N_t = 70$, (b) $T = 0.5$, and (c) $t_f = 25.0$. The small figures show the behaviour of the average fidelity for large δ.

We observe the same dependence on the parameters N_t, T and t_f as seen before for the case where we control the x- and y-field. But while for controlling the x- and y-field the average fidelity saturates to a universal value, there exists no universal saturation in the case of procedure B as becomes obvious by considering the plots of the average fidelity versus large δ (see the small figures contained in Figs. 8(a), 8(b), and 8(c). We dare the following explanation:

In contrast to procedure A controlling only the x-field does not enable universal quantum computation which means that we only may implement the unitaries contained in a Lie subgroup of $SU(d)$. The Lie algebra of this subgroup is generated by the set $\{-iH_0, -iS_{1x}\}$ (see Section 4.3). While $SU(d)$ is a compact Lie group with a finite Haar measure defined on it, an arbitrary Lie-subgroup of $SU(d)$ is locally compact but not necessarily compact. That is, we cannot act on the assumption that the reachable set of unitary operators for control of the x-field forms a compact group. Hence, the uniform Haar measure, which measures uniformly distributed random unitaries, may be infinite. Furthermore, the reachable set of unitaries for a system at time t_f is dependent on the value of t_f. The control fields of Figs. 8(a) and 8(b) differ in their acting time, i.e. in the product $t_f = N_t T$. Therefore the reachable set may differ in these cases and explain the different saturation values. The fact that $\bar{F}$ of the cases plotted in 8(c), which all correspond to the same t_f, saturates for all fields to the same value, seems to confirm this explanation.

4.6 Search for smoothened optimal control fields

For mathematical and computational convenience we have chosen the controls to be piecewise constant functions. However, practical implementations require the imposition of constraints on the control fields, for instance on the frequency spectrum, to generate smoother controls. In practice a jump in the control leads to very high frequency components in the power spectrum of the Fourier transformed control fields. In order to produce optimal control fields which are smoother than the piecewise constant controls, we Fourier transform the piecewise constant optimal fields, apply spectral filtering techniques to the Fourier transformed fields and after that transform back to the time domain. To begin with we calculate in the subsequent chapter the Fourier transform of the piecewise constant control fields and point out its properties.

4.6.1 Fourier transform

We derive in the following an expression for the Fourier transform of the piecewise constant control fields. At this we focus on the case where we switch between controls pointing in the x- and y-direction (procedure A). The control field in this case is described by the vector

$$\vec{h}(t) = \begin{pmatrix} h_x(t) \\ h_y(t) \\ 0 \end{pmatrix}. \tag{4.6.1}$$

In order to derive a concise expression for the control field, we write it in terms of the Heaviside function

$$\theta(x) = \begin{cases} 1, & x \geq 0 \\ 0, & x < 0 \end{cases}. \tag{4.6.2}$$

Using the Heaviside function, we define box functions $\theta_x^n(t)$ and $\theta_y^n(t)$ as follows:

$$\theta_x^n(t) := \theta[t - 2(n-1)T] - \theta[t - (2n-1)T] = \begin{cases} 1, & 2(n-1)T \leq t < (2n-1)T \\ 0, & \text{otherwise} \end{cases}, \tag{4.6.3}$$

$$\theta_y^n(t) := \theta[t - (2n-1)T] - \theta[t - 2nT] = \begin{cases} 1, & (2n-1)T \leq t < 2nT \\ 0, & \text{otherwise} \end{cases}. \tag{4.6.4}$$

In terms of $\theta_x^n(t)$ and $\theta_y^n(t)$ the control fields $h_x(t)$ and $h_y(t)$ may be written as

$$h_x(t) = \sum_{n=1}^{N_t/2} h_{x,n} \theta_x^n(t), \tag{4.6.5}$$

$$h_y(t) = \sum_{n=1}^{N_t/2} h_{y,n} \theta_y^n(t). \tag{4.6.6}$$

The Fourier transform of the fields $h_x(t)$ and $h_y(t)$ corresponds to the Fourier transform of a sum of box functions which is equal to the sum of the Fourier transformed box functions. At this point we note that for the case, where we control only the x-field (procedure B) and hence apply in each time interval T a field in x-direction, we have to replace the factor $2(n-1)$ by $(n-1)$ and the factor $(2n-1)$ by n in (4.6.3) and in (4.6.5) we have to sum from 1 to N_t instead of summing from 1 to $N_t/2$. Up to these modifications the calculation of the Fourier transform of the field $h_x(t)$ which follows here for procedure A is valid as well for procedure B.

Next, we look at the Fourier transform of the box functions $\theta_a(t)$ for some real positive parameter a defined as

$$\theta_a(t) = \begin{cases} 1, & -a \le t < a \\ 0, & \text{otherwise} \end{cases}, \tag{4.6.7}$$

and $\theta_b(t)$ with b_1, b_2 being real and $b_1 < b_2$,

$$\theta_b(t) = \begin{cases} 1, & b_1 \le t < b_2 \\ 0, & \text{otherwise} \end{cases}. \tag{4.6.8}$$

The Fourier transform of these two single box functions can be derived as:

$$\widehat{\theta_a}(\omega) = \frac{1}{\sqrt{2\pi}} \int_{-\infty}^{+\infty} \theta_a(t) e^{i\omega t} dt = \frac{1}{\sqrt{2\pi}} \int_{-a}^{a} e^{i\omega t} dt = \sqrt{\frac{2}{\pi}} \int_{0}^{a} \cos(\omega t) dt$$

$$= \sqrt{\frac{2}{\pi}} \frac{\sin(\omega a)}{\omega} = \sqrt{\frac{2}{\pi}} a \operatorname{sinc}(\omega a), \tag{4.6.9}$$

$$\widehat{\theta_b}(\omega) = \frac{1}{\sqrt{2\pi}} \int_{-\infty}^{+\infty} \theta_b(t) e^{i\omega t} dt = \frac{1}{\sqrt{2\pi}} \int_{b_1}^{b_2} e^{i\omega t} dt$$

$$= \frac{1}{\sqrt{2\pi} i\omega} \left(e^{i\omega b_2} - e^{i\omega b_1} \right). \tag{4.6.10}$$

We state that the Fourier transform of the even box function $\theta_a(t)$ is real and determined by the *sinc (sinus cardinalis) function*, $\operatorname{sinc}(x) := \frac{\sin x}{x}$, which is a non-periodic damped sine function and also known as *sampling function* (see Fig. 9).

The peak of $\widehat{\theta_a}(\omega)$ at $\omega = 0$ is equal to $\sqrt{\frac{2}{\pi}} a$ and occurs due to the convergence of $\operatorname{sinc}(x)$ to 1 in the limit $x \to 0$. The other peaks are occurring with a period of $2\pi/a$ relative to each other, caused by the period of $\sin(\omega a)$, and their amplitudes are decaying with $1/\omega$.
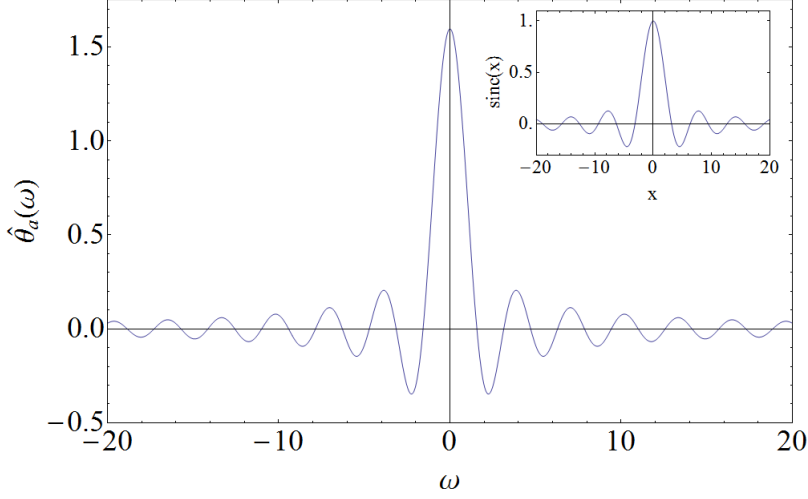
Figure 9: The Fourier transform of the even box function $\theta_a(t)$, here plotted for $a = 2.0$, is determined by the sinc function.

The Fourier transform of a box function which is not even, as the function $\theta_b(t)$ for $b_1 \neq -b_2$, however, is not real but complex, given by a superposition of two complex exponential functions. Our control fields $h_x(t)$ and $h_y(t)$ are described by box functions which are obviously not even wherefore their Fourier transforms, $\widehat{h_x}(\omega)$ and $\widehat{h_y}(\omega)$, become complex as we see in the following:

$$
\begin{aligned}
\widehat{h_x}(\omega) &= \frac{1}{\sqrt{2\pi}} \int_{-\infty}^{\infty} h_x(t) e^{i\omega t} dt \\
&= \frac{1}{\sqrt{2\pi}} \int_{-\infty}^{\infty} \sum_{n=1}^{N_t/2} h_{x,n} \theta_x^n(t) e^{i\omega t} dt \\
&= \frac{1}{\sqrt{2\pi}} \sum_{n=1}^{N_t/2} h_{x,n} \int_{-\infty}^{\infty} \theta_x^n(t) e^{i\omega t} dt \\
&= \frac{1}{\sqrt{2\pi}} \sum_{n=1}^{N_t/2} h_{x,n} \int_{2(n-1)T}^{(2n-1)T} e^{i\omega t} dt \\
&= \frac{1}{\sqrt{2\pi} i\omega} \sum_{n=1}^{N_t/2} h_{x,n} \left(e^{(2n-1)i\omega T} - e^{2(n-1)i\omega T} \right).
\end{aligned}
\tag{4.6.11}
$$

We note that the Fourier transform of the n-th box function $\theta_x^n(t)$ is given by

$$
\frac{1}{\sqrt{2\pi} i\omega} h_{x,n} \left(e^{(2n-1)i\omega T} - e^{2(n-1)i\omega T} \right).
\tag{4.6.12}
$$

Analogously we derive the Fourier transformed y-field as

$$
\widehat{h_y}(\omega) = \frac{1}{\sqrt{2\pi} i\omega} \sum_{n=1}^{N_t/2} h_{y,n} \left(e^{2ni\omega T} - e^{(2n-1)i\omega T} \right).
\tag{4.6.13}
$$

We intend to calculate the real and imaginary part of $\widehat{h_x}(\omega)$ and $\widehat{h_y}(\omega)$ and define for this purpose

$$
\begin{aligned}
f_{Re}^x(\omega) &:= \sin\left[(2n-1)\omega T\right] - \sin\left[2(n-1)\omega T\right], & \text{(4.6.14a)} \\
f_{Re}^y(\omega) &:= \sin\left[2n\omega T\right] - \sin\left[(2n-1)\omega T\right], & \text{(4.6.14b)} \\
f_{Im}^x(\omega) &:= \cos\left[(2n-1)\omega T\right] - \cos\left[2(n-1)\omega T\right], & \text{(4.6.14c)} \\
f_{Im}^y(\omega) &:= \cos\left[2n\omega T\right] - \cos\left[(2n-1)\omega T\right]. & \text{(4.6.14d)}
\end{aligned}
$$

These four functions are combinations of two sine and cosine functions, respectively, and they are periodic for the following reason. At first we note that the fundamental period of the trigonometric functions $f_1(x) = \sin(kx)$ and $f_2(x) = \cos(kx)$ is equal to $2\pi/k$. Now assume, we consider two periodic functions $f(x) = f(x + a)$ and $g(x) = g(x + b)$ with periods a and b, respectively, and the combination of these; $h(x) = f(x) + g(x)$. The periods a and b are assumed to be given by $a = r_1 s$ and $b = r_2 s$ with r_1 and r_2 being rational numbers and s being some arbitrary real number. Under this assumption the combined function $h(x)$ is periodic as well having a period of rs where r is obtained as the least common multiple of the rational numbers r_1 and r_2. The least common multiple of two rational numbers may be found as the least common multiple of the numerators divided by the highest common fraction of the denominators. Thus, the period of the functions defined in Eqs. (4.6.14a) to (4.6.14d) is equal to $2\pi/T$ for any positive integer n since the least common multiple of $1/n_1$ and $1/n_2$ for two positive integers n_1 and n_2 with $n_1 = n_2 + 1$ is equal to 1.

In terms of (4.6.14a) to (4.6.14d) the real part of the Fourier transformed fields is given by

$$\mathrm{Re}[\widehat{h_x}(\omega)] = \frac{1}{\sqrt{2\pi}\omega} \sum_{n=1}^{N_t/2} h_{x,n} f_{Re}^x(\omega), \tag{4.6.15}$$

$$\mathrm{Re}[\widehat{h_y}(\omega)] = \frac{1}{\sqrt{2\pi}\omega} \sum_{n=1}^{N_t/2} h_{y,n} f_{Re}^y(\omega), \tag{4.6.16}$$

and the imaginary part by

$$\mathrm{Im}[\widehat{h_x}(\omega)] = -\frac{1}{\sqrt{2\pi}\omega} \sum_{n=1}^{N_t/2} h_{x,n} f_{Im}^x(\omega), \tag{4.6.17}$$

$$\mathrm{Im}[\widehat{h_y}(\omega)] = -\frac{1}{\sqrt{2\pi}\omega} \sum_{n=1}^{N_t/2} h_{y,n} f_{Im}^y(\omega). \tag{4.6.18}$$

We point out that the real part of the Fourier transforms is even while the imaginary part is odd. The power spectrum (absolute square) of the Fourier transformed fields may be calculated as follows:

$$|\widehat{h}_j(\omega)|^2 = \mathrm{Re}[\widehat{h}_j(\omega)]^2 + \mathrm{Im}[\widehat{h}_j(\omega)]^2, \quad j = x, y. \tag{4.6.19}$$

For the sake of completeness we note the *Parseval's theorem* which reveals the unitarity of the Fourier transform:

$$\int_{-\infty}^{+\infty} |h_j(t)|^2 dt = \int_{-\infty}^{+\infty} |\widehat{h}_j(\omega)|^2 d\omega, \quad j = x, y. \tag{4.6.20}$$

In order to analyse the shape of the Fourier transforms, we consider at first constant fields $h_x(t)$ and $h_y(t)$, i.e. we set all components equal to 1. The real and imaginary part of the Fourier transform simplifies then to

$$\mathrm{Re}[\widehat{h}_j(\omega)] = \frac{1}{\sqrt{2\pi}\omega} \sum_{n=1}^{N_t/2} f_{Re}^j(\omega), \tag{4.6.21}$$

$$\mathrm{Im}[\widehat{h}_j(\omega)] = -\frac{1}{\sqrt{2\pi}\omega} \sum_{n=1}^{N_t/2} f_{Im}^j(\omega), \tag{4.6.22}$$

with $j = x, y$. In Fig. 10 the real, imaginary part and the power spectrum of the Fourier transform are plotted for such constant fields using the parameters $N_t = 70$ and $T = 0.5$. The calculation of the Fourier transform and its real, imaginary part and power spectrum is done analytically using Mathematica.
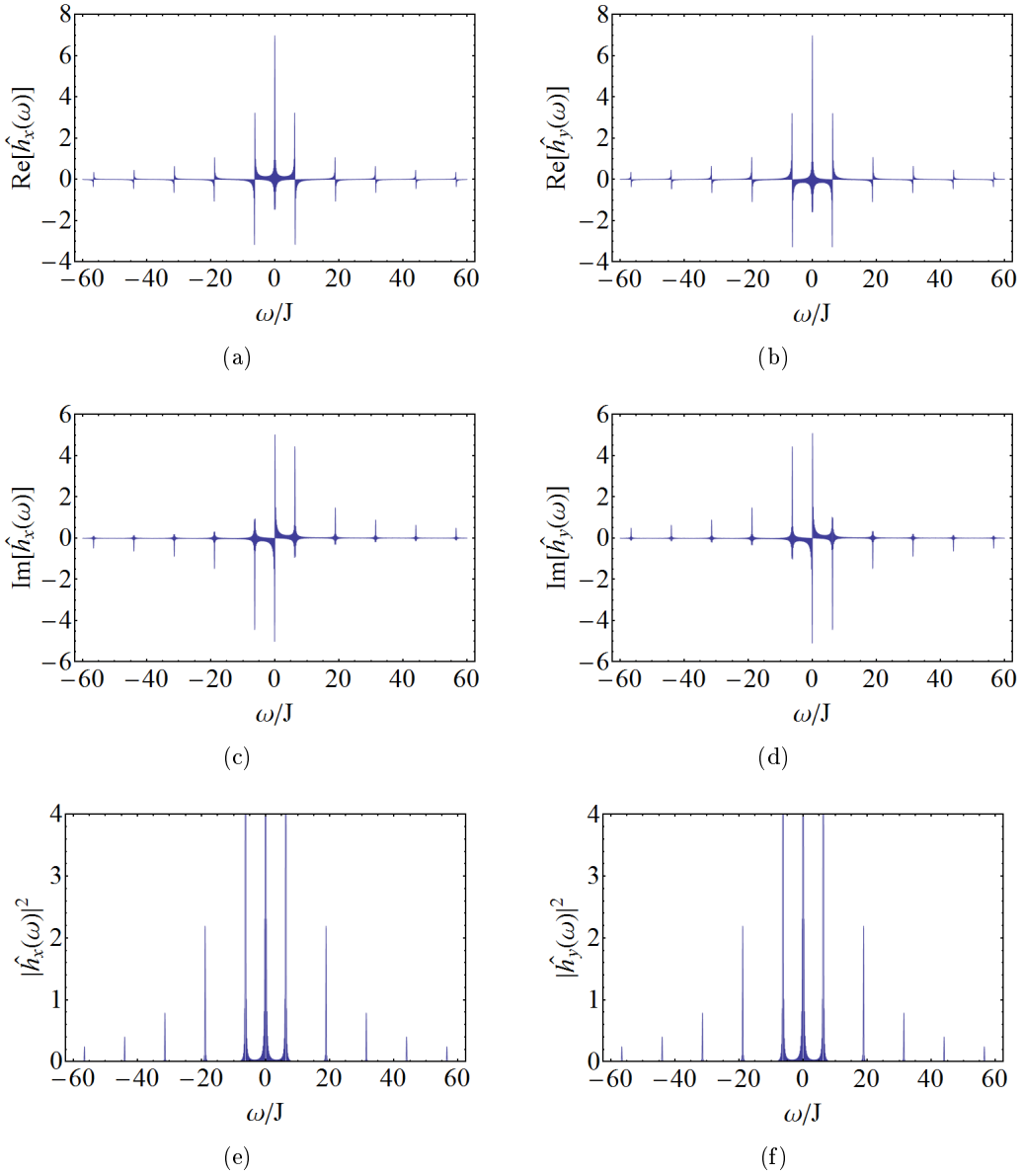
39

Figure 10: Real, imaginary part and power spectrum of a Fourier transformed constant field (all components set to 1) which is far from optimal, for $N_t = 70$ and $T = 0.5$. The left column contains the plots corresponding to the Fourier transformed x-field, the right column the equivalent plots for the y-field. (a)/(b) $\mathrm{Re}[\widehat{h}_j(\omega)]$, (c)/(d) $\mathrm{Im}[\widehat{h}_j(\omega)]$, and (e)/(f) $|\widehat{h}_j(\omega)|^2$, $j = x, y$.

We analyse the peak occurrence in the plots of Fig. 10. If we do not take into account the positive peak at $\omega = 0$ of the real part and the two peaks (one positive, one negative) of the imaginary part which are converging to the point $\omega = 0$ for $N_t \to \infty$, we notice that the other peaks and pair of peaks (real part), respectively, occur with a period of $2\pi/T$. This period corresponds to the one of the functions $f_{Re}^j(\omega)$ and $f_{Im}^j(\omega)$. The peaks are located either exactly at $\pi/T + k \cdot 2\pi/T$ for integers k as in the case of the imaginary part or are converging for $N_t \to \infty$ to these locations from the left and from the right as in the case of the real part, resulting in two peaks, one in the negative, one in the positive. The appearance of the additional peak at $\omega = 0$ of the real part is caused by the factor $1/\omega$ as may be seen calculating the limit of the real part for $\omega \to 0$. In order to do this, we expand the function $\frac{\sin(\omega a)}{\omega}$, with a being an arbitrary real multiplication factor, into Taylor series:

$$\sin(\omega a) = \sum_{k=0}^{\infty} (-1)^k \frac{(\omega a)^{2k+1}}{(2k+1)!}, \tag{4.6.23}$$

and hence,

$$\frac{\sin{(\omega a)}}{\omega} = \sum_{k=0}^{\infty} (-1)^k \frac{\omega^{2k} a^{2k+1}}{(2k+1)!}. \tag{4.6.24}$$

The limit for $\omega \to 0$ evaluates to

$$\lim_{\omega^{\pm} \to 0} \frac{\sin{(\omega a)}}{\omega} = a, \tag{4.6.25}$$

where $\omega^+ \to 0$ and $\omega^- \to 0$ denote the two possible directions from which we may converge to zero, namely starting in the positive $(+)$ or starting in the negative $(-)$. We note that the singularity of $\frac{\sin{(\omega a)}}{\omega}$ at $\omega = 0$ is removable since the limit (4.6.25) exists and is finite. Using Eqs. (4.6.14a), (4.6.14b), and (4.6.25), the limit of the real part for $\omega \to 0$ may be calculated straightforward:

$$\begin{aligned}
\lim_{\omega^{\pm} \to 0} \mathrm{Re}[\widehat{h_x}(\omega)] &= \lim_{\omega^{\pm} \to 0} \frac{1}{\sqrt{2\pi}\omega} \sum_{n=1}^{N_t/2} f_{Re}^x(\omega) \\
&= \frac{1}{\sqrt{2\pi}} \sum_{n=1}^{N_t/2} \lim_{\omega^{\pm} \to 0} \frac{1}{\omega} f_{Re}^x(\omega) \\
&= \frac{1}{\sqrt{2\pi}} \sum_{n=1}^{N_t/2} [(2n-1)T - 2(n-1)T] \\
&= \frac{1}{\sqrt{2\pi}} \sum_{n=1}^{N_t/2} T \\
&= \frac{1}{\sqrt{2\pi}} \cdot \frac{N_t}{2} \cdot T, \tag{4.6.26}
\end{aligned}$$

and analogously

$$\lim_{\omega^{\pm} \to 0} \mathrm{Re}[\widehat{h_y}(\omega)] = \frac{1}{\sqrt{2\pi}} \cdot \frac{N_t}{2} \cdot T. \tag{4.6.27}$$

On the other hand, in order to calculate the imaginary part in the limit $\omega \to 0$, we make use of the series expansion for $\frac{\cos{(\omega a)}}{\omega}$:

$$\cos{(\omega a)} = \sum_{k=0}^{\infty} (-1)^k \frac{(\omega a)^{2k}}{(2k)!}, \tag{4.6.28}$$

and hence,

$$\frac{\cos{(\omega a)}}{\omega} = \sum_{k=0}^{\infty} (-1)^k \frac{\omega^{2k-1} a^{2k}}{(2k)!}. \tag{4.6.29}$$

The limit for $\omega \to 0$ is therefore derived as

$$\lim_{\omega^{\pm} \to 0} \frac{\cos{(\omega a)}}{\omega} = \lim_{\omega^{\pm} \to 0} \frac{1}{\omega} = \pm\infty, \tag{4.6.30}$$

and we note

$$\lim_{\omega^{\pm} \to 0} \left(\frac{\cos{(\omega a)}}{\omega} - \frac{\cos{(\omega b)}}{\omega} \right) = 0, \quad \text{for arbitrary real numbers } a \text{ and } b. \tag{4.6.31}$$

The singularity of $\frac{\cos{(\omega a)}}{\omega}$ at $\omega = 0$ is a pole since the limit (4.6.31) is infinite. Using Eqs. (4.6.14c), (4.6.14d), and (4.6.31), the limit of the imaginary part for $\omega \to 0$ evaluates to

$$\lim_{\omega^{\pm} \to 0} \mathrm{Im}[\widehat{h}_j(\omega)] = \frac{1}{\sqrt{2\pi}} \sum_{n=1}^{N_t/2} \lim_{\omega^{\pm} \to 0} \frac{1}{\omega} f_{Im}^j(\omega) = 0, \quad j = x, y. \tag{4.6.32}$$

The two peaks, one in the positive, one in the negative, which are located close to $\omega = 0$ for $N_t = 70$, are converging to the point $\omega = 0$ for $N_t \to \infty$. We note that the height of the other peaks is equal to $\pm \frac{1}{\sqrt{2\pi}} \cdot \frac{1}{\omega} \cdot N_t$ in the case of the imaginary part since $f_{Im}^x(\omega) = -2$ and $f_{Im}^y(\omega) = 2$ for $\omega = \pi/T + k \cdot 2\pi/T$ and any integer k. In the case of the real part the height of the peaks are as well proportional to N_t/ω. Up to now we have considered a constant field where all components are set to 1. The height of the peaks will of course be dependent on this constant value and be the higher (in the negative or the positive) the larger this value is which means the stronger the field is. If the values of the field components are different, the sharp peaks may disappear and split instead into several peaks which form kind of wave packets or say distributions of a certain width. Negative values of the field components may shift the occurrence of the peaks and lead to additional and/or missing peaks depending on whether constructive or destructive interference is dominating. We note that the underlying fundamental period of $2\pi/T$ may be visible in the majority of cases.
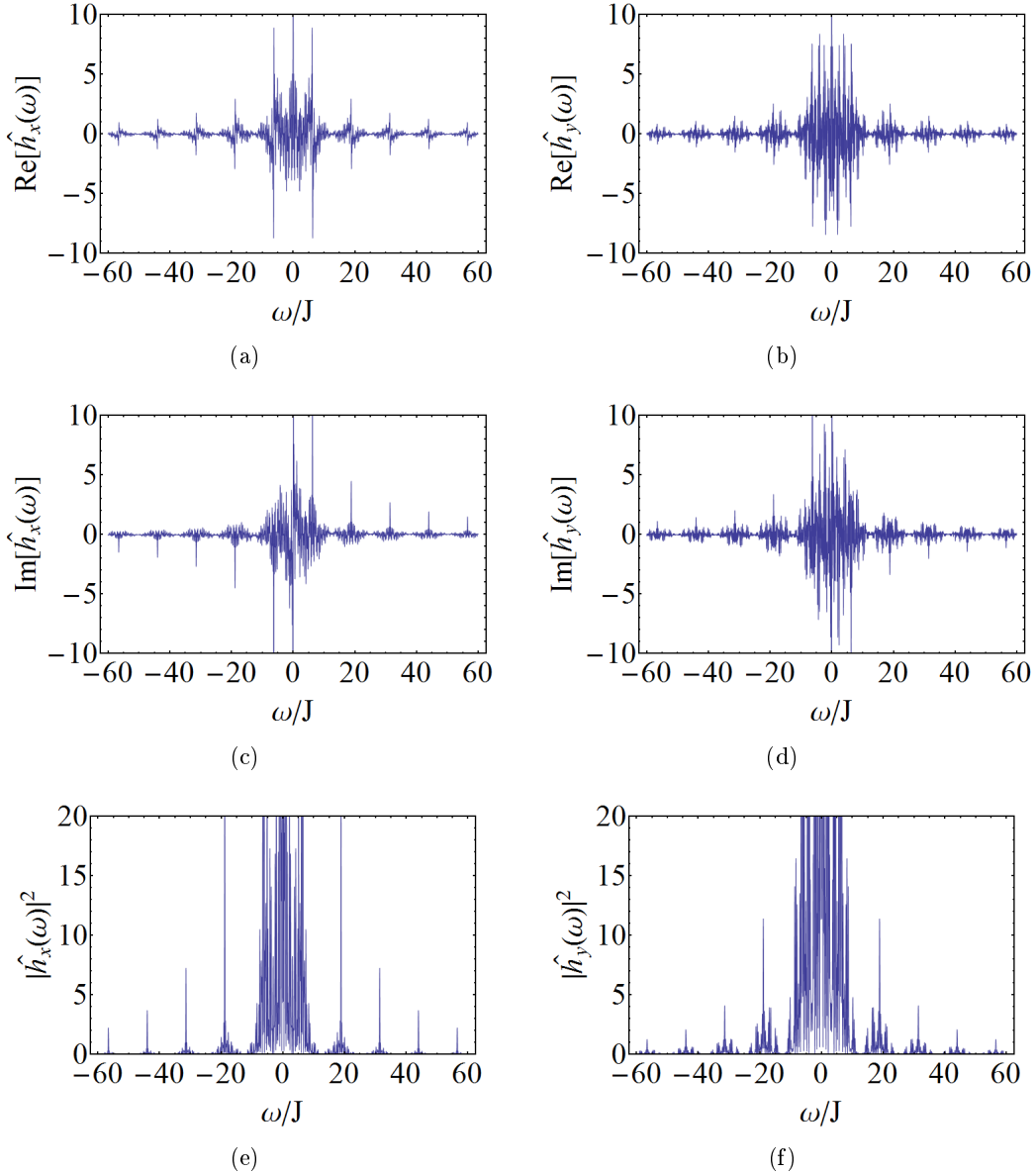

Figure 11: The same plots as in Fig. 10, but done here for a Fourier transformed optimal control field reached for $N_t = 70$ and $T = 0.5$. This optimal field is the same as the one of Fig. 3.

Figure 11 shows the real, imaginary part and power spectrum of a Fourier transformed optimal control field. The used optimal field corresponds to the one plotted in Fig. 3. We notice that the shape of the Fourier transformed optimal field is determined by the shape of the underlying sum over the Fourier transforms of box functions. There is no information contained in the Fourier transform which would allow to distinguish between optimal and not optimal fields.

4.6.2 Smoothing filters

We search for optimal control fields which are smoother than our implemented piecewise constant controls and nevertheless approximate the considered target gates well with high corresponding fidelities. For this purpose we put constraints on the frequency spectrum which is generated by the Fourier transforms of the optimal piecewise constant control fields $h_j(t)$ $(j = x, y)$. We formulate the spectral constraint by means of a so-called frequency filter function $f_j(\omega)$ [17] which is applied to the Fourier transformed fields. After operating with the filter function on the Fourier transforms of the optimal fields, we return to the time domain and recalculate the time dependent control fields by doing inverse Fourier transforms. The thus obtained filtered fields are denoted $\widetilde{h}_j(t)$. In order to derive a concise expression for $\widetilde{h}_j(t)$, we use here the shorthand $\mathcal{F}$ for the Fourier transform and $\mathcal{F}^{-1}$ for its inverse:

$$\widetilde{h}_j(t) = \mathcal{F}^{-1}[f_j(\omega)\mathcal{F}[h_j(t)]], \quad j = x, y, \tag{4.6.33}$$

where $\mathcal{F}[h_j(t)]$ is equivalent to the above introduced notation $\widehat{h}_j(\omega)$. We note that any real filter function $f_j(\omega)$ has to be an even function in ω, i.e. $f_j(\omega) = f_j(-\omega)$, since $\widetilde{h}_j(t)$ is real valued.

Proof. $h_j(t)$ real, i.e. $h_j^*(t) = h_j(t) \Rightarrow \widehat{h}_j^{\,*}(\omega) = \int_{-\infty}^{+\infty} h_j(t)e^{-i\omega t}dt = \widehat{h}_j(-\omega)$, together with $\widetilde{h}_j(t)$ real, i.e $\widetilde{h}_j^*(t) = \widetilde{h}_j(t)$ whereas $\widetilde{h}_j(t)$ and $\widetilde{h}_j^*(t)$ are given by $\widetilde{h}_j(t) = \int_{-\infty}^{+\infty} f_j(\omega)\widehat{h}_j(\omega)e^{-i\omega t}d\omega$ and $\widetilde{h}_j^*(t) = \int_{-\infty}^{+\infty} f_j^*(\omega)\widehat{h}_j(-\omega)e^{+i\omega t}d\omega$, it follows directly that $f_j(\omega)$ must fulfill $f_j^*(\omega) = f_j(-\omega)$, $f_j(\omega)$ real $\Rightarrow f_j(\omega) = f_j(-\omega)$ $\qquad\square$

In principle, all frequency filters may as well be implemented in the time domain provided that a time-dependent filter function which effects the desired filtering is known. Multiplication in the Fourier space is equivalent to convolution in the inverse Fourier space. Therefore any frequency filter can be realized in the time domain or at least approximated by convolution with the Fourier transform of the frequency filter. Since we desire to find smoother fields, we have to use filter functions which attenuate high frequencies. Attenuating low frequencies on the other hand would enhance the edges in the time domain. In the frequency domain there exist straightforward filters which attenuate high frequencies as low-pass or Gaussian filters wherefore we will perform the filtering in the frequency space.

As in the previous chapter we perform the following calculations of smoothened control fields only for procedure A since an expression for the field $\widetilde{h}_x(t)$ by using procedure B can be derived straightforward, just by replacing $2(n-1)$ by $(n-1)$ and $(2n-1)$ by n as well as the sum from 1 to $N_t/2$ by a sum from 1 to N_t in the corresponding formula.

Low-pass filter:

At first we consider low-pass filtering. We will implement the simplest low-pass filter which is the *ideal low-pass*. That is, we apply in the frequency domain a filter function to the Fourier transformed fields which removes all frequency components above a certain cut-off frequency ω_0 and below $-\omega_0$, only passing low-frequency signals. An ideal low-pass filter perfectly passes low frequencies while high-frequency signals are cut perfectly, not only attenuated. The filter function effecting the desired filtering corresponds then to a combination of Heaviside functions, namely to the box function

$$f_j(\omega) = \theta(\omega + \omega_0) - \theta(\omega - \omega_0), \quad j = x, y, \tag{4.6.34}$$

which is even as can be seen by inspection. We note that the rectangular function is the frequency response of the low-pass filter while the sinc function is the impulse response in the time domain, i.e. the Fourier transform of the even box function is given by a sinc function as we already have seen. After applying the filter functions $f_x(\omega)$ and $f_y(\omega)$ to the Fourier transformed optimal control fields, we calculate the 'smoothened' fields $\widetilde{h}_x(t)$ and $\widetilde{h}_y(t)$ via inverse Fourier transform:

$$
\begin{aligned}
\widetilde{h}_x(t) &= \frac{1}{\sqrt{2\pi}} \int_{-\infty}^{+\infty} f_x(\omega)\widehat{h_x}(\omega)e^{-i\omega t}d\omega \\
&= \frac{1}{\sqrt{2\pi}} \int_{-\infty}^{+\infty} [\theta(\omega + \omega_0) - \theta(\omega - \omega_0)]\widehat{h_x}(\omega)e^{-i\omega t}d\omega \\
&= \frac{1}{\sqrt{2\pi}} \int_{-\omega_0}^{\omega_0} \widehat{h_x}(\omega)e^{-i\omega t}d\omega \\
&= \frac{1}{\sqrt{2\pi}} \int_{-\omega_0}^{\omega_0} \frac{1}{\sqrt{2\pi}i\omega} \sum_{n=1}^{N_t/2} h_{x,n} \left(e^{(2n-1)i\omega T} - e^{2(n-1)i\omega T} \right) e^{-i\omega t}d\omega \\
&= \frac{1}{2\pi i} \sum_{n=1}^{N_t/2} h_{x,n} \int_{-\omega_0}^{\omega_0} \frac{1}{\omega} \left(e^{i\omega[(2n-1)T-t]} - e^{i\omega[2(n-1)T-t]} \right) d\omega \\
&= \frac{1}{2\pi i} \sum_{n=1}^{N_t/2} h_{x,n} \left(\int_{-\omega_0}^{\omega_0} \frac{1}{\omega}e^{i\omega[(2n-1)T-t]}d\omega - \int_{-\omega_0}^{\omega_0} \frac{1}{\omega}e^{i\omega[2(n-1)T-t]}d\omega \right). \quad (4.6.35)
\end{aligned}
$$

The integral $I(\omega_0 a) := \int_{-\omega_0}^{\omega_0} \frac{1}{\omega}e^{i\omega a}d\omega$ which we regard as a function of $\omega_0 a$ for some real variable a can be decomposed into two parts:

$$
\begin{aligned}
I(\omega_0 a) &= \int_{-\omega_0}^{\omega_0} \frac{1}{\omega}[\cos(\omega a) + i\sin(\omega a)]d\omega \\
&= \int_{-\omega_0}^{\omega_0} \frac{\cos(\omega a)}{\omega}d\omega + i \int_{-\omega_0}^{\omega_0} \frac{\sin(\omega a)}{\omega}d\omega. \quad (4.6.36)
\end{aligned}
$$

In order to assign a value to the first integral in (4.6.36) we have to make use of the Cauchy principal value since we intend to integrate over a pole ($\omega = 0$) of the integrand. By means of the Cauchy principal value $\mathcal{P}$ we may write

$$
\mathcal{P} \int_{-\omega_0}^{\omega_0} \frac{\cos(\omega a)}{\omega}d\omega = \lim_{\epsilon \to 0} \left(\int_{-\omega_0}^{-\epsilon} \frac{\cos(\omega a)}{\omega}d\omega + \int_{+\epsilon}^{\omega_0} \frac{\cos(\omega a)}{\omega}d\omega \right). \quad (4.6.37)
$$

Since $\cos(\omega a)$ is an even function while ω is odd which means that $\frac{\cos(\omega a)}{\omega}$ is an odd function in ω, the Cauchy principal value defined in (4.6.37) is equal to zero. On the other hand, $\frac{\sin(\omega a)}{\omega}$ is an even function in ω since $\sin(\omega a)$ is odd. The singularity of $\frac{\sin(\omega a)}{\omega}$ at $\omega = 0$ is removable for which reason we do not need the Cauchy principal value for evaluating the second integral in (4.6.36). After these considerations $I(\omega_0 a)$ simplifies to

$$
I(\omega_0 a) = 2i \int_0^{\omega_0} \frac{\sin(\omega a)}{\omega}d\omega, \quad (4.6.38)
$$

and the expression for $\widetilde{h}_x(t)$ to

$$
\begin{aligned}
\widetilde{h}_x(t) &= \frac{1}{2\pi i} \sum_{n=1}^{N_t/2} h_{x,n} \left(2i \int_0^{\omega_0} \frac{\sin\{\omega[(2n-1)T-t]\}}{\omega}d\omega - 2i \int_0^{\omega_0} \frac{\sin\{\omega[2(n-1)T-t]\}}{\omega}d\omega \right) \\
&= \frac{1}{\pi} \sum_{n=1}^{N_t/2} h_{x,n} \left(\int_0^{\omega_0} \frac{\sin\{\omega[(2n-1)T-t]\}}{\omega}d\omega - \int_0^{\omega_0} \frac{\sin\{\omega[2(n-1)T-t]\}}{\omega}d\omega \right).
\end{aligned}
$$
$$(4.6.39)$$

Analogously we obtain

$$\widetilde{h}_y(t) = \frac{1}{\pi} \sum_{n=1}^{N_t/2} h_{y,n} \left(\int_0^{\omega_0} \frac{\sin\{\omega[2nT-t]\}}{\omega} d\omega - \int_0^{\omega_0} \frac{\sin\{\omega[(2n-1)T-t]\}}{\omega} d\omega \right). \quad (4.6.40)$$

The integral $\mathrm{Si}(\omega_0 a) := \int_0^{\omega_0} \frac{\sin(\omega a)}{\omega} d\omega$, regarded as a function of $\omega_0 a$, can be rewritten using the series expansion for $\sin(\omega a)$ (see Eq. (4.6.24)) as

$$\begin{aligned}
\mathrm{Si}(\omega_0 a) &= \int_0^{\omega_0} \sum_{k=0}^{\infty} (-1)^k \frac{\omega^{2k} a^{2k+1}}{(2k+1)!} d\omega \\
&= \sum_{k=0}^{\infty} (-1)^k \frac{(\omega a)^{2k+1}}{(2k+1)(2k+1)!} \bigg|_0^{\omega_0} \\
&= \sum_{k=0}^{\infty} (-1)^k \frac{(\omega_0 a)^{2k+1}}{(2k+1)(2k+1)!}.
\end{aligned} \quad (4.6.41)$$

At first we remark that $\mathrm{Si}(\omega_0 a) = \int_0^{\omega_0} \frac{\sin(\omega a)}{\omega} d\omega$ is given by an infinite series which converges for all $\omega_0 a$. Considering the series or by applying substitution rules on the integral ($u = -\omega a$ and $v = -u$, respectively), we see that the following relations hold:

$$\mathrm{Si}(\omega_0 a) = \int_0^{\omega_0} \frac{\sin(\omega a)}{\omega} d\omega = \int_0^{\omega_0 a} \frac{\sin\omega}{\omega} d\omega \quad \text{and} \quad \mathrm{Si}(-\omega_0 a) = -\mathrm{Si}(\omega_0 a). \quad (4.6.42)$$

We point out that the integral $\mathrm{Si}(\omega_0 a)$ is known as the *sine integral* with $\omega_0 a$ being the upper limit of the integral and the integrand being the sinc function, $\mathrm{sinc}(\omega) = \frac{\sin\omega}{\omega}$, which has the normalization $\int_{-\infty}^{+\infty} \mathrm{sinc}(\omega) d\omega = 2\int_0^{\infty} \mathrm{sinc}(\omega) d\omega = \pi$. Hence, $\mathrm{Si}(\omega_0 a)$ converges in the limit $\omega_0 a \to \pm\infty$ to $\pm\pi/2$. The integral $\mathrm{Si}(\infty) = \int_0^{\infty} \frac{\sin\omega}{\omega} d\omega$ is known as the *Dirichlet integral*. The sinc function possesses a removable singularity at $\omega = 0$. Removable, since the limit $\lim_{\omega\to 0} \mathrm{sinc}(\omega)$ exists and is finite, namely equal to 1. Moreover, this function is equivalent to the 0-th order spherical Bessel function of the first kind, $j_0(\omega)$. At last, we note that the indefinite integral (or antiderivative) of $\mathrm{sinc}(\omega)$ cannot be expressed in terms of elementary analytical functions, such as polynomials, ratios of polynomials, exponential and trigonometric functions and their inverses, as the above derived expression for $\mathrm{Si}(\omega_0 a)$ reveals. After these considerations the control field $\widetilde{h}_x(t)$ can be written as follows:

$$\begin{aligned}
\widetilde{h}_x(t) &= \frac{1}{\pi} \sum_{n=1}^{N_t/2} h_{x,n} \left(\int_0^{\omega_0[(2n-1)T-t]} \frac{\sin\omega}{\omega} d\omega - \int_0^{\omega_0[2(n-1)T-t]} \frac{\sin\omega}{\omega} d\omega \right) \\
&= \frac{1}{\pi} \sum_{n=1}^{N_t/2} h_{x,n} \left(\sum_{k=0}^{\infty} (-1)^k \frac{\{\omega_0[(2n-1)T-t]\}^{2k+1}}{(2k+1)(2k+1)!} - \sum_{k=0}^{\infty} (-1)^k \frac{\{\omega_0[2(n-1)T-t]\}^{2k+1}}{(2k+1)(2k+1)!} \right) \\
&= \frac{1}{\pi} \sum_{n=1}^{N_t/2} h_{x,n} \sum_{k=0}^{\infty} \frac{(-1)^k}{(2k+1)(2k+1)!} \left(\{\omega_0[(2n-1)T-t]\}^{2k+1} - \{\omega_0[2(n-1)T-t]\}^{2k+1} \right).
\end{aligned}$$
$$(4.6.43)$$

The field $\widetilde{h}_y(t)$ is given entirely equivalent by

$$
\begin{aligned}
\widetilde{h}_y(t) &= \frac{1}{\pi} \sum_{n=1}^{N_t/2} h_{y,n} \left(\int_0^{\omega_0[2nT-t]} \frac{\sin\omega}{\omega} d\omega - \int_0^{\omega_0[(2n-1)T-t]} \frac{\sin\omega}{\omega} d\omega \right) \\
&= \frac{1}{\pi} \sum_{n=1}^{N_t/2} h_{y,n} \sum_{k=0}^{\infty} \frac{(-1)^k}{(2k+1)(2k+1)!} \left(\{\omega_0[2nT-t]\}^{2k+1} - \{\omega_0[(2n-1)T-t]\}^{2k+1} \right).
\end{aligned}
$$
(4.6.44)

We conclude that the calculation of the control fields $\widetilde{h}_x(t)$ and $\widetilde{h}_y(t)$ requires in each case the computation of two sine integrals, indefinite series which cannot be expressed in terms of elementary functions. We compute the sine integrals numerically using the routine cisi provided by the authors of [14]. The cut-off frequency ω_0 is treated as a parameter.

Gaussian filter:

Instead of removing all frequencies above a given cut-off frequency, we now consider so-called Gaussian filters which only retain the Fourier components around a certain centre frequency $\pm\omega_c$. We define the Gaussian filter function in the frequency domain for some real positive parameter γ according to [17] as

$$
f_j(\omega) = e^{-\gamma(\omega-\omega_c)^2} + e^{-\gamma(\omega+\omega_c)^2}, \quad j = x,y \quad \text{and} \quad \gamma > 0.
$$
(4.6.45)

This filter function is chosen to be even as required of any real filter function and effects that only the frequency components around $\pm\omega_c$ are allowed in the resulting pulse. We note that both the frequency and the impulse response of the Gaussian filter are Gaussian functions since the Fourier transform of a Gaussian is a Gaussian again. Gaussian filters act as low-pass filters and have a similar effect depending on the width of the Gaussian function as ideal low-pass filters depending on the cut-off frequency.

If we like to allow the frequencies around several centre frequencies $\pm\omega_k$, say around m different frequencies, the total filter function $f_j^{tot}(\omega)$ is obtained by just summing over single filter functions $f_j^k(\omega)$, each of them corresponding to one of the different centre frequencies:

$$
f_j^{tot}(\omega) = \sum_{k=1}^{m} f_j^k(\omega) = \sum_{k=1}^{m} \left(e^{-\gamma(\omega-\omega_k)^2} + e^{-\gamma(\omega+\omega_k)^2} \right), \quad j = x,y.
$$
(4.6.46)

In order to ensure that the total filter function $f_j^{tot}(\omega)$ is restricted to values in the interval $(0,1]$ we use an ascending order for the frequencies ω_k, i.e. $\omega_k < \omega_{k+1}$, and assume that each of the functions $e^{-\gamma(\omega-\omega_k)^2}$ is operating only on the interval $[C_k, C_{k+1}]$ where $C_k < C_{k+1}$ with C_k, C_{k+1} being positive real numbers and $C_k < \omega_k$, $C_{k+1} > \omega_k$. On the other hand, the functions $e^{-\gamma(\omega+\omega_k)^2}$ are assumed to operate only on the intervals $[-C_{k+1}, -C_k]$.

We summarize briefly several important properties of the Gaussian functions $g_\pm(\omega) = e^{-\gamma(\omega\pm\omega_c)^2}$. The position of the centre of the peak is equal to $\mp\omega_c$ for the curves $g_\pm(\omega)$ and the peak's height equal to 1. The area under the curves $g_\pm(\omega)$ evaluates to

$$
\int_{-\infty}^{+\infty} g_\pm(\omega)d\omega = \int_{-\infty}^{+\infty} e^{-\gamma(\omega\pm\omega_c)^2}d\omega = \sqrt{\frac{\pi}{\gamma}}.
$$
(4.6.47)

The full width at half maximum of the Gaussian functions $g_\pm(\omega)$ is independent of the value of ω_c for which reason we can set ω_c equal to zero and look at the curve $e^{-\gamma\omega^2}$. We search for values of ω where $e^{-\gamma\omega^2}$ is equal to $\frac{1}{2}$. Hence, we have to set $\gamma\omega^2 = \ln 2$. From this equation it follows directly that $e^{-\gamma\omega^2}$ reaches its half maximum at the points $\omega = \pm\sqrt{\frac{\ln 2}{\gamma}}$ and $e^{-\gamma(\omega\pm\omega_c)^2}$

at the points $\omega = \mp\omega_c \pm \sqrt{\frac{\ln 2}{\gamma}}$, respectively. Thus, we derive the full width at half maximum as FWHM $= 2\sqrt{\frac{\ln 2}{\gamma}}$.

We apply the general Gaussian filter function (4.6.46) to the Fourier transformed control fields and recalculate the 'smoothened' fields $\widetilde{h}_x(t)$ and $\widetilde{h}_y(t)$ doing inverse Fourier transform:

$$
\begin{aligned}
\widetilde{h}_x(t) &= \frac{1}{\sqrt{2\pi}} \int_{-\infty}^{+\infty} f_x(\omega)\widehat{h_x}(\omega)e^{-i\omega t}d\omega \\
&= \frac{1}{2\pi i} \sum_{n=1}^{N_t/2} h_{x,n} \int_{-\infty}^{+\infty} \sum_{k=1}^{m} \left(e^{-\gamma(\omega-\omega_k)^2} + e^{-\gamma(\omega+\omega_k)^2} \right) \frac{1}{\omega} \left(e^{i\omega[(2n-1)T-t]} - e^{i\omega[2(n-1)T-t]} \right) d\omega \\
&= \frac{1}{\pi} \sum_{n=1}^{N_t/2} h_{x,n} \int_{0}^{\infty} \sum_{k=1}^{m} \left(e^{-\gamma(\omega-\omega_k)^2} + e^{-\gamma(\omega+\omega_k)^2} \right) \frac{1}{\omega} (\sin\{\omega[(2n-1)T-t]\} - \sin\{\omega[2(n-1)T-t]\})d\omega \\
&= \frac{1}{\pi} \sum_{k=1}^{m} \sum_{n=1}^{N_t/2} h_{x,n} \int_{C_k}^{C_{k+1}} \frac{1}{\omega} e^{-\gamma(\omega-\omega_k)^2} (\sin\{\omega[(2n-1)T-t]\} - \sin\{\omega[2(n-1)T-t]\})d\omega,
\end{aligned}
$$

$$(4.6.48)$$

and the field $\widetilde{h}_y(t)$ is analogously given by

$$
\widetilde{h}_y(t) = \frac{1}{\pi} \sum_{k=1}^{m} \sum_{n=1}^{N_t/2} h_{y,n} \int_{C_k}^{C_{k+1}} \frac{1}{\omega} e^{-\gamma(\omega-\omega_k)^2} (\sin\{\omega[2nT-t]\} - \sin\{\omega[(2n-1)T-t]\})d\omega.
$$

$$(4.6.49)$$

Equations (4.6.48) and (4.6.48) give an expression for control fields filtered by a general Gaussian filter function of the form (4.6.46). Considering Fourier transforms of optimal control fields (see Fig. 11 as an example), we state that the dominating frequencies of the spectra are located close to $\omega = 0$ which is why it seems reasonable to choose as filter function just the single function defined in Eq. (4.6.45) with $\omega_c = 0$ and analyse the shape of the smoothened control fields as well as the corresponding fidelity by varying the parameter γ of the Gaussian. For $\omega_c = 0$ the filter function simplifies to

$$
f_j(\omega) = e^{-\gamma\omega^2}, \quad j = x, y. \tag{4.6.50}
$$

In order to calculate the smoothened x-fields by applying the filter function in Eq. (4.6.50), we have to evaluate integrals of the form

$$
\int_0^\infty \frac{1}{\omega} e^{-\gamma\omega^2} (\sin\{\omega[(2n-1)T-t]\} - \sin\{\omega[2(n-1)T-t]\})d\omega. \tag{4.6.51}
$$

In general, an integral of the form $\int_0^\infty \frac{1}{x} e^{-p^2 x^2} \sin(ax)dx$ evaluates to the infinite sum (see [18])

$$
\sqrt{\pi} \sum_{k=0}^{\infty} \frac{(-1)^k}{k!(2k+1)} \left(\frac{a}{2p} \right)^{2k+1} = \frac{\pi}{2} \mathrm{erf}\left(\frac{a}{2p} \right), \tag{4.6.52}
$$

where $\mathrm{erf}(x)$ is the error function

$$
\mathrm{erf}(x) = \frac{2}{\sqrt{\pi}} \int_0^x e^{-t^2}dt = \frac{2}{\sqrt{\pi}} \sum_{k=0}^{\infty} (-1)^k \frac{x^{2k+1}}{k!(2k+1)}. \tag{4.6.53}
$$

Thus, the integral in Eq. (4.6.51) is given by

$$
\frac{\pi}{2} \left\{ \mathrm{erf}\left[\frac{(2n-1)T-t}{2\sqrt{\gamma}} \right] - \mathrm{erf}\left[\frac{2(n-1)T-t}{2\sqrt{\gamma}} \right] \right\}. \tag{4.6.54}
$$

Finally, we obtain for the smoothened field $\widetilde{h}_x(t)$

$$\widetilde{h}_x(t) = \frac{1}{2} \sum_{n=1}^{N_t/2} h_{x,n} \left\{ \text{erf}\left[\frac{(2n-1)T-t}{2\sqrt{\gamma}}\right] - \text{erf}\left[\frac{2(n-1)T-t}{2\sqrt{\gamma}}\right] \right\}, \quad (4.6.55)$$

and for $\widetilde{h}_y(t)$

$$\widetilde{h}_y(t) = \frac{1}{2} \sum_{n=1}^{N_t/2} h_{y,n} \left\{ \text{erf}\left[\frac{2nT-t}{2\sqrt{\gamma}}\right] - \text{erf}\left[\frac{(2n-1)T-t}{2\sqrt{\gamma}}\right] \right\}. \quad (4.6.56)$$

We compute the error functions contained in the expressions for the filtered fields numerically using an intrinsic Fortran function.

4.6.3   Unitary evolution

In order to determine the fidelity corresponding to the 'smoothened' control fields, we have to calculate the time evolution operator $U(t)$ which is governed by the Hamiltonian $H(t)$. For this purpose we have to solve the equation of motion for $U(t)$, that is, the differential equation

$$i\frac{d}{dt}U(t) = H(t)U(t), \quad (4.6.57)$$

with $H(t) = H_0 + \vec{\widetilde{h}}(t) \cdot \vec{S}_1 = H_0 + \widetilde{h}_x(t)S_{1x} + \widetilde{h}_y S_{1y}$ and $\vec{\widetilde{h}}(t) = (\widetilde{h}_x(t), \widetilde{h}_y(t), 0)$ being the smoothened controlled field. If we write the $d \times d$ matrices $U(t)$ and $H(t)U(t)$ as d^2-dimensional vectors (d: dimension of the Hilbert space), then Eq. (4.6.57) defines a set of d^2 coupled *first-order* ordinary differential equations (ODEs), having the form

$$i\frac{d}{dt}U_{kl}(t) = \sum_{j=1}^{d} H_{kj}(t)U_{jl}(t), \quad k,l = 1,...,d. \quad (4.6.58)$$

We are considering here a so-called *initial value problem*. At the starting value $t_0 = 0$ the time evolution operator is given by $U(0) = \mathbb{1}$ and we desire to find it at some final time $t_f = N_t T$. For our purposes it is essential that the unitarity of the time evolution operator is preserved. Instead of solving the described set of first-order ODEs by using standard Runge-Kutta methods which are, however, not preserving the unitarity, we calculate the evolution operator $U(t)$ in the following way:

We discretize the evolution time of the system during the action of the control into sufficiently small time steps of length τ. The total action time of the control field is given by $t_f = N_t T$. We divide each time interval T into a certain number of time steps m_T. The time length τ between two steps is equal to T/m_T and the total number of steps seen over the whole evolution time t_f of the system is equal to $m_f = N_t m_T$. We assume that during the evolution time τ between two steps the total Hamiltonian is constant, i.e. $H(t) = H^{(k)}$ for $k\tau \le t < (k+1)\tau$ with $k \in \{0,...,m_f-1\}$. Hence, the unitary $U^{(k)}(\tau)$ describing the time evolution during the $(k+1)$-th time interval with length τ is given exactly by $U^{(k)}(\tau) = e^{-iH^{(k)}\tau}$, exactly under the assumption of constant Hamiltonians $H^{(k)}$. The total time evolution operator $U(t_f)$ of the system at the final time t_f can accordingly be derived as the product

$$U(t_f) = \prod_{k=m_f-1}^{0} e^{-iH^{(k)}\tau} = e^{-iH^{(m_f-1)}\tau} \cdot .... \cdot e^{-iH^{(1)}\tau} \cdot e^{-iH^{(0)}\tau}. \quad (4.6.59)$$

The constant Hamiltonians $H^{(k)}$ are given by

$$H^{(k)} = H_0 + \vec{\widetilde{h}}(k\tau) \cdot \vec{S}_1 = H_0 + \widetilde{h}_x(k\tau)S_{1x} + \widetilde{h}_y(k\tau)S_{1y}. \quad (4.6.60)$$

This kind of product-formula approximation becomes more and more accurate with increasing number of time steps and the simultaneous decrease of the distance τ between two steps. We mention that for our purpose it is not difficult to choose τ so small that the time evolution operator can be computed to requisite accuracy. Considering Eq. (4.6.59) we state that the unitary property of the time evolution operator is preserved for any number of time steps m_T, and hence the method is unconditionally stable (see Refs. [19, 20]). In the case of a piecewise constant control field the results for the unitary obtained with this procedure can be considered as being exact. Moreover, for the piecewise constant controlled fields defined by procedures A and B (recall Section 4.3), the obtained results for the unitary are entirely exact for any number of steps m_T. If we set $m_T = 1$ the approach, which we have described here, is equivalent to procedures A and B. This is an important condition for calculating $U(t_f)$ as accurate as possible, since we are starting from optimal piecewise constant control fields which we 'smoothen' by doing Fourier and inverse Fourier transforms.

4.6.4 Results

We apply two different filtering techniques, on the one hand ideal low-pass filtering (recall Eq. (4.6.34) where the corresponding filter function is defined) and on the other hand Gaussian filtering whereas we use the filter function (4.6.50). In order to analyse the results stemming from low-pass filtering, we introduce the dimensionless cut-off frequency ω_0/J. Hence, any value given to the cut-off has to be understood as being dimensionless. The results of filtered and smoothened optimal fields shown below correspond to the implementation of the gates $11X$ and $1CNOT$ using procedure A. For the sake of completeness we will show at the very end of this chapter one smoothened field which implements the gate $11X$ and is achieved using procedure B.

As we will show in the following discussion, the effect of the filtering procedure is strongly dependent on the shape of the optimal control fields. For this reason we introduce two quantities which allow to characterize the optimal control field in consideration. At first we quantify the strength of the control field. In order to derive a reasonable quantity for the magnitude, we consider the absolute values (amplitudes) of the field components and define an average amplitude for the x- and y-field, respectively, as follows

$$\bar{A}_x := \frac{1}{N_t/2} \sum_{i=1}^{N_t/2} |h_{x,i}| \quad \text{and} \quad \bar{A}_y := \frac{1}{N_t/2} \sum_{i=1}^{N_t/2} |h_{y,i}|, \tag{4.6.61}$$

whereas we have assumed procedure A and N_t time steps. The average amplitude of the x-field is denoted $\bar{A}_x$, the one of the y-field $\bar{A}_y$. Using procedure B we have to replace $N_t/2$ by N_t in the expression for $\bar{A}_x$. While for procedure B we have obtained one value which describes the strength of the control field, in the case of procedure A we have two averages, for each field direction one. Average amplitudes for the x- and y-field at hand, we now define a total average amplitude $\bar{A}$ for procedure A, reflecting the strength of the whole control field, as

$$\bar{A} := \frac{\bar{A}_x + \bar{A}_y}{2}. \tag{4.6.62}$$

This total average may be understood in the following way: Per unit time there is acting a control field of average strength $\bar{A}$ either in x- or in y-direction.

We continue focussing on the variance in the absolute field values since the optimal control fields considered are not constant seen over the whole evolution time of the system but consist of N_t switches between different values. The variance in the absolute values of the x- and y-field, respectively, which we denote by var_x and var_y, may be calculated for procedure A and N_t time intervals as

$$\text{var}_x = \frac{1}{N_t/2 - 1} \sum_{i=1}^{N_t/2} (|h_{x,i}| - \bar{A}_x)^2 \quad \text{and} \quad \text{var}_y = \frac{1}{N_t/2 - 1} \sum_{i=1}^{N_t/2} (|h_{y,i}| - \bar{A}_y)^2. \tag{4.6.63}$$

Again, using procedure B we must substitute N_t for $N_t/2$ in the formula for var_x. For procedure A we define additionally an average variance of all absolute field values, denoted var, as

$$\text{var} := \frac{\text{var}_x + \text{var}_y}{2}, \tag{4.6.64}$$

which is simply the mean of var_x and var_y and quantifies the variance in the absolute values of the whole field. To assign a value to the average amplitude and the variance of an optimal control field, we always use the dimensionless quantities $\bar{A}/J$ and var/J^2 even if not explicitly mentioned.

Now we have the instruments at hand in order to discuss the filtering of optimal control fields. To begin with we consider Figs. 12 and 13 which each illustrate the smoothing of an optimal control field if an ideal low-pass filter is applied. Together with the optimal piecewise constant field there are shown filtered fields for different cut-off frequencies ω_0. The control field of Fig. 12 implements the spin-flip gate $11X$ to a very high accuracy, the one of Fig. 13 the controlled gate 1CNOT. Both fields are achieved for 70 time steps of length 0.5. In each case Fig. (a) shows the x-field and (b) the y-field.

(a)   (b)
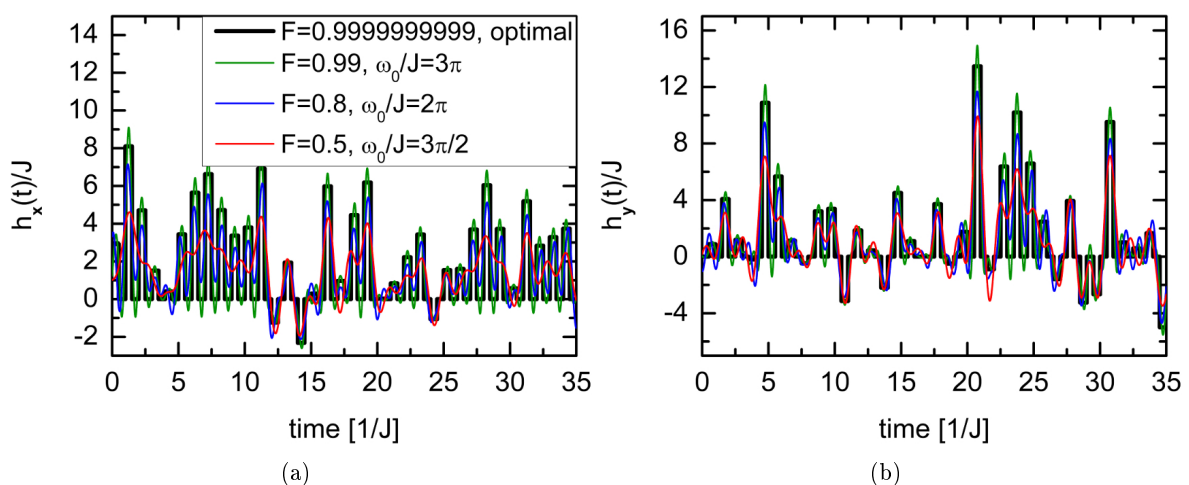
Figure 12: Gate $11X$: Filtered optimal control field plotted for different cut-off frequencies ω_0. (a) x-field and (b) y-field. The optimal piecewise constant field is plotted for comparison (black curve) and corresponds to the one of Figs. 3 and 11, achieved for the parameters $N_t = 70$ and $T = 0.5$. Its Magnitude and variance are: $\bar{A}/J = 3.4$ and $\text{var}/J^2 = 7.8$.

(a)   (b)
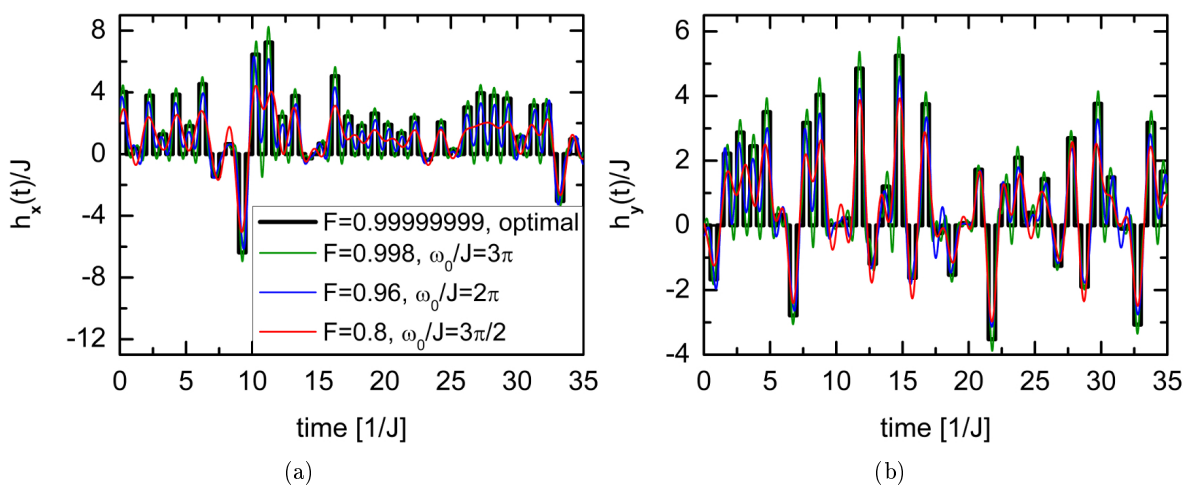
Figure 13: Gate 1CNOT: Filtered optimal control field plotted for different cut-off frequencies ω_0. (a) x-field and (b) y-field. The optimal piecewise constant field is plotted for comparison (black curve) and specified by $N_t = 70$, $T = 0.5$, $\bar{A}/J = 2.4$, and $\text{var}/J^2 = 2.6$.

We see that for smaller cut-offs the fields become smoother, while simultaneously the fidelity is decreasing. Furthermore we notice that in Fig. 12 the fidelity has dropped down to 0.5 at a cut-off frequency of $3\pi/2$ whereas in Fig. 13 the fidelity is still 0.8 at the same cut-off. This behaviour is related to the average amplitude of the fields. The optimal piecewise constant fields of Figs. 12 and 13 have an average amplitude of 3.4 and 2.4, respectively. We will observe later in this chapter that the fidelity of weaker filtered fields decays less rapidly depending on the cut-off frequency.

In Fig. 14(a) we compare the behaviour of the fidelity for ideal low-pass and Gaussian filtering depending on the cut-off frequency ω_0 and on the full width at half maximum FWHM, respectively. To this end we use the control field shown before in Fig. 12 which approximates the spin-flip gate $11X$ with very high fidelity.

(a)

(b)   (c)
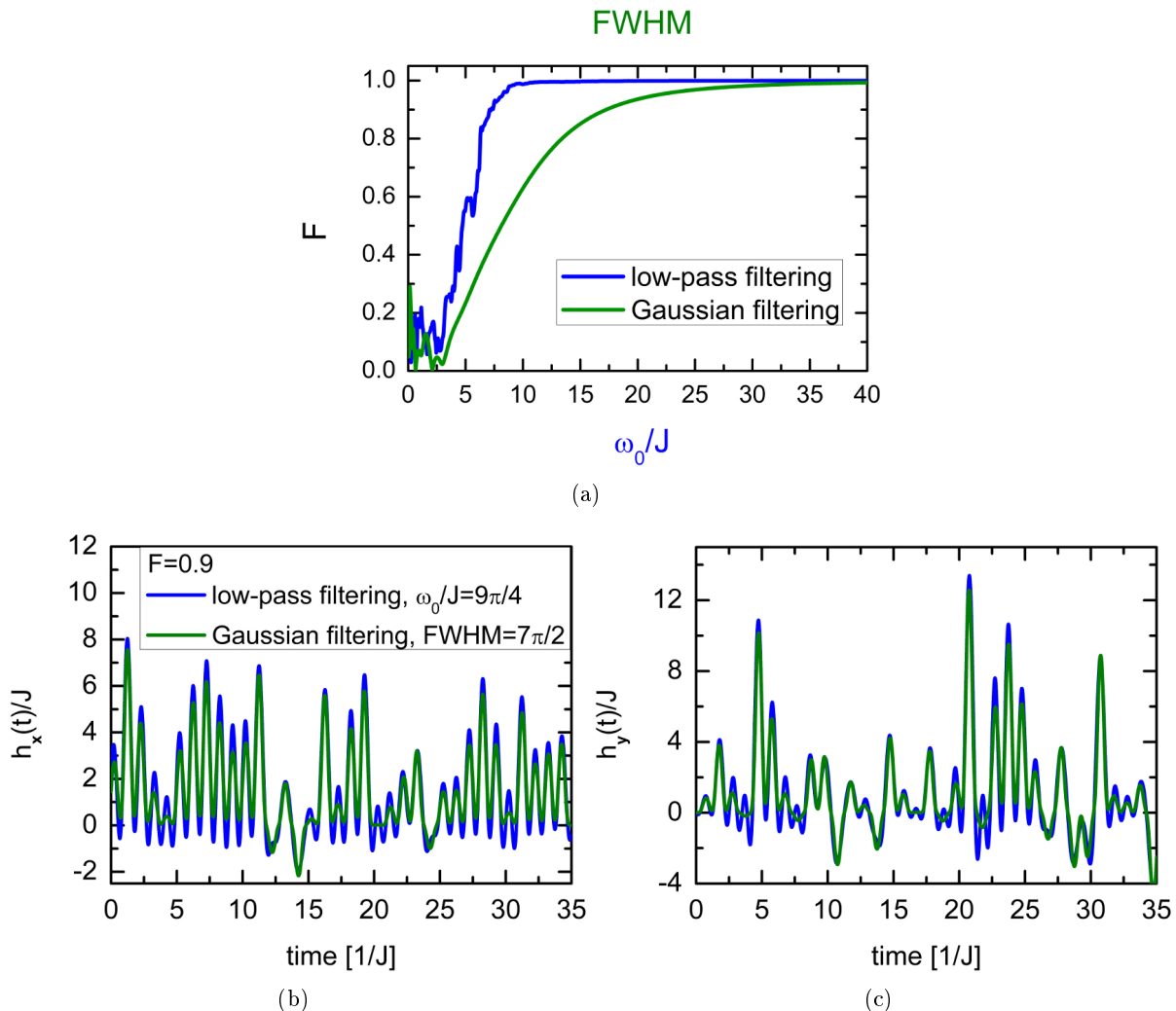
Figure 14: Gate $11X$, implemented by the same control field as the one of Fig. 12. The fidelity F depending on ω_0 (ideal low-pass filtering) and on FWHM (Gaussian filtering), respectively, is plotted in Fig. (a). The filtered and smoothened control field corresponding to a fidelity of 0.9 is shown for both, low-pass and Gaussian filtering, in Figs. (b) (x-field) and (c) (y-field).

We observe that in the case of Gaussian filtering the decay of the fidelity with decreasing FWHM (green curve) is smooth due to the Gaussian filter function $e^{-\gamma\omega^2}$ (where $\text{FWHM} = 2\sqrt{\frac{\ln 2}{\gamma}}$) which effects a monotone continuous attenuation of high frequencies. In contrast, the fidelity curve versus ω_0 corresponding to the ideal low-pass filter (blue curve) shows a rapid decay with decreasing ω_0 in the range where ω_0/J reaches values around 2π. The decay curve is characterized by small peaks and appears much less smooth compared to the case of Gaussian filtering. This feature may be explained having in mind that the low-pass filter function is a non-continuous box function. Considering the power spectrum of the Fourier transformed optimal control field (see Fig.

11), we see that around 2π there are distributed frequencies with high peaks effecting the rapid decay of the fidelity visible in 14(a). Figures 14(b) (x-field) and 14(c) (y-field) present the filtered control fields corresponding to a fidelity of 0.9 in Fig. 14(a), both for low-pass (blue field) and Gaussian (green field) filtering. The smoothened control fields look similar in both cases. The Gaussian filtered field appears slightly smoother.

In the following we concentrate fully on ideal low-pass filtering and examine the behaviour of the fidelity depending on the cut-off frequency in more detail. In particular, we are interested how the magnitude and variance of the optimal control fields influence this behaviour. In order to generate optimal control fields which are differing in their average amplitude and variance, we start from initial guesses taking 70 time steps of length 1.5. Since for this choice the total evolution time $t_f = N_t T$ is sufficiently large, the optimization program returns optimal control fields with values close to the initial guess. Therefore we are able to control the amplitude and variance of the optimal control fields by varying the initial guess in an appropriate way.

In Fig. 15 we analyse the fidelity versus ω_0 for six optimal control fields which induce the implementation of the spin-flip gate $11X$ (a) and of the controlled gate $1CNOT$ (b), respectively. The fields differ clearly in their average amplitude and are achieved for positive constant initial guesses which is why they all have an almost vanishing variance. We observe that the fidelity is less affected by the smoothing if the corresponding optimal control field is weak. The rapid decay of the fidelity at certain values of ω_0 may be explained by considering the power spectrum of the Fourier transformed fields (collected in the Appendix A.2: Figures 24 and 25 contain the power spectra of the Fourier transformed fields corresponding to Figs. 15(a) and 15(b), respectively). We note that at the cut-offs where the fidelity is decaying rapidly, there are occurring sharp peaks in the corresponding power spectra. Those sharp peaks are characteristic for control fields which are almost 'constant'. Constant in this context means for the use of procedure A that the amplitude of the field is constant in time while its direction is continuously switching from x- to y-direction.
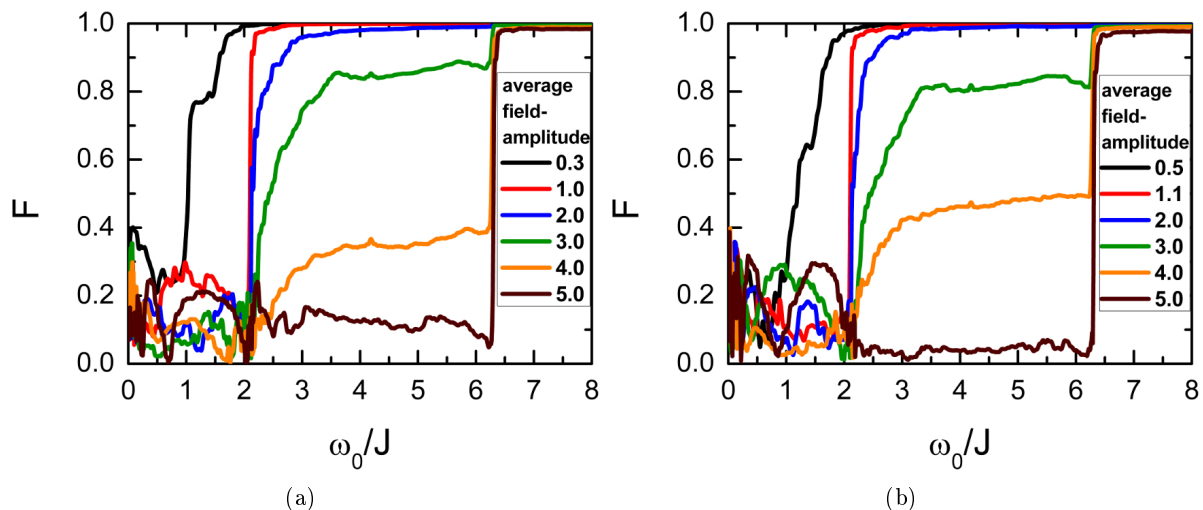

(a)   (b)

Figure 15: Gates $11X$ (a) and $1CNOT$ (b): Fidelity F versus ω_0 corresponding to six different low-pass filtered optimal control fields. All optimal fields are achieved for $N_t = 70$ and $T = 1.5$ and have a variance (var/J^2) between 0.1 and 0.4, but they differ clearly in their average amplitude (see legend where the values of the dimensionless quantity $\bar{A}/J$ are given).

We continue focussing on the implementation of $11X$ and analyse how the behaviour of F versus ω_0 changes, when the field values are far away from being constant, by increasing the variance and including negative field values. While the optimal control fields of Fig. 15(a) are characterized by field amplitudes which are all positive and by a small variance between 0.1 and 0.4, the optimal fields of Fig. 16(a) have a larger variance in the range 1.1 to 1.3 and the field values are arbitrarily distributed around the average amplitude including as well negative values. Curves

of the same colour in Figs. 15(a) and 16(a) have a similar average amplitude. Comparing the curves corresponding to fields of similar magnitude, we notice that in Fig. 16(a) the drop in F with decreasing cut-off frequency starts already at larger ω_0 in comparison to Fig. 15(a) and occurs less rapid over a larger ω_0-range. This feature is related in particular to the including of negative field values. Negative field amplitudes effect that the sharp peaks in the power spectra of the Fourier transformed fields (see Appendix A.2: Figure 26) disappear splitting into a wider distribution of peaks. The larger variance contributes as well to the broadening of the peak distributions in the power spectra.

The dependence of the fidelity curve versus ω_0 on the variance is examined in Fig. 16(b) for optimal control fields of similar magnitude whose field values are chosen arbitrary including again negative values. We observe that the fidelity is more affected by low-pass filtering if the variance of the fields is increased. A larger variance leads to higher peaks in the power spectra of the Fourier transformed fields (see Fig. 27 in Appendix A.2).

(a)   (b)
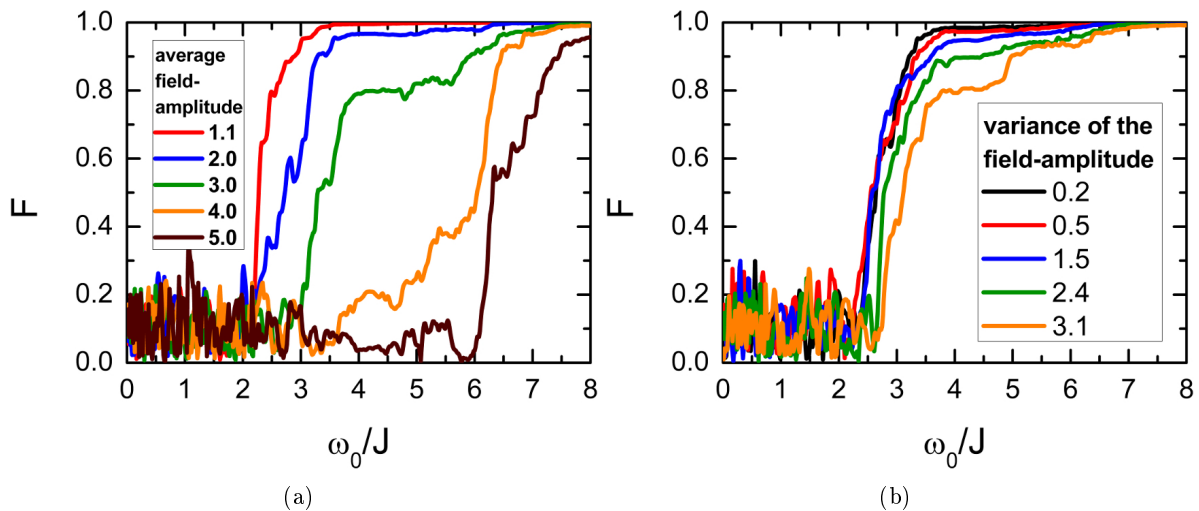
Figure 16: Gate $11X$: Fidelity F versus ω_0 corresponding to different low-pass filtered optimal control fields which are characterized by: (a) The optimal control fields are achieved for the same parameters as the fields of Fig. 15 and have a similar average amplitude for equal colour. But their variance is larger, ranging between 1.1 and 1.3 for all fields. (b) The optimal control fields all have an average amplitude between 1.9 and 2.1 but differ clearly in their variance which is specified in the legend.

After having discussed the behaviour of F versus ω_0 for optimal control fields of fixed parameters N_t and T which were differing in their average amplitude, variance and the occurrence of negative field amplitudes, we now analyse how the fidelity is affected by varying the length T of the time steps in the optimal piecewise constant control. For this purpose we plot the fidelity versus $\omega_0 T$. Plotting versus $\omega_0 T$ eliminates the effect of the oscillation period in the Fourier transform which is dependent on T. Figure 17 contains plots for optimal control fields which differ in T. The fields have a similar magnitude, small variance and include only positive field amplitudes. Although the plotting versus $\omega_0 T$ eliminates the influence of the different period of the oscillating part in the Fourier transform, there can be observed a clear difference depending on T. For smaller T the fidelity is less affected by the smoothing. This feature is reminiscent of the behaviour which shows the fidelity for random noise affected optimal control fields (recall Fig. 5(a) in Section 4.5.1 where the sensitivity of the fidelity is analysed for optimal control fields which differ in T).
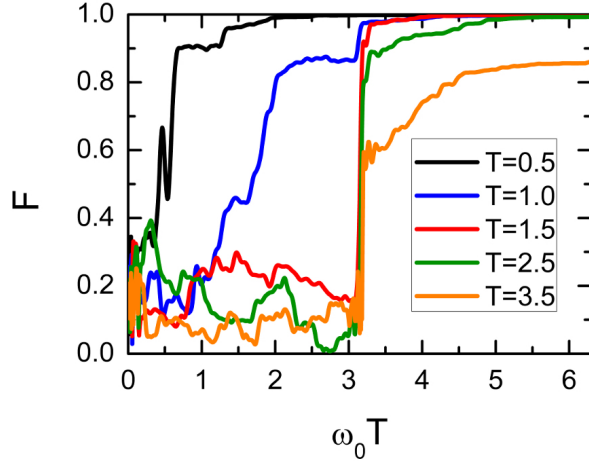
Figure 17: Gate 11X: Fidelity F plotted versus $\omega_0 T$ for five different low-pass filtered optimal control fields which all have an average amplitude between 1.0 and 1.1 as well as a small variance between 0.1 and 0.6. They are achieved for 70 time intervals but differ in the parameter T.

In order to complete this chapter, we show three further low-pass filtered and hence smoothened optimal control fields corresponding to a fidelity of 0.9 (see Figs. 18, 19, and 20). We recall that smooth fields with high fidelities may be achieved if the control field is small and the switching time T short. The smoothened control fields of Figs. 18 and 19, which implement the gates 11X and 1CNOT, respectively, are obtained using procedure A, while the smoothened field shown in Fig. 20 results from procedure B.
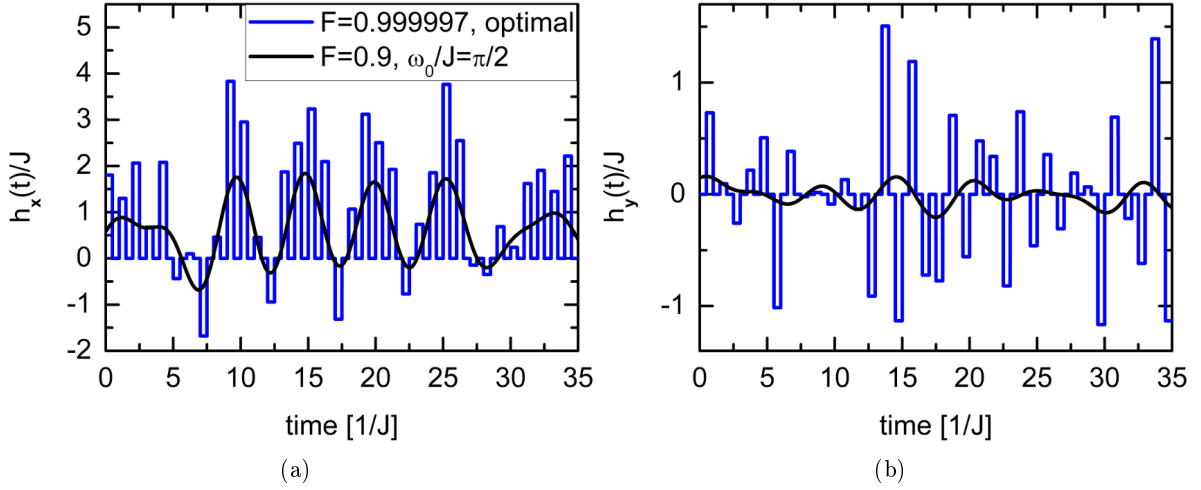
Figure 18: Gate 11X: Smoothing by low-pass filtering of an optimal control field which is achieved for the parameters $N_t = 70$ and $T = 0.5$ and has an average amplitude and a variance of 1.1 and 0.6, respectively. The optimal piecewise constant field is low-pass filtered and plotted for a cut-off frequency of $\pi/2$. The smoothened field corresponds to a fidelity of still 0.9. The optimal field is plotted for comparison. (a) x-field and (b) y-field. The behaviour of the fidelity versus ω_0 is shown for this field in Fig. 17 (black curve).

(a)   (b)
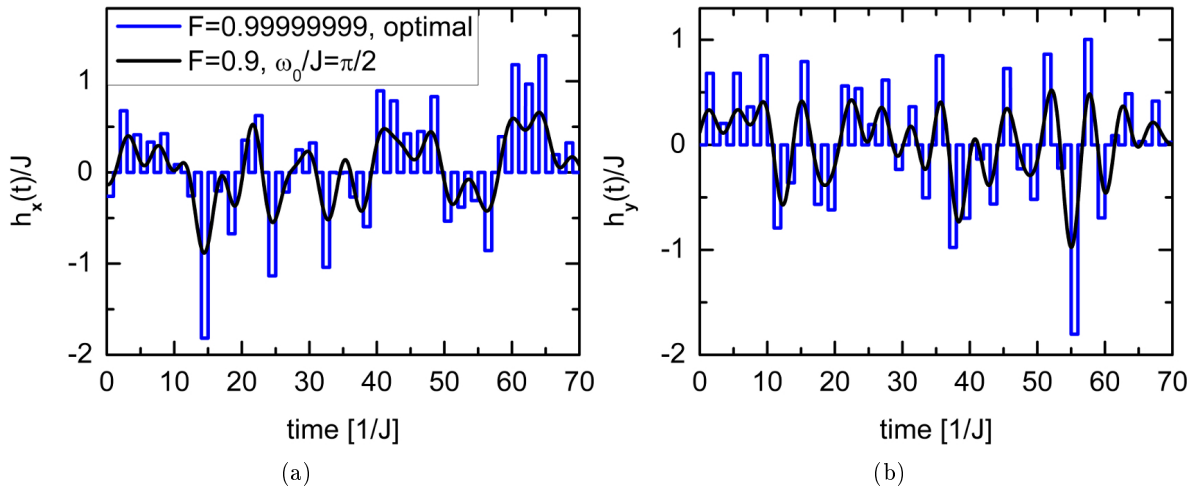
Figure 19: The equivalence of Fig. 18 for the gate 1CNOT. The filtered optimal control field is reached for $N_t = 70$ and $T = 1.0$ and its average magnitude and variance are: $\bar{A}/J = 0.6$ and $\mathrm{var}/J^2 = 0.1$.
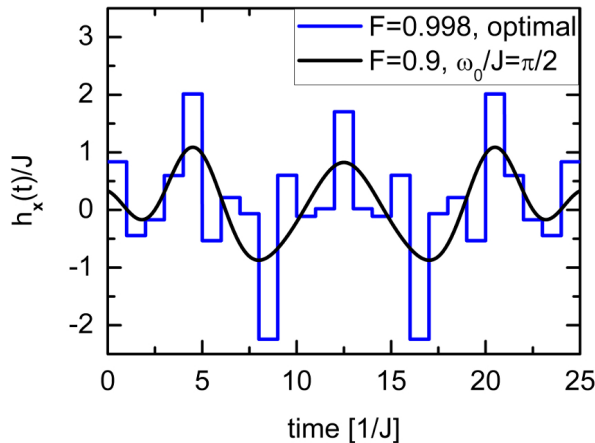

Figure 20: Gate $11X$: One and only example of a weak low-pass filtered and smoothened optimal field which is achieved using procedure B. The optimal piecewise constant field consists of 25 time intervals of length 1 and is plotted for comparison. Its average magnitude and variance are: $\bar{A}_x/J = 0.7$ and $\mathrm{var}_x/J^2 = 0.5$.

5 Generalization to Heisenberg spin chains of arbitrary length

In this section we generalize the isotropic Heisenberg spin-$\frac{1}{2}$ chain of length three, which we have considered up to now, to a chain of arbitrary length and control this system analogously to the three-spin case by locally operating on the first spin in the chain. We recall that a Heisenberg chain of arbitrary length can be controlled by operating on one of the spins at its ends [1]. From a controllability perspective we can treat the N-spin chain completely analogously to the three-spin chain since the algebraic properties of the system's Hamiltonian are preserved. At first we describe the calculation of the generalized Hamiltonian and compare in the following the results stemming from the implementation of a generalized spin-flip and CNOT gate for two-, three- and four-spin chains. We note that the dimension of the Hilbert space is doubled with every additional spin. Hence, the optimization program works slowlier for every added spin due to the time-consuming matrix multiplication and the well-known feature that controlling a system in a larger Hilbert space requires a longer total evolution time. Applied to our case this means that we need more time steps in the computation of the time evolution operator. For these reasons it was not possible to control a chain consisting of more than four spins, simply because the optimization routine in use was too slow.

5.1 Calculation of the Hamiltonian

We study an isotropic Heisenberg spin-$\frac{1}{2}$ chain of length N. The Hilbert space of such a system has a dimension of 2^N. We write the total Hamiltonian of the spin chain analogously to the three-spin system as

$$H = H_0 + H_c, \tag{5.1.1}$$

with H being a $2^N \times 2^N$ Hermitian matrix. The Hamiltonian H_0 describes the free evolution of the system containing the Heisenberg nearest-neighbour interaction and may be written for a chain of length N as

$$H_0 = J \sum_{k=1}^{N-1} (X_{k,k+1} + Y_{k,k+1} + Z_{k,k+1}), \tag{5.1.2}$$

where J denotes the coupling constant which we set equal to one. The interaction parts $X_{k,k+1}$, $Y_{k,k+1}$ and $Z_{k,k+1}$ are defined as

$$X_{k,k+1} := S_{kx} \cdot S_{k+1,x}, \tag{5.1.3}$$

$$Y_{k,k+1} := S_{ky} \cdot S_{k+1,y}, \tag{5.1.4}$$

$$Z_{k,k+1} := S_{kz} \cdot S_{k+1,z}. \tag{5.1.5}$$

The control Hamiltonian H_c is given as in the three-spin case by

$$H_c = h_x(t)S_{1x} + h_y(t)S_{1y}. \tag{5.1.6}$$

The generalized spin matrices S_{kx} can be calculated as the tensor product

$$S_{kx} = \mathbb{1} \otimes \ldots \otimes \mathbb{1} \otimes S_x \otimes \mathbb{1} \otimes \ldots \otimes \mathbb{1}, \tag{5.1.7}$$

which consists of N factors with S_x being located at the k-th place ($k \in \{1, .., N\}$). The identity $\mathbb{1}$ is a 2×2 matrix as in all subsequent formula. The matrices S_{ky} and S_{kz} may be derived analogously. We note that S_{1x} and S_{1y} imply S_{1z} in the Lie completion for arbitrary N since $[S_{1x}, S_{1y}] = i\hbar S_{1z}$ holds for any number of spins. Therefore, the control Hamiltonian (5.1.6) enables complete controllability of the system.

Using the relation

$$(A \otimes B \otimes \ldots) \cdot (C \otimes D \otimes \ldots) = AC \otimes BD \otimes \ldots, \tag{5.1.8}$$

which is valid for complex matrices A, B, C, and D of dimensions $m \times n$, $p \times q$, $n \times r$ and $q \times s$, respectively, we derive $X_{k,k+1}$ as the tensor product

$$X_{k,k+1} = \mathbb{1} \otimes \ldots \otimes \mathbb{1} \otimes S_x \otimes S_x \otimes \mathbb{1} \otimes \ldots \otimes \mathbb{1}, \tag{5.1.9}$$

where the k-th and $k + 1$-th factor are equal to S_x while the other $N - 2$ factors are given by the identity matrix $\mathbb{1}$. The y- and z-part of the Heisenberg interaction $Y_{k,k+1}$ and $Z_{k,k+1}$ are obtained analogously.

The gate $11X$ which flips the last spin in the three-spin chain is generalized to the gate X_N which flips the last spin in a N-spin chain

$$X_N = \mathbb{1} \otimes \mathbb{1} \otimes \ldots \otimes \mathbb{1} \otimes X, \tag{5.1.10}$$

where all factors are equal to the identity beside the N-th which is equal to the Pauli matrix X and effects the spin-flip of the last qubit. Additionally, we define a generalized controlled-NOT gate as follows

$$\text{CNOT}_N = \mathbb{1} \otimes \mathbb{1} \otimes \ldots \otimes \mathbb{1} \otimes \text{CNOT}, \qquad\qquad (5.1.11)$$

which operates on all spins by the identity beside on the last two on which the CNOT gate is acting. We remark that in the case of three spins we have $X_3 = 11X$ and $\text{CNOT}_3 = 1\text{CNOT}$ which are our well-known three-qubit gates whose implementation we already discussed. In the following chapter we compare the implementation of X_N and CNOT_N by controlling the x- and y-field (procedure A) for spin chains consisting of two, three, and four spins. The dynamic time evolution operator can be calculated for any number of spins as in Eq. (4.3.3) by inserting the generalized Hamiltonian.

5.2 Comparison between two, three, and four spins

The proceeding in the implementation of gates for a Heisenberg spin chain of arbitrary length is completely analogous to the three-spin case and will therefore not be repeated here. Again, we use natural units and set $\hbar = 1$ in all numerical calculations.

5.2.1 Minimal time

We are interested in finding a minimal time which is at least required to achieve respective gates to high accuracy. When having discussed the implementation of gates for the three-spin chain, we already mentioned that the evolution time of the system has to be sufficiently high in order to generate high fidelities. For evolution times below a certain minimal time it was not possible to approximate the gate in consideration with high fidelity. This feature could be observed for all implemented gates. At this point we intend to estimate this minimal time for the implementation of the gates X_N and CNOT_N (defined by Eqs. (5.1.10) and (5.1.11)) whereas we let them operate on a two-, three- and four-spin chain and compare the results for varying spin. In the case of two and three spins we proceed as follows: Starting from an evolution time t_f which is certainly too short to enable the implementation of the gate, we increase t_f taking discrete time steps. For any value of t_f we perform runs over increasing N_t. As minimal time we fix the shortest evolution time for which we achieved at any number of time intervals N_t control fields with gate errors below 10^{-5}. While for two spins we are able to increase t_f in steps of 0.1 due to the fast working optimization program, we take in the case of three spins steps of 1.0.

In contrast, for four spins the computational burden becomes such high that only a very limited number of runs can be done by starting from a fixed T and varying N_t or reversely. We therefore decide to fix the minimal time as soon as the evolution time is large enough to enable an implementation of the gate with error in the range 10^{-2}. Due to the limited number of collected samples we are not able to distinguish between the gates X_N and CNOT_N and estimate that the minimal time is of the same order for both gates in the case of four spins. In Table 6 the results are listed.

	X_N	CNOT_N
2 spins	6.4	7.4
3 spins	18	25
4 spins	80	80

Table 6: Minimal time in $[1/J]$ depending on the number of spins

5.2.2 Sensitivity of the fidelity

In this chapter we briefly compare the sensitivity of the fidelity to random noise for the implementation of the gate X_N with respect to a varying number N of spins in the Heisenberg chain. In order to eliminate the influence of the parameters N_t and T, we generate control fields of fixed parameters N_t and T which effect the implementation of X_N for $N = 2, 3, 4$. We choose
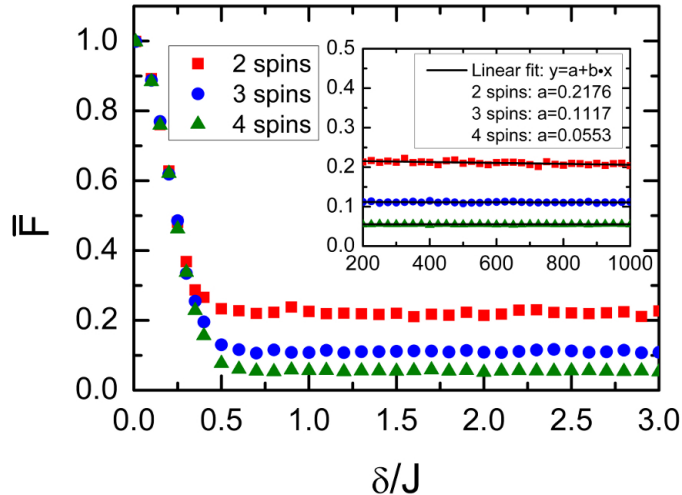
Figure 21: Average fidelity $\bar{F}$ versus δ for three random noise affected optimal fields which implement the gate X_N in the case of two, three, and four spins. The optimal fields are specified by the parameters $N_t = 300$ and $T = 1.0$. The small figure shows the behaviour of $\bar{F}$ for large δ.

$N_t = 300$ and $T = 1.0$, a choice corresponding to a sufficiently large evolution time so that for all three cases it is ensured that the gate X_N can be approximated to high accuracy. In Fig. 21 we show the decay of the average fidelity $\bar{F}$ versus δ for three random noise affected optimal fields which implement the gate X_N in the case of two, three, and four spins, respectively. We observe that the fidelity is dropping similarly independent of the number of spins since the optimal control fields are achieved all for the same parameters. However, the saturation value is higher for smaller number of spins. We recall Section 4.5.1 where we derived that the value of the saturation is dependent on the dimension d of the Hilbert space (see Eq. (4.5.4)), namely $1/d$. Thus, we expect for two, three, and four spins a saturation of $1/4 = 0.25$, $1/8 = 0.125$, and $1/16 = 0.0625$, respectively. The small figure in 21 contains a linear fit of the average fidelity curve in the range of large δ in order to obtain a value for the saturation. The linear fitting produces saturation values of 0.2176 ($N = 2$), 0.1117 ($N = 3$), and 0.0553 ($N = 4$) which fit to order 10^{-2} with what we expected.

We point out that the fidelity corresponding to optimal control fields which are achieved in minimal time is more sensitive to random noise for more spins since the minimal time and number of time steps needed increases with increasing number of spins (recall Figs. 5 and 7 which illustrate the behaviour of $\bar{F}$ depending on the parameters N_t, T, and t_f in the three-spin case).

6   An application: Error correction circuit

In this chapter we sketch one possible application of an operator controlled Heisenberg spin-$\frac{1}{2}$ chain. To this end we consider firstly the error correction circuit in Fig. 22. This circuit gives an example how quantum error correction can be performed without need of measurements using only unitary operations and ancilla systems which are prepared in standard states. The single-qubit state $\alpha \ket{0} + \beta \ket{1}$ is encoded in three (codeword) qubits as $\alpha \ket{000} + \beta \ket{111}$. We assume that the initial state has been perfectly encoded and let the three qubits independently of each other pass through a bit-flip channel (illustrated in Fig. 22 as the red framed X on each line of the codeword qubits). Suppose a bit flip occurred on at most one qubit, then the circuit in Fig. 22 provides a perfectly working procedure in order to detect the error and recover the correct quantum state. The error diagnose is achieved by a combination of controlled gates, namely of CNOT gates and a Toffoli gate. We refer to Section 2.4.2 where the action of the CNOT and Toffoli gate is described and their matrix representation given. Their circuit symbols are illustrated in Fig. 23. The black solid circles indicate the control qubits while the the target
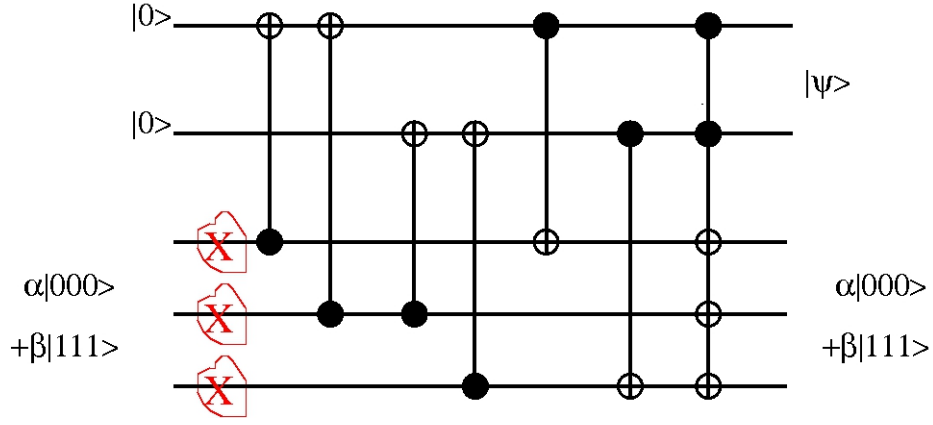
Figure 22: Error correction circuit which consists of two ancilla qubits and three codeword qubits which encode a single logical qubit. The circuit corrects a single bit-flip error on the wires of the three codeword qubits. The red framed X represent possible random flips of at most one qubit [21].
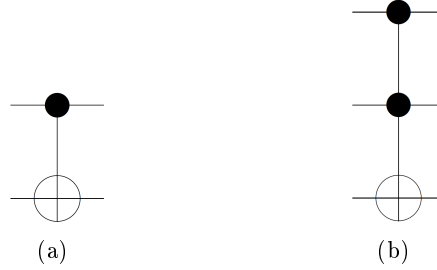

Figure 23: Circuit symbols: (a) CNOT and (b) Toffoli gate.

qubits are identified by the symbol $\oplus$ which highlights that the action of the CNOT and Toffoli gate on the target qubit is addition modulo two. In Fig. 22 the Toffoli gate acts on more than one target, namely on three. The effect on each target $|t_i\rangle$, with $i = 1, 2, 3$, is $|t_i\rangle \to |t_i \oplus c_1 c_2\rangle$, where $|c_1\rangle$ and $|c_2\rangle$ are the states of the control qubits.

The two ancillary are initialized both in the state $|0\rangle$ before starting error correction and have to be reinitialized each time error correction is performed. The three controlled gates acting as last gates in the circuit are controlled by the ancilla qubits and effect the recovering of the correct quantum state while the error itself is detected by the four preceding gates. If no bit flip occurred on the wires of the codeword qubits, the final state $|\psi\rangle$ of the ancilla system is $|00\rangle$. If the upper erroneous X gate on the left has acted, the state of the ancillas is $|10\rangle$, if the middle one has acted $|11\rangle$ and if the lower one has acted $|01\rangle$. We note again that this error correction circuit works only if at most one erroneous X gate has acted.

Such a quantum error correction circuit as in Fig. 22 could be realized by applying local operator control on a Heisenberg spin-$\frac{1}{2}$ chain of length five. The relevant unitary U which effects the error correction results from Fig. 22 by multiplying the CNOT gates and the Toffoli gate from the left to the right:

$$U = \text{CNOT}_{Q_1 A_1} \text{CNOT}_{Q_2 A_1} \text{CNOT}_{Q_2 A_2} \text{CNOT}_{Q_3 A_2} \text{CNOT}_{A_1 Q_1} \text{CNOT}_{A_2 Q_3} \text{Toffoli}_{A_1 A_2 Q_1 Q_2 Q_3},$$
$$(6.0.1)$$

where the subscripts denote the control and target qubits (in this order) on which the respective gate is acting. The unitary U can be implemented by applying a control field to one of the spins at the end of the Heisenberg spin chain [1]. In principle, the order of the qubits in the chain makes no difference except that the matrix representation of U is modified. It seems,

however, reasonable to control one of the ancilla qubits and put it hence at one end of the chain. Moreover, we could apply a control field to both ancillary qubits which allows to initialize them directly to $|0\rangle$. But since the system is complete controllable by control of one spin at the end, the initialization could as well be done indirectly by quantum control.

The question arises whether the unitary U may be implemented by controlling only the x-field. We will not represent U here in its matrix representation since it is a large $2^5 \times 2^5$ matrix but we summarize some of its properties. It is a permutation matrix, i.e that one entry in each row and column is equal to 1 while the others are 0. The trace does not vanish which is why we may conclude that $-iU$ is not contained in the Lie algebra $\mathcal{L}_X$ generated by $\{-iH_0, -iS_{1x}\}$. Furthermore, we note that U is not Hermitian. These collected properties complicate the answering to the arisen question and we have to let it unanswered.

However, implementing U by applying a control field in x- and y-direction to one spin at the end of the chain, is just a question of time. Since the algorithm used throughout this work does not enable the implementation in 'reasonable' time, we are not able to present results at this point.

7 Conclusions

In this work we were concerned with operator control achieved by local control of an isotropic Heisenberg spin-$\frac{1}{2}$ chain. We have mainly discussed a three-spin chain which we extended at the end to a chain of arbitrary length. In order to find optimal control fields, we have maximized the fidelity between target gate and dynamic unitary over the field amplitudes. The found optimal fields have been analysed regarding their time dependence and pulse shape. We have examined the fidelity with respect to its robustness if (classical) random noise occurs and to the behaviour if the optimal fields are smoothened by attenuating high-frequencies in the Fourier space. Here, we review briefly the main results. At first we have seen that local control of a Heisenberg chain, namely applying a control field to the first spin, enables the implementation of gates to high accuracy. Concretely, we have shown that spin-flip gates and even entangling gates with universal property like CNOT and $\sqrt{\text{SWAP}}$ gates can be achieved with optimal fidelities. Moreover, we have observed that the achievement of those gates is equally 'hard'. That is, the number of time steps and the minimal evolution time needed is similar for all considered gates. Even a rotation operator close to the identity could not be implemented in significant shorter time. We have examined the issue of minimal time by comparing the implementation of gates for Heisenberg chains of two, three, and four spins. It seems that the minimal time is exponentially increasing in the number of spins.

Quantum control systems are in practice open systems introducing noise. We have analysed the sensitivity of the fidelity to classical noise. For this purpose we have affected the optimal fields by random noise. We have seen that the fidelity is less sensitive, hence more robust, to noise the smaller the pulse timings T are. If the pulse duration is fixed and the evolution time increased, then the fidelity becomes more sensitive the longer the systems evolves under the noise. We have assumed piecewise constant functions for the controls. In order to smoothen the piecewise constant optimal controls, we have removed high frequencies in the Fourier space by applying ideal-low pass and Gaussian filters. We have shown that smooth control fields with high fidelities may be reached if the field amplitude is weak and the variance in the amplitude small. The work has been completed by describing how a quantum error correction circuit may be implemented by local control of a Heisenberg five-spin chain.

8 Acknowledgments

A Appendix

A.1 Basis of the dynamical Lie algebra for controlling the x-field only

Based on notes of D. Burgarth, we calculate a basis for the dynamical Lie algebra $\mathcal{L}_X$ corresponding to the quantum control system (4.3.5) which consists of an isotropic Heisenberg three-spin-$\frac{1}{2}$ chain whereas a control field pointing into x-direction only is applied to the first spin in the chain. The Lie algebra is generated by the set $\{-iH_0, -iH_1\}$ and its dimension is 18 as may be computed by using the algorithm described in Table I of Ref. [8]. The Hamiltonian H_0 is the Heisenberg interaction Hamiltonian defined in (4.2.2) and H_1 represents the control part of the full system's Hamiltonian: $H_1 = S_{1x}$. In order to simplify the calculation we neglect trivial constants and redefine the Hamiltonians H_0 and H_1 as

$$H_0 := XX1 + YY1 + ZZ1 + 1XX + 1YY + 1ZZ, \tag{A.1.1}$$
$$H_1 := X11, \tag{A.1.2}$$

whereas the sign $\otimes$ for the Tensor product is omitted in all terms and where 1 denotes the 2×2 unit matrix and X, Y, Z denote the usual Pauli matrices. A basis for the Lie algebra generated by $\{-iH_0, -iH_1\}$ may be derived by finding a complete set of linearly independent (repeated) commutators of the set of generators and linear combinations of it. The calculation is straightforward and given in the following without much explanations. Expressions in round brackets have to be understood as matrix multiplications, not Tensor products.

$$[H_0, H_1] = (YX - XY)Y1 + (ZX - XZ)Z1 \tag{A.1.3}$$
$$= -2iZXY + 2iYZ1 \tag{A.1.4}$$
$$= 2i(YZ1 - ZY1) \tag{A.1.5}$$

$$H_2 := YZ1 - ZY1 \tag{A.1.6}$$

$$[H_1, H_2] = (XY - YX)Z1 - (XZ - ZX)Y1$$
$$= 2iZZ1 + 2iYY1$$
$$= 2i(ZZ1 + YY1) \tag{A.1.7}$$

$$H_3 := ZZ1 + YY1 \tag{A.1.8}$$

$$[H_2, H_3] = (YZ - ZY)11 - 1(YZ - ZY)1 + 1(ZY - YZ)1 - (ZY - YZ)11$$
$$= 2iX11 - 2i1X1 - 2i1X1 + 2iX11$$
$$= 4i(X11 - 1X1) \tag{A.1.9}$$

$$H_4 := 1X1 \tag{A.1.10}$$

$$[H_4, H_0] = Y(XY - YX)1 + Z(XZ - ZX)1 + 1(XY - YX)1 + 1(XZ - ZX)1$$
$$= 2iYZ1 - 2iZY1 + 2i1ZY - 2i1YZ$$
$$= 2i(YZ1 - ZY1 + 1ZY - 1YZ) \tag{A.1.11}$$

$$H_5 := 1ZY - 1YZ \tag{A.1.12}$$

$$[H_5, H_4] = 1(ZX - XZ)Y - 1(YX - XY)Z$$
$$= 2i1YY + 2i1ZZ$$
$$= 2i(1YY + 1ZZ) \tag{A.1.13}$$

$$H_6 := 1YY + 1ZZ \tag{A.1.14}$$

$$[H_5, H_6] = 1(ZY - YZ)1 - 11(ZY - YZ) + 11(YZ - ZY) - 1(YZ - ZY)1$$
$$= -2i1X1 + 2i11X + 2i11X - 2i1X1$$
$$= 4i(11X - 1X1) \tag{A.1.15}$$

$$H_7 := 11X \tag{A.1.16}$$

$$[H_3, H_6] = Z(ZY - YZ)Y - Y(YZ - ZY)Z$$
$$= -2iZXY + 2iYXZ$$
$$= 2i(YXZ - ZXY) \tag{A.1.17}$$

$$H_8 := YXZ - ZXY \tag{A.1.18}$$

$$[H_8, H_1] = (YX - XY)XZ - (ZX - XZ)XY$$
$$= -2iZXZ - 2iYXY$$
$$= -2i(ZXZ + YXY) \tag{A.1.19}$$

$$H_9 := ZXZ + YXY \tag{A.1.20}$$

We define

$$\widetilde{H}_{10} := H_0 - H_3 - H_6 = XX1 + 1XX, \tag{A.1.21}$$

where the $\widetilde{}$ denotes that this matrix is not linearly independent of the other elements which are derived up to now.

$$
\begin{aligned}
[\widetilde{H}_{10}, H_3] &= [(XZ)(XZ) - (ZX)(ZX)]1 + Z(XZ - ZX)X \\
&\quad + [(XY)(XY) - (YX)(YX)]1 + Y(XY - YX)X \\
&= -2iZYX + 2iYZX \\
&= 2i(YZX - ZYX)
\end{aligned}
\tag{A.1.22}
$$

$$
H_{11} := YZX - ZYX
\tag{A.1.23}
$$

$$
\begin{aligned}
[\widetilde{H}_{10}, H_6] &= X(XY - YX)Y + 1[(XY)(XY) - (YX)(YX)] \\
&\quad + X(XZ - ZX)Z + 1[(XZ)(XZ) - (ZX)(ZX)] \\
&= 2iXZY - 2iXYZ \\
&= 2i(XZY - XYZ)
\end{aligned}
\tag{A.1.24}
$$

$$
H_{12} := XZY - XYZ
\tag{A.1.25}
$$

$$
\begin{aligned}
[H_1, H_{11}] &= (XY - YX)ZX - (XZ - ZX)YX \\
&= 2iZZX + 2iYYX \\
&= 2i(ZZX + YYX)
\end{aligned}
\tag{A.1.26}
$$

$$
H_{13} := ZZX + YYX
\tag{A.1.27}
$$

$$
\begin{aligned}
[H_7, H_{12}] &= XZ(XY - YX) - XY(XZ - ZX) \\
&= 2iXZZ + 2iXYY \\
&= 2i(XZZ + XYY)
\end{aligned}
\tag{A.1.28}
$$

$$
H_{14} := XZZ + XYY
\tag{A.1.29}
$$

$$
\begin{aligned}
[H_{11}, H_5] &= Y1(XY - YX) - Z[(YZ)(XY) - (ZY)(YX)] \\
&\quad - Y[(ZY)(XZ) - (YZ)(ZX)] + Z1(XZ - ZX) \\
&= 2iY1Z - 2iZ1Y \\
&= 2i(Y1Z - Z1Y)
\end{aligned}
\tag{A.1.30}
$$

$$
H_{15} := Y1Z - Z1Y
\tag{A.1.31}
$$

$$
\begin{aligned}
[H_{15}, H_1] &= (YX - XY)1Z - (ZX - XZ)1Y \\
&= -2iZ1Z - 2iY1Y \\
&= -2i(Z1Z + Y1Y)
\end{aligned}
\tag{A.1.32}
$$

$$H_{16} := Z1Z + Y1Y \tag{A.1.33}$$

$$\begin{aligned}
[H_{14}, H_5] &= X1(ZY - YZ) + X(YZ - ZY)1 - X(ZY - YZ)1 - X1(YZ - ZY) \\
&= -2iX1X + 2iXX1 + 2iXX1 - 2iX1X \\
&= 4i(XX1 - X1X)
\end{aligned} \tag{A.1.34}$$

$$H_{17} := XX1 - X1X \tag{A.1.35}$$

$$\begin{aligned}
[H_{13}, H_2] &= (ZY - YZ)1X + 1(YZ - ZY)X - 1(ZY - YZ)X - (YZ - ZY)1X \\
&= -2iX1X + 2i1XX + 2i1XX - 2iX1X \\
&= 4i(1XX - X1X)
\end{aligned} \tag{A.1.36}$$

$$H_{18} := 1XX - X1X \tag{A.1.37}$$

The set $\{-iH_0, -iH_1, -iH_2, -iH_3, -iH_4, -iH_5, -iH_6, -iH_7, -iH_8, -iH_9, -iH_{11}, -iH_{12}, -iH_{13},$ $-iH_{14}, -iH_{15}, -iH_{16}, -iH_{17}, -iH_{18}\}$ forms a basis for $\mathcal{L}_X$ whereas H_0 may be replaced by $\widetilde{H}_{10}$. We remark that by linear combination of $\widetilde{H}_{10}$, H_{17} and H_{18} the elements $XX1$, $X1X$ and $1XX$ can be generated.

Having this basis for the Lie algebra $\mathcal{L}_X$ at hand, we may answer the question whether a gate is achievable by controlling only the x-field or not, at least for the gates $11X$, $1X1$, and $1\sqrt{\text{SWAP}}$. The answer is, 'yes, they are', i.e. that they are contained in the reachable set of the control system, namely in the Lie group $e^{\mathcal{L}_X}$ which corresponds to the algebra $\mathcal{L}_X$. The reasoning for stating this becomes clear considering the elements of $\mathcal{L}_X$. We have seen that the elements $-i(11X)$ and $-i(1X1)$ are contained in the algebra. Hence, the gates $11X$ and $1X1$ can be reached due to the relations

$$-i(11X) = e^{-i\frac{\pi}{2}(11X)}, \tag{A.1.38}$$

$$-i(1X1) = e^{-i\frac{\pi}{2}(1X1)}. \tag{A.1.39}$$

The square root of swap $1\sqrt{\text{SWAP}}$ is generated up to an irrelevant phase by $e^{-i\frac{\pi}{8}S_{23}}$ (recall Eq. (2.4.18)), where S_{23} is defined as

$$S_{23} = 1XX + 1YY + 1ZZ. \tag{A.1.40}$$

We point out that $-iS_{23}$ is an element of $\mathcal{L}_X$ as may be seen by linear combining the basis elements.

A.2 Fourier transform of optimal control fields: Power spectrum
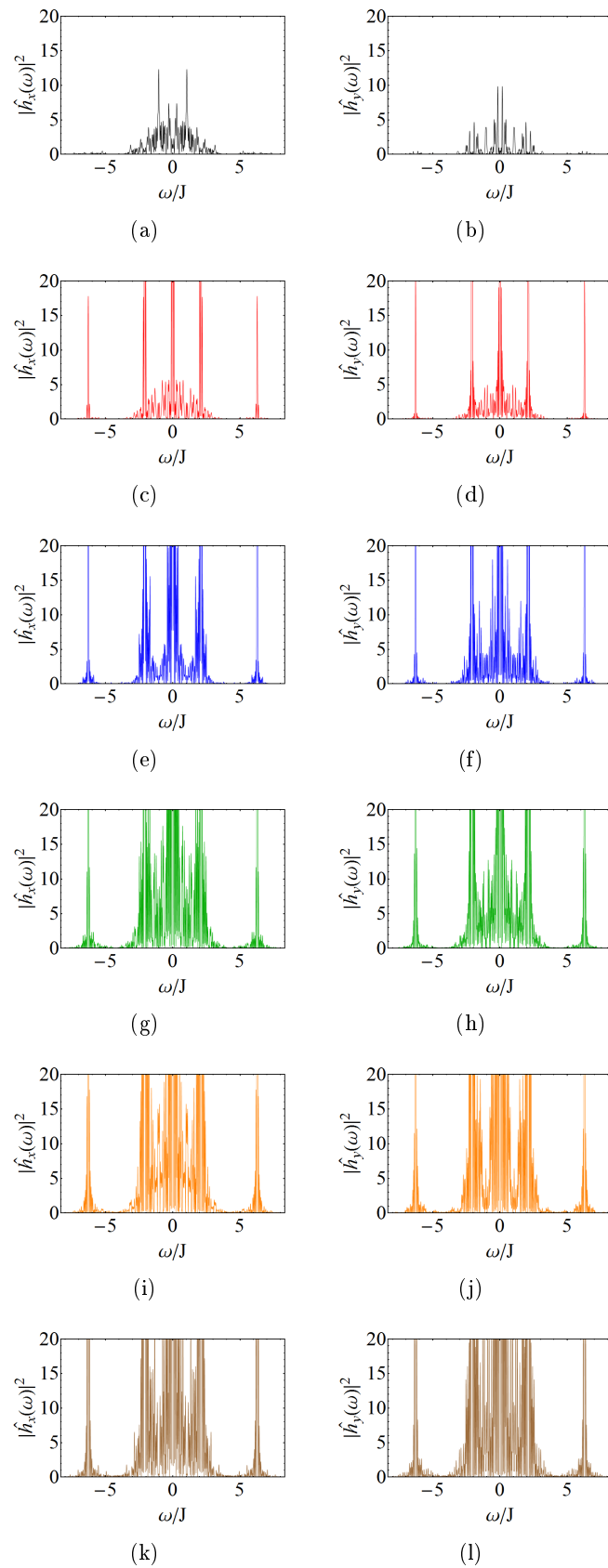

Figure 24: Power spectrum for the optimal control fields of Fig. 15(a). The colours correspond to the ones in Fig. 15(a).
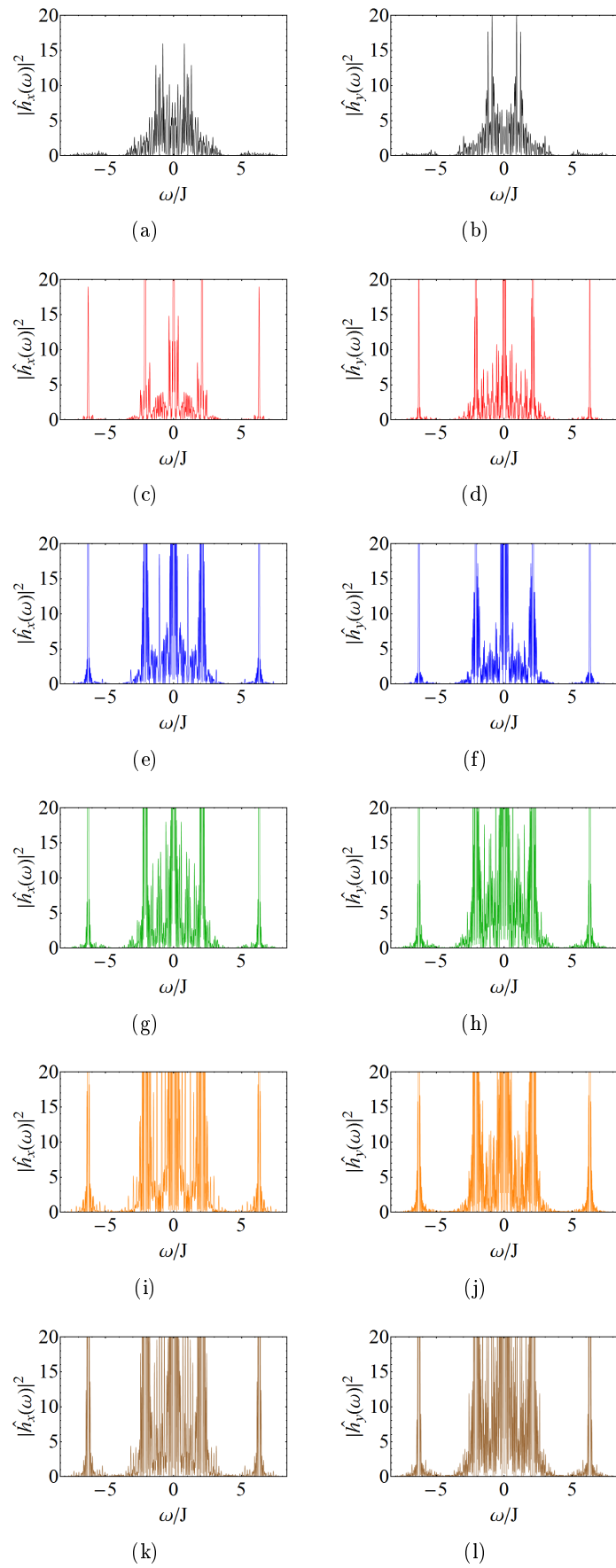
Figure 25: Power spectrum for the optimal control fields of Fig. 15(b). The colours correspond to the ones in Fig. 15(b).
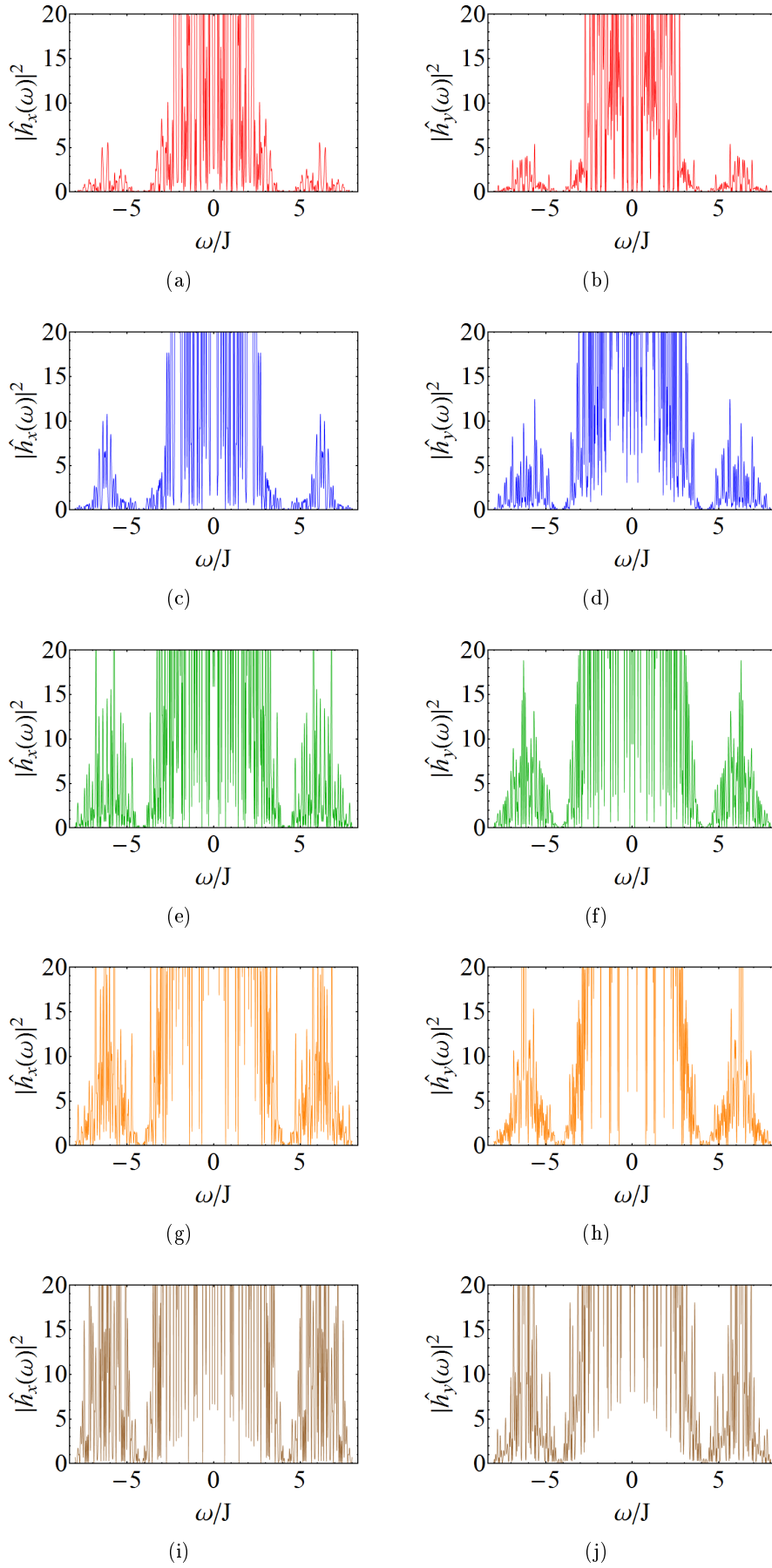
66

Figure 26: Power spectrum for the optimal control fields of Fig. 16(a). The colours correspond to the ones in Fig. 16(a).
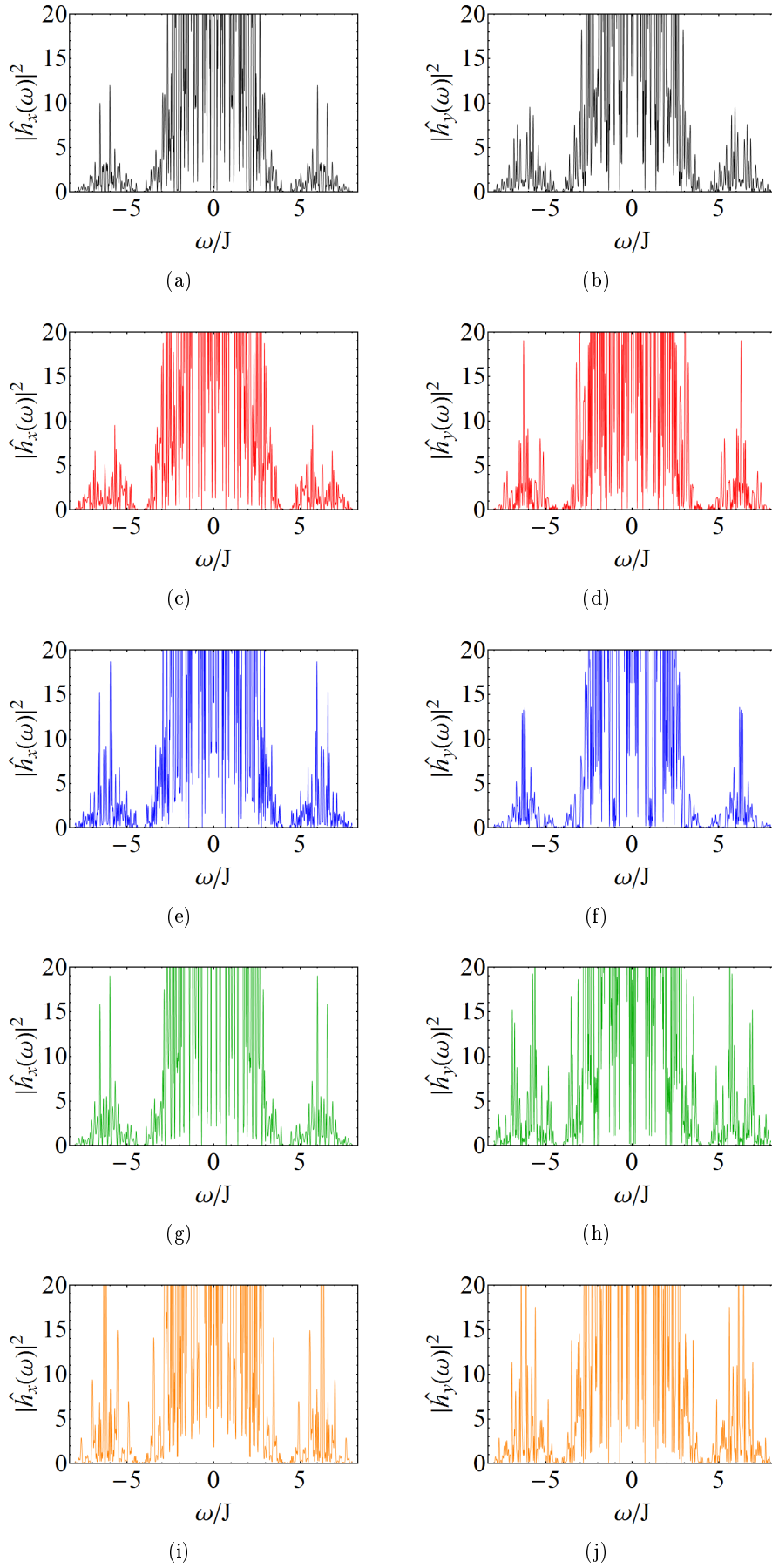
Figure 27: Power spectrum for the optimal control fields of Fig. 16(b). The colours correspond to the ones in Fig. 16(b).
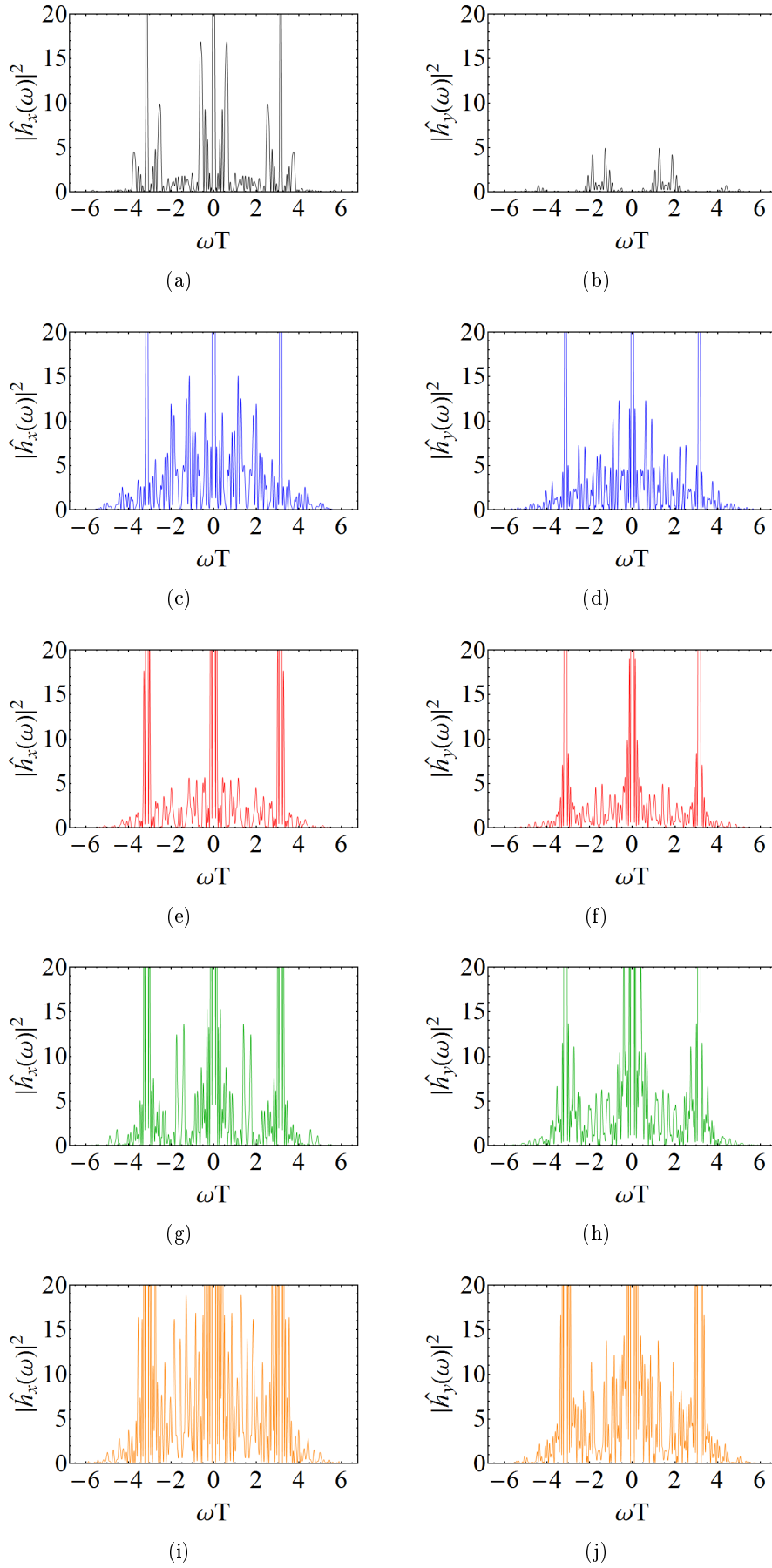
Figure 28: Power spectrum for the optimal control fields of Fig. 17. The colours correspond to the ones in Fig. 17.

References

[1] D. Burgarth, S. Bose, C. Bruder, and V. Giovannetti, Phys. Rev. A **79**, 060305(R) (2009).

[2] D. D'Alessandro, *Introduction to Quantum Control and Dynamics* (Taylor & Francis, Boca Raton, 2008).

[3] M. A. Nielsen and I. L. Chuang, *Quantum Computation and Quantum Information* (Cambridge University Press, Cambridge, 2000).

[4] P. Kaye, R. Laflamme, and M. Mosca, *An Introduction to Quantum Computing* (Oxford University Press, Oxford, 2007).

[5] M. A. Nielsen, Phys. Lett. A **303**, 249 (2002).

[6] E. Bagan, M. Baig, and R. Muñoz-Tapia, Phys. Rev. A **67**, 014303 (2003).

[7] D. Dong and I. R. Petersen, arXiv:0910.2350v1.

[8] S. G. Schirmer, H. Fu, and A. I. Solomon, Phys. Rev. A **63**, 063410 (2001).

[9] D. D'Alessandro, Systems & Control Letters **47**, 87 (2002).

[10] S. Lloyd, Phys. Rev. Lett. **75**, 346(4) (1995).

[11] N. Weaver, J. of Math. Phys. **41**, 240 (2000).

[12] L. H. Pedersen, N. M. Møller, and K. Mølmer, Phys. Lett. A **367**, 47 (2007).

[13] S. G. Schirmer, I. C. H. Pullen, and P. J. Pemberton-Ross, Phys. Rev. A **78**, 062339 (2008).

[14] W. H. Press, S. A. Teukolsky, W. T. Vetterling, and B. P. Flannery, *Numerical Recipes in Fortran 77 and 90: The Art of Scientific and Parallel Computing* (Cambridge University Press, Cambridge, 1997).

[15] X. Wang, A. Bayat, S. G. Schirmer, and S. Bose, Phys. Rev. A **81**, 032312 (2010).

[16] P. T. Callaghan, *Principles of Nuclear Magnetic Resonance Microscopy* (Oxford University Press, Oxford/New York, 1991).

[17] J. Werschnik and E. K. U. Gross, J. Phys. B: At. Mol. Opt. Phys. **40**, R175 (2007).

[18] I. S. Gradshteyn and I. M. Ryzhik, *Tables of integrals, series, and products* (Academic Press, New York, 1965).

[19] H. D. Raedt, A. H. Hams, K. Michielsen, and K. D. Raedt, Comp. Phys. Commun. **132**, 1 (2000).

[20] A. H. Hams and H. D. Raedt, Phys. Rev. E **62**, 4365 (2000).

[21] N. D. Mermin, *Quantum Computer Science: An Introduction* (Cambridge University Press, New York, 2007).